Thermal stabilizers as paradoxical PINK1 activators for the treatment of Parkinson's disease

Luc Truong

Department of Pharmacology and Therapeutics

McGill University, Montreal

July, 2019

A thesis submitted to McGill University in partial fulfillment of the requirements of the degree of Master of Science

TABLE OF CONTENTS

i. List of main body figures

ii. List of Appendix figures

iii. Abstract

PINK1 is a pivotal kinase in the mitochondrial quality control (MQC) pathway. It selectively accumulates on damaged mitochondria and phosphorylates ubiquitin (Ub), as well as the ubiquitin-like domain (Ubl) of Parkin, an E3 ubiquitin ligase. This recruits Parkin to the damaged mitochondria and leads to its activation. Active Parkin then proceeds to ubiquitinate a variety of mitochondrial substrates. A positive feedback loop is thus established, in which Parkin provides more Ub for PINK1 to phosphorylate, in turn recruiting and activating more Parkin. The Ub and phospho-Ub (pUb) decoration of damaged mitochondria ultimately isolates them for arrest, repair, or mitochondrial autophagy (mitophagy). Importantly, loss-of-function mutations in PINK1 and Parkin cause autosomal recessive juvenile Parkinson's disease (ARJPD), a neurodegenerative condition characterized by the loss of dopaminergic neurons in the substantia nigra. It is thought that the accumulation of mitochondrial damage caused by the dysfunction of the MQC pathway underpins the pathogenesis of ARJPD. In this project, we explore the possibility of pharmacologically activating PINK1 in order to bolster the MQC pathway. Most small-molecule kinase-targeted drugs, however, are designed as ATP-competitive inhibitors. Incidentally, reports have shown that certain kinase inhibitors can paradoxically activate the very kinases they are meant to inhibit by inducing their oligomerization, accelerating subcellular localization, or promoting dimerization. Our goal was to exploit this paradoxical kinase activation phenomenon for the pharmacological activation of PINK1. We screened kinase inhibitors for PINK1 thermal stabilizers as a proxy for their ability to impart a conformational change that may underlie PINK1 paradoxical activation. The top thermal stabilizers were then characterized *in vitro* and in mammalian cells. We discovered that CYC116 and PRT062607 are Type I inhibitors of *Tribolium castaneum* PINK1 auto- and substrate phosphorylation, but that PRT062607 is the sole *Homo sapiens* PINK1 inhibitor. Crucially, we report that in HeLa and U2OS cells, PRT062607 induced no stabilization of PINK1 or increase in pUb. However, PRT062607 slightly increased mitophagy in U2OS cells overexpressing GFP-Parkin. Notwithstanding, the thermal stabilizers' characterization remains to be completed, and we aim to crystallize PINK1 bound to a thermal stabilizer in order to test our *in silico* predictions and to guide the development of PINK1 modulators.

iv. French abstract

PINK1 est une kinase essentielle dans la voie de contrôle de qualité mitochondriale (CQM). Elle s'accumule sélectivement sur les mitochondries endommagées et phosphoryle l'ubiquitine (Ub) et le domaine « ubiquitine-like » de Parkin (Ubl), une ligase d'ubiquitine E3. Ces événements recrutent Parkin aux mitochondries endommagées et mènent à son activation. Parkin se met alors à ubiquitiner une variété de substrats mitochondriaux. Une boucle de rétroaction s'établi, avec Parkin fournissant de l'Ub à PINK1 qui par la suite le phosphoryle, activant Parkin de nouveau. Décorées avec de l'Ub et de la phospho-Ub (pUb), les mitochondries endommagées sont isolées pour cesser leur mouvement, les réparer, ou les cibler pour l'autophagie (la mitophagie). Des mutations perte-de-fonction de PINK1 et de Parkin causent la maladie de Parkinson autosomique récessive (ARJPD), une condition neurodégénérative se caractérisant par la perte de neurones dopaminergiques dans la substance noire. Le consensus est que l'accumulation de mitochondries endommagées causée par le dysfonctionnement de la voie de CQM est sous-jacente à la pathogénèse de l'ARJPD. Nous explorons dans ce projet la possibilité d'activer PINK1 pharmacologiquement pour augmenter la compétence de la voie CQM. Cependant, la majorité des petites molécules ciblant les kinases sont conçues en tant qu'inhibiteur. Incidemment, des études ont montré que certains inhibiteurs peuvent activer paradoxalement les kinases qu'ils sont censés inhiber en induisant leur oligomérisation, en accélérant leur localisation, ou en encourageant leur dimérisation. Notre but était d'exploiter ce phénomène d'activation de kinase paradoxale afin d'activer PINK1 pharmacologiquement. Nous avons criblé une librairie d'inhibiteurs de kinases pour dépister des stabilisateurs thermiques de PINK1 comme proxy pour leur capacité de causer un changement conformationel qui pourrait mener à l'activation paradoxale de PINK1. Les meilleurs stabilisateurs thermiques ont été caractérisés *in vitro* et dans des cellules mammifères. Nous avons découvert que CYC116 et PRT062607 sont des inhibiteurs Type I de PINK1 *Tribolium castaneum*, mais que seul PRT062607 inhibe PINK1 *Homo sapiens*. Nous rapportons que PRT062607 n'induit pas la stabilisation de PINK1 ni la production de pUb dans les cellules HeLa et U2OS, mais qu'il augmente légèrement la mitophagie dans les cellules U2OS surexprimant GFP-Parkin. Nonobstant, il reste à compléter la caractérisation des stabilisateurs thermiques, et nous visons à cristalliser PINK1 liée à un stabilisateur thermique afin de tester nos prédictions *in silico* et de guider le développement de modulateurs de PINK1.

v. Acknowledgements

This project would not have been possible without the insight, expertise, and guidance of Dr. Jean-François Trempe. Additionally, I would like to express my gratitude for the help of Shafqat Rasool, who initially trained me as an undergraduate student and has continuously supported me over the span of 3 and a half years. I would also like to thank Andrew Bayne for his unwavering assistance and his contribution to shaping me as a scientist, and Nathalie Croteau for having performed the Thermal Shift Assay and her generous day-to-day help. Last but not least, I thank Yang (Sophie) Lu, Anthony Duchesne, Dylan Pelletier, Dr. Simon Veyron, Tara Shomali, Dr. Marta Vranas, and Nimra Khan, who over the years have made the Trempe Lab an exceptional work environment.

I would like to thank Dr. Mark Hancock (McGill SPR-MS Facility) for his help with the operation of our mass spectrometer. I would also like to thank Dr. John Hanrahan (McGill Department of Physiology) for lending us his RT-PCR system, and Dr. Terry Hébert (McGill Department of Pharmacology) for lending us one of his plate-readers.

I would like to thank Dr. Mohamed Eldeeb from Dr. Edward Fon's lab (Montreal Neurological Institute) for having performed the FACS assay and data analysis.

I would like to thank FRQS for awarding me the GÉPROM Summer Studentship in 2016 and the Master's Training Grant in 2019; NSERC for awarding me the Undergraduate Summer Research Award in 2017 and the Alexander Graham Bell Canadian Graduate Scholarship in 2018; and the McGill Department of Pharmacology for awarding me the Graduate Research Enhancement and Travel Award in 2018. Additionally, I would like to thank NSERC, CIHR, Parkinson Society Canada, and the Michael J. Fox Foundation for funding my project.

vi. Contribution of authors

I performed all experiments in this thesis except the Thermal Shift Assay (performed by Nathalie Croteau) and the FACS Mitophagy Assay (performed by Dr. Mohamed Eldeeb).

All experiments were conceptualized and planned by Dr. Jean-François Trempe and myself.

1. Introduction

1.1. Parkinson's disease is linked to mitochondrial dysfunction

Parkinson's disease (PD) is a neurodegenerative illness characterized by motor symptoms such as bradykinesia, rigidity, and tremors (Gibb and Lees, 1988), as well as non-motor symptoms such as REM sleep abnormalities, loss of olfaction, and psychosis (Kalia and Lang, 2015). With age as a major risk factor, these debilitating symptoms are thought to be caused by the selective decay of dopaminergic neurons in the pars compacta of the substantia nigra (Dickson et al, 2009; Poewe et al, 2017). The projected number of PD patients is predicted to double to over 9 million in the next 10 years, making it a pressing burden to the world's ageing population (Dorsey et al. 2007). Despite the existence of some treatments aimed at symptomatic relief, there currently exists no disease-modifying intervention for PD (Grimes et al, 2012). However, research efforts over the last three decades have discovered a causal link between the underlying pathogenesis of PD and mitochondrial dysfunction. These findings, reviewed and discussed in this section, have produced promising targets for pharmacological PD treatment.

The link between mitochondrial dysfunction and PD was first observed after individuals unknowingly self-administered 1-methyl-4-phenyl-1,2,3,6-tetrahydropyridine (MPTP), a neurotoxic impurity from the clandestine synthesis of an opioid analgesic (Langston et al, 1983). In the brain, MPTP is metabolized into 1-methyl-4-phenylpyridinium (MPP+) (Ransom et al, 1987) which acts as a complex I inhibitor of the mitochondrial respiratory chain (Nakamura et al, 2000). The dysfunction of the electron transport chain leads to the formation of highly reactive oxygen species (ROS), which accumulate and cause a variety of mitochondrial damage; for example, ROS can induce DNA damage, alter membrane properties, react with polypeptides, and affect ion homeostasis (Sena and Chandel, 2013; Guo et al, 2013). Within days, the users developed Parkinsonian symptoms – rigidity, postural imbalance, and tremors, which were partially rescued by giving L-dopa, the dopamine precursor. These symptoms were reproduced when MPTP, along with other complex I inhibitors such as rotenone and paraquat, were administered to rodents and non-human primates (Burns et al, 1983; 1984). Post-mortem analysis revealed that following the administration of complex I inhibitors, individuals and animals display the characteristic loss of melanin in their substantia nigra, indicative of the local destruction of dopaminergic neurons.

These findings gave rise to an interesting question: why did these mitochondrial insults only significantly affect these specific neurons, causing a Parkinsonian phenotype, when there are plenty of mitochondria elsewhere in the body? It is believed that substantia nigra pars compacta dopaminergic neurons are exquisitely susceptible to mitochondrial damage because they are exceptionally reliant on mitochondrial function (Surmeier et al, 2011): they have broad action potentials, and they are pacemaking neurons. More importantly, they intake large amounts of calcium ions via their $Ca_v1.3$ voltage-gated calcium channels without expressing calbindin, a calcium ion buffering protein (Guzman et al, 2010). This obliges them to mobilize their already-taxed mitochondria for excess calcium storage and exposes them to oxidative stress (Surmeier et al (2), 2011). Under such working conditions, these neurons are extraordinarily sensitive to the effects of exogenous mitochondrial insults.

In parallel, complex I deficiencies (Schapira et al, 1989) and mitochondrial DNA (mtDNA) damage (Bender et al, 2006) were also found in post-mortem PD patient brain tissue. However, the overwhelming majority of these patients did not self-administer complex I inhibitors. It is believed that although most PD cases are idiopathic, PD arises from environmental factors, such as pesticide exposure or traumatic brain injury (Dick et al, 2007; Poewe et al, 2017), or genetic factors (Foltynie et al, 2002; Martin et al, 2011), or a combination thereof. For the purposes of foundational research, genetically-caused PD is of great value as it highlights the biochemical players whose dysfunction precipitates the development of the disease. In doing so, we are given clues pertaining to the underlying pathogenesis of PD. Locus mapping and Genome-wide Association Studies (GWAS) (Chang et al, 2017) have revealed several genes whose mutations either increase the risk of developing PD or cause autosomal dominant or recessive forms of PD. For example, autosomal dominant late-onset PD is caused by mutations in *SNCA* (Singleton et al, 2003) and *PARK8* (Khan et al, 2005), encoding α-synuclein and Leucine-rich Repeat Kinase 2, respectively; and autosomal recessive juvenile PD is caused by mutations in *PARK2* (Kitada et al, 1998; Gasser 2001; Yi et al, 2019) and *PARK6* (Bentivoglio et al, 2001; Valente et al, 2002; 2004; Gandhi S et al, 2006), encoding Parkin and PTEN-induced kinase 1 (PINK1), respectively. For clarity and pertinence to this project's aims, Parkin, and especially PINK1, will receive more attention in this Introduction.

Early *in vivo* models of Parkin and PINK1 mutations were used to narrow down the possible molecular mechanisms underlying these rare forms of monogenic PD. Parkin knock-out (KO) mice with increased mtDNA damage (by transgenically incorporating a deficient mtDNA polymerase) have severe nigrostriatal degeneration (Pickrell et al, 2015). Parkin-null *Drosophila* exhibit flight and climb defects, in addition to shorter lifespan, apoptotic muscle degeneration, and male sterility (Greene et al, 2003). Combined with observations of abnormalities in mitochondrial morphology, these phenotypes are all linked to mitochondrial dysfunction. The PINK1 loss-of-function mutant *Drosophila* model exhibits the same muscular defects, sterility, and morphological aberrations of its mitochondria, but overexpression of Parkin in the PINK1 mutant flies was shown to rescue this phenotype (Park et al, 2006; Clark et al, 2006). The converse, i.e. overexpression of PINK1 in a Parkin-null fly, did not rescue the phenotype. These reports were the first to suggest that PINK1 and Parkin work in the same pathway, but that the function of PINK1 in mitochondrial quality control (MQC) is upstream of Parkin's. Importantly, these reports placed mitochondrial dysfunction in the forefront of PD pathogenesis and aetiology (Beilina et al, 2005; Silvestri et al, 2005; Sim et al, 2006; Schapira, 2008).

1.2. PINK1 and Parkin orchestrate mitophagy

Over the past 10 years, numerous follow-up studies have established highly reproducible paradigms to probe this MQC pathway, revealing its details and proposing targets for therapeutic intervention. It has now been firmly established that PINK1 is a kinase that recruits the E3 cytosolic ubiquitin ligase Parkin by selectively accumulating on damaged mitochondria (Narendra et al, 2008) and phosphorylating ubiquitin (Ub) as well as the ubiquitin-like domain of Parkin (Ubl) (Kondapalli et al, 2012). These concurrent events activate Parkin, which subsequently ubiquitinates nearby mitochondrial substrates, providing more targets for PINK1 to phosphorylate. This creates a positive feedback loop in which Parkin's activity provides more substrates for PINK1 while the generation of phospho-Ub (pUb) continues to recruit and activate more Parkin. Eventually, this process of decorating the mitochondrion with Ub and pUb recruits autophagic adaptors which complete the process of macroautophagy of the mitochondrion (mitophagy) (Pickrell and Youle, 2015; Pickles et al, 2018). The remainder of this introduction aims to flesh out the details and nuances of this pathway in order to rationalize the goals of this project.

1.2.1. PINK1 is a mitochondrial damage-sensing ubiquitin kinase

PINK1 is the Ser/Thr kinase that is the sparkplug in this MQC pathway. The structure of its insect orthologs, solved by X-ray crystallography (Kumar et al, 2017; Schubert et al, 2017; Okatsu et al, 2018), reveals that it assumes the canonical kinase fold **(Figure 1)** (Taylor and Radzio-Andzelm, 1994): it has a small N-terminal lobe made of mostly β strands, and a larger C-terminal C-lobe made of mostly α helices. These two lobes are connected by a "hinge" that forms the back of the ATP binding pocket. Sandwiched between the two lobes is the catalytic region, where the phosphorylation of its substrates takes place. Specifically, it contains an activation segment spanning a perfectly conserved Asp-Phe-Gly (DFG) motif to an Ala-Pro-Glu (APE) motif. The DFG aspartate (Asp384 in human PINK1 (HsPINK1)) coordinates a magnesium ion which in turn coordinates the γ-phosphate of adenosine triphosphate (ATP). As well, its N-lobe contains a Gly-rich loop, a gatekeeper methionine (Met294 in TcPINK1; Met318 in HsPINK1) that controls entry into the ATP binding pocket, and a so-called "αC helix" that regulates some of its activities. Finally, the N-lobe contains a catalytic loop with another perfectly conserved His-Arg-Asp (HRD) motif. The HRD catalytic aspartate (Asp337 in TcPINK1; Asp362 in HsPINK1) acts as an electron-donating moiety which increases the nucleophilicity of the substrate's client OH-group **(Figures 2, 3)**. In a phosphorylation reaction, this OH-group attacks the γ-Phosphorus, producing ADP and receiving the phosphoryl group (Johnson et al, 1996; Nolen et al, 2004; Endicott et al, 2012).

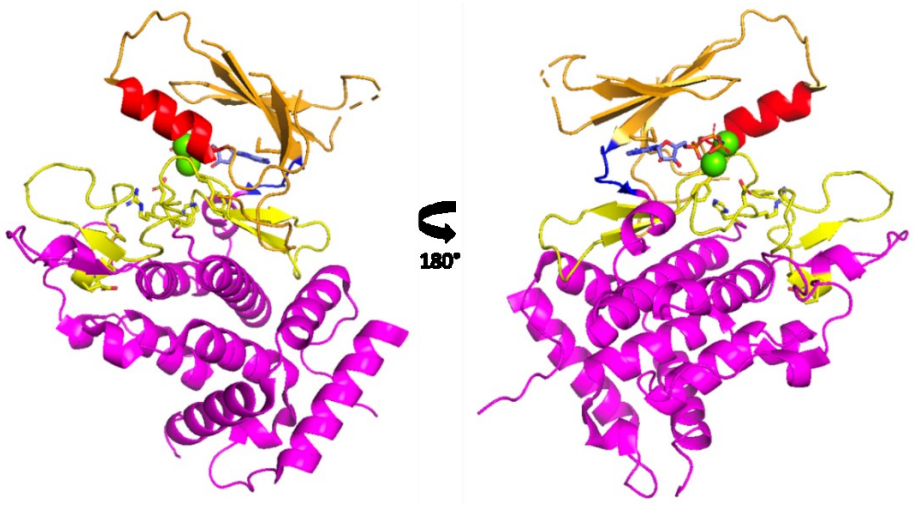

Figure 1: TcPINK1 assumes the canonical kinase fold. X-ray crystal structure of TcPINK1 (153-570 with phosphomimetics S205D, S377D, T386E, and T530E (referred to as

"TcPINK1^{DDEE}"; PDB: 5yj9)). The following structural features have been highlighted in color: the N-lobe, in orange; the C-lobe, in magenta; the hinge, in blue; the catalytic segment, in yellow; and the αC helix, in red. The HRD, APE, and DFG motif sidechains are shown. The gatekeeper Met294 is also shown. Adenylyl-imidodiphosphate (AMP-PNP), an unhydrolyzable ATP analog, is shown in blue and Mg^{2+} cofactors are shown in green.

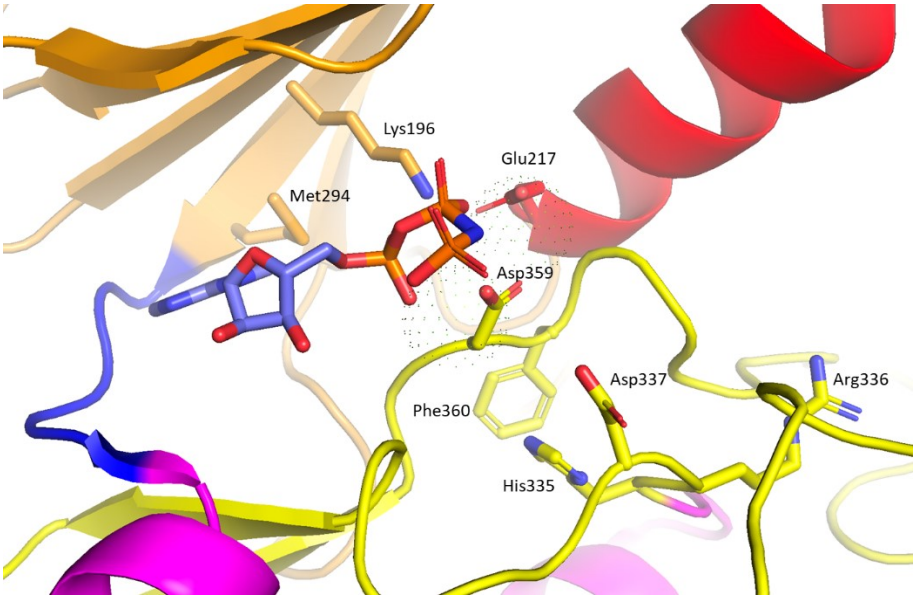

Figure 2: Focus on the catalytic region of active TcPINK1. DFG-in and αC helix-in TcPINK1^{DDEE} (PDB: 5yj9) in complex with AMP-PNP. Structural features are colored as in **Figure 1**. HRD and DFG motif sidechains are shown. Lys196, Glu217 and the gatekeeper Met294 are also shown. Mg^{2+} ions are made transparent for clarity.

Beyond its overall structure, the functionalities of PINK1 can be appreciated by analyzing its primary sequence. Although all of its functions revolve around the mitochondrial estate, it is encoded by the nuclear genome. Its N-terminus, spanning residues 1 to 94, contains a mitochondrial targeting sequence (MTS) from residues 1 to 34, and an outer mitochondrial membrane localization signal (OMS) from residues 74 to 94 (Okatsu et al, 2015). Its residues from 94 to 110 consist of a transmembrane domain (TMD), and a linker from residue 110 to 156 which connects this N-terminal region to the kinase domain. This domain has structural similarity to Calcium/calmodulin-dependent protein kinase 2 (CamKII) (Trempe and Fon, 2013), and runs from residue 156 to 509. Its kinase domain contains three "Inserts", numbered from 1 to 3, which are

not conserved with respect to other kinases and moderately conserved across orthologs. From residue 509 to its C-terminus, PINK1 harbors a poorly conserved "C-terminal extension" (CTE).

PINK1 is constitutively expressed and localizes to the outer mitochondrial membrane (OMM), where its MTS interacts with the translocase of the OMM complex (TOM) surface receptors Tom20 and Tom22 (Sekine and Youle, 2018). Driven by the membrane potential ($\Delta\psi$) across the inner mitochondrial membrane (IMM), PINK1's N-terminus is imported through the Tom40 channel subunit (Jin et al, 2010; Lazarou et al, 2012) into the intermembrane space (IMS), before interacting with Tim23 of the translocase of the IMM complex (TIM) (Neupert and Hermann, 2007; Wiedemann and Pfanner, 2017). The MTS then protrudes into the mitochondrial matrix and stalls as the MTS reveals hydrophobic "stop-transfer" residues to Tim23, preventing further import by the presequence translocase-associated motor (PAM) complex. In the matrix, the MTS is met by the protease MPP (mitochondrial processing peptidase). MPP cleaves the MTS at an unknown site (Greene et al, 2012); then, PINK1/presenilin-associated rhomboid-like protease (PARL) cleaves PINK1 within the IMM at the TMD between Ala103 and Phe104 (Deas et al, 2011; Meissner et al, 2011). It is unclear how PARL manages to reach the PINK1 TMD while it is located inside Tim23; some reports have suggested that additional proteins may be involved in assisting PARL or promoting the lateral translation of the TMD (Sekine and Youle, 2018). Regardless, the cleaved (or "processed") 52 kDa form of PINK1 is then retro-translocated back out of the Tim23 and Tom40 channels and into the cytosol. There, exposure of its hydrophobic and bulky N-terminal Phe104 sidechain attracts the E3 ligase enzymes UBR1, UBR2, and UBR4, which ubiquitinate and degrade PINK1 via the N-end-rule proteasome pathway (Tasaki et al, 2005; Yamano and Youle, 2013). This seemingly futile process of synthesis, import, and degradation repeats itself continuously on the surface of functional mitochondria, resulting in a low steady-state abundance of PINK1.

Damaged mitochondria are characterized by mtDNA aberrations, accumulation of misfolded proteins, and loss of $\Delta\psi$ (Sekine and Youle, 2018). These defects are potentially self-sustaining and compromise the normal function of the mitochondrion. Moreover, dysfunctional mitochondria jeopardize the fate of the entire cell, given that mitochondria contribute to electrolyte homeostasis through their ion buffering capacity, and to energy homeostasis through their involvement in glycolysis and oxidative phosphorylation. As well, dysregulated mitochondrial function can lead

to excess production of ROS, further spreading the damage to more macromolecules and tissues (Sena and Chandel, 2013; Guo et al, 2013). It is in the context of damaged mitochondria that the biological purpose of PINK1's constitutive expression and mitochondrial localization is revealed. When $\Delta\psi$ is lost (which can be artificially induced by carbonyl cyanide m-chlorophenyl hydrazone (CCCP) treatment), PINK1 proceeds to the TOM complex but fails to reach the TIM complex because of an insufficiency in membrane potential to drive its import. It therefore does not reach MPP and PARL and does not get processed. It is instead stabilized on the OMM via interactions between Tom20 and its OMS (Okatsu et al, 2015; Sekine and Youle, 2018). Since PINK1 is constitutively expressed, it accumulates on the OMM, its local concentration gradually increasing. It likewise accumulates on mitochondrial regions containing misfolded protein aggregates, although the underlying mechanism is less clear (Jin and Youle, 2013). Nevertheless, PINK1 acts as a mitochondrial damage sensor, localizing to all mitochondria but accumulating specifically on the damaged ones. As the concentration of PINK1 increases, so does the probability that two PINK1 proteins are situated in proximity. When such an event occurs, PINK1 undergoes an intermolecular autophosphorylation (or *transphosphorylation*) event in which one PINK1 phosphorylates the other (Okatsu et al, 2012; 2013; Rasool et al, 2018). It is believed that its interaction with Tom7 poises it for temporary dimerization and transphosphorylation (Hasson et al, 2013; Bausewein et al, 2017). As in many other kinases (Beenstock et al, 2016), autophosphorylation structurally primes PINK1 to phosphorylate its substrates ubiquitin (Ub), and the ubiquitin-like domain of Parkin (Ubl), ultimately leading to Parkin recruitment.

The importance of PINK1 autophosphorylation is demonstrated and discussed at length in an article that our group published in February 2018, and to which I contributed during my graduate studies (Rasool et al, 2018). Here, for continuity and contextualization, that article will be summarized briefly. It had been previously observed that human PINK1 (HsPINK1) expressed in mammalian cells is autophosphorylated at two key residues: Ser228, located upstream of the αC-helix, and Ser402, located on the activation segment **(Figures 1, 2, 3)** (Okatsu et al, 2012). Transfected with S228A HsPINK1 mutants, cells failed to recruit Parkin. However, cells transfected with S402A mutants did not fail to recruit Parkin at lower temperatures, and S402N mutants displayed wild-type (WT) levels of Parkin recruitment (Narendra et al, 2013). This indicated that only Ser228 autophosphorylation was indispensable for PINK1 function, but it was unclear what underpinning mechanisms made this true. We investigated the role of Ser228

autophosphorylation by testing two mutants: Ser228 to alanine (an unphosphorylatable residue with a non-polar sidechain) or to asparagine (an unphosphorylatable residue, but polar nonetheless). It is important to note that much of the *in vitro* work on PINK1 has been done using insect orthologs of PINK1, such as *Tribolium castaneum* or *Pediculus humanus corporis* PINK1 (TcPINK1 and PhPINK1, respectively), as they are better recombinantly expressed in heterologous systems, yield larger amounts of PINK1 upon purification, and display better activity *in vitro* (Woodroof et al, 2011). The equivalent residue for Ser228 is Ser202 in PhPINK1, and Ser205 in TcPINK1. Thus, we created TcPINK1 S205A and S205N mutants. These mutants failed to phosphorylate Ub or Ubl *in vitro* and in cells. By transverse relaxation-optimized spectroscopy (TROSY) nuclear magnetic resonance (NMR), we showed that TcPINK1 could not bind Ub or Ubl in the absence of the autophosphorylation at Ser205. Intriguingly, intact protein mass spectrometry (MS) data indicated that the S205A and S205N mutants were still able to phosphorylate *themselves* (at other serines and threonines). This meant that the Ser205 mutants were still catalytically active, but failed to recognize and phosphorylate non-self substrates. Furthermore, mammalian cells expressing endogenous Parkin transfected with S228A HsPINK1 displayed no pUb signal (Rasool et al, 2018). Although the PINK1:Ub/Ubl binding sites were mapped, the precise intramolecular changes caused by Ser228/Ser205 autophosphorylation remained elusive.

The structural consequences of PINK1 autophosphorylation were initially observed by Hydrogen-Deuterium exchange tandem-MS (HDX-MS), which measures solvent exchange rates of protein segments to infer solvent exposure and degree of folding (Konermann et al, 2011). By comparing an autophosphorylated versus a dephosphorylated form of TcPINK1, an increase in exchange was specifically observed in regions circumscribed within the catalytic region and surrounding the Ser205 autophosphorylation site (Rasool et al, 2018). Given that Ser205 is located some 25 Å away from the catalytic loop, the increase was interpreted as an allosteric effect caused by the autophosphorylation resulting in the reorganization of the catalytic region and the αC-helix (Rasool and Trempe, 2018).

Three PINK1 insect ortholog structures obtained by X-ray crystallography have now shed light on the rearrangements caused by autophosphorylation and Ub binding. Coincidentally, these three structures represent three distinct steps that occur when PINK1 phosphorylates its substrates: an

apo TcPINK1 structure (meaning, unbound TcPINK1) (Kumar et al, 2017; PDB: 5oat); a structure of TcPINK1 binding an unhydrolyzable ATP analog (Okatsu et al, 2018; PDB: 5yj9); and, a co-crystal structure of PhPINK1 bound to its substrate Ub (Schubert et al, 2018; PDB: 6eqi). While the TcPINK1 structures confirmed the general fold of the kinase (Taylor and Radzio-Andzelm, 1994), the PhPINK1 structure revealed the relationship between autophosphorylation and Ub binding **(Figure 3)**. In PhPINK1, the phosphoryl on Ser202 interacts with Arg282 and Asn283, thus rearranging Insert 3. This enables Insert 3 to participate in the N-lobe-centered interface between PhPINK1 and Ub, which also implicates the Gly-rich loop along with the bulky residues Phe196 and Tyr198. This face of PINK1 engages Ub around its His68, Val70, and Ile44 hydrophobic patch, and phosphorylates Ub at Ser65 (Kondapalli et al, 2012; Koyano et al. 2014). Following PINK1 activation and Ub phosphorylation, Parkin is recruited.

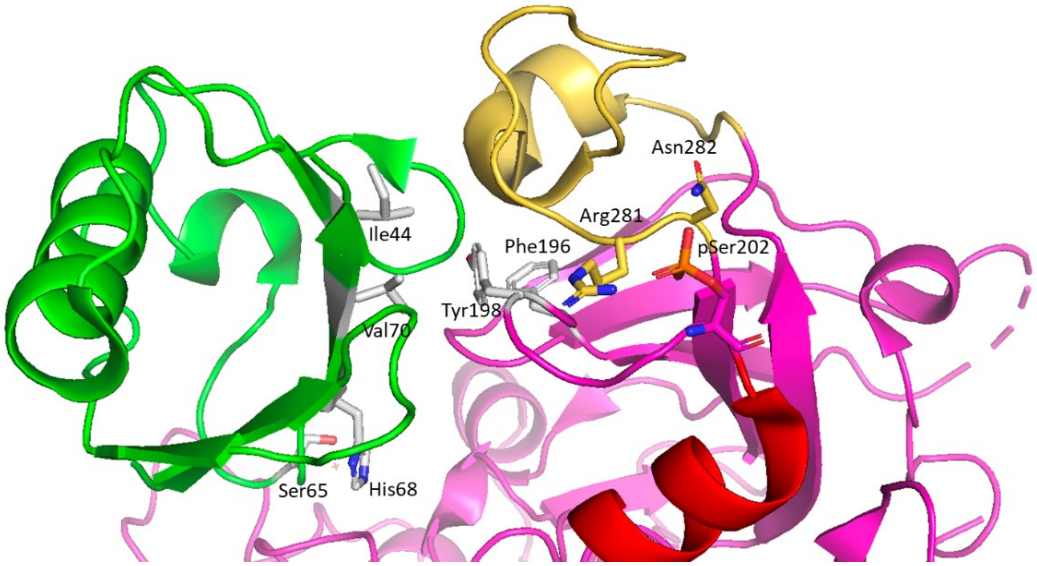

Figure 3: pSer202 primes the binding interface between PhPINK1 and Ub. X-ray crystal structure of PhPINK1 (143-575) bound to Ub (PDB: 6eqi). The following features were highlighted in color: PhPINK1, in magenta; Ub, in green; Insert 3, in beige; the αC helix, in red. Sidechains crucial for interface formation and PhPINK1:Ub binding are displayed and labeled.

1.2.2. Parkin is a PINK1-dependent ubiquitin ligase

In order to relay the status of mitochondrial health, PINK1 phosphorylation activity is coupled to Parkin ubiquitination activity (Trempe and Fon, 2013). In general, ubiquitination of substrates occurs at lysine sidechains or the N-amino-terminus and is indispensable for targeted protein degradation (Hershko and Ciechanover, 1998). The process of ubiquitination is carried out by three classes of proteins: E1 activating, E2 conjugating, and E3 ligating enzymes (Komander and Rape, 2012; Buetow and Huang, 2016; Zheng and Shabek, 2017). The E1 enzyme consumes ATP to activate Ub by forming a thioester bond between its catalytic cysteine and the carboxy-terminus of Ub. It then transfers the Ub to the E2 conjugating enzyme via another thioester bond. The E2 enzyme then interacts with an E3 ligase to finalize the ubiquitination of a substrate. There are three classes of E3 enzymes: RING-type, HECT-type, and RING-HECT hybrids (or RBR-type). RING (Really Interesting New Gene)-type enzymes are essentially scaffolds, binding to both the E2 and the substrate, allowing the E2 to directly ubiquitinate the substrate. HECT (Homologous to the E6-AP Carboxyl Terminus)-type enzymes ubiquitinate the substrate themselves after having the Ub transferred to their own catalytic cysteine. Finally, RING-HECT hybrids have at least two RING domains linked together by an in-between-RING (IBR) domain. They bind the E2 enzyme on one domain, transfer the Ub onto another domain's catalytic cysteine, and then ubiquitinate the substrate. Parkin is an example of a RING-HECT hybrid E3 Ub ligase which contains additional domains: a ubiquitin-like domain (Ubl), a linker, and an extra RING domain called RING0. Moreover, the IBR is immediately followed by the Repressor Element of Parkin (REP), a small helix that binds the RING1 domain (Trempe et al, 2013; Seirafi et al, 2015; Sauvé et al, 2015). These add-on elements are catered to Parkin's relationship with PINK1 and its role in MQC.

Numerous lines of evidence, from *in vitro* assays to crystallography, show that Parkin remains repressed by several intramolecular interactions until it binds pUb and is itself phosphorylated by PINK1 (Chaugule et al, 2011; Wauer and Komander, 2013; Trempe et al, 2013; Riley et al, 2013; **Figure 4**). Firstly, the Ubl and the REP occlude the RING1 E2 binding site. Secondly, the catalytic Cys431 on RING2 is inaccessible due to interactions with RING0. Activation of Parkin therefore requires a large conformational rearrangement to unlock both the E2 binding site and the RING2 catalytic site.

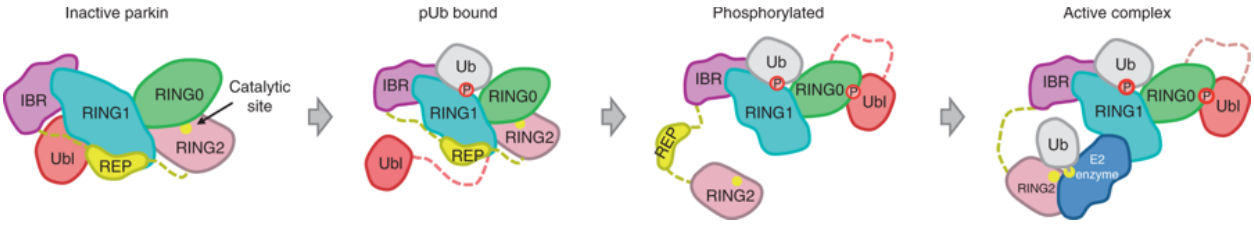

Figure 4: Mechanism of PINK1-dependent Parkin activation (Sauvé et al, 2018). Domain names and phosphorylation events are annotated.

On damaged mitochondria, PINK1 phosphorylates nearby pre-existing Ub moieties, most likely near mitochondrial-endoplasmic reticulum (ER) contact sites (Tang et al, 2017; McLelland et al, 2018). Parkin is then attracted from the cytosol to the OMM where it binds pUb through interactions with RING0 and IBR, as well as RING1 via the His302, Arg305, and Tyr312 sidechains (Sauvé et al, 2015). The binding of pUb triggers the allosteric release of the Ubl on the opposite side of RING1 **(Figure 4)**. Since the Ubl interacts with RING1 with the same interface with which it would bind PINK1, this allows it to be phosphorylated by PINK1 at Ser65. Parkin is now recruited to the damaged mitochondrion with pUb acting as its receptor (Okatsu et al, 2015), while its Ubl is phosphorylated (pUbl) and free from RING1. The pUbl swings around and binds to RING0, where the phospho-Ser65 interacts with Lys161, Lys211, and Arg163 (Sauvé et al, 2018; Gladkova et al, 2018). This releases the REP and displaces the resident RING2, exposing its catalytic Cys431, and finalizing the activation mechanism of Parkin. Meanwhile, the vacated RING1 is now able to strongly bind E2 conjugating enzymes. Thus, Parkin activity is exquisitely dependent on PINK1 catalytic activity and localization.

Once activated, Parkin ubiquitinates a panoply of mitochondrial substrates. Numerous groups have reported different sets of Parkin substrates. It has been shown to ubiquitinate Mitofusin1/2 (Mfn1/2), a large guanosine triphosphatase (GTPase) that controls the topography of the OMM and membrane fusion (Santel et al, 2003). Subsequently, the +AAA ATPase p97 targets Lys48-ubiquitinated Mfn1/2 for extraction out of the OMM and ultimate degradation (Tanaka et al, 2010). As such, Parkin targeting of Mfn1/2 is thought to mitigate the spread of mitochondrial damage by preventing mergers between damaged and healthy mitochondria, in favor of mitochondrial fission orchestrated by dynamin-related protein 1 (Drp1). Mfn2 has also been reported to localize at mito-

ER contact sites, and Parkin-mediated ubiquitination of Mfn2 might contribute to the separation of damaged mitochondria from the ER network to facilitate mitophagy. In addition to Mfn1/2, cell-based studies have indicated that the voltage-dependent anion channels 1/2/3 (VDAC1/2/3) and Miro1 are ubiquitinated by Parkin (Geisler et al, 2010; Chan et al 2011). Miro1 serves as an adaptor between kinesin and mitochondria, giving rise to mitochondrial motility (Wang et al, 2011). Its degradation would bring mitochondrial movement to a halt; this is thought to help sequester damaged mitochondria for autophagy. Recent proteomic data (Martinez et al, 2017; Ordureau et al, 2018) have confirmed these proteins as Parkin substrates among hundreds of other substrates, including subunits of the TOM complex, Hexokinase 1 (involved in glycolysis), mitoNEET/CISD1 (which has unknown function (Geldenhuys et al, 2014)), and mitochondrial Rho GTPase 1 (RHOT1; involved in mitochondrial anterograde transport). The breadth and seemingly indiscriminating nature of Parkin substrates showcases its promiscuity, which is thought to help broadcast an amplified signal of mitochondrial damage following PINK1 activation.

Ub itself can accept Ub moieties since it contains lysines (and an N-terminus), yielding linear or branched polyUb chains. While Parkin ubiquitinates certain substrates site-specifically (such as Mfn1/2), it has been reported that Parkin can build large polyUb chains on any of the several lysines of Ub with little preference (Durcan et al, 2014). Although PINK1 can phosphorylate short polyUb chains *in vitro* (Rasool et al, 2018), it is predicted that in cells, while stabilized on the OMM by TOM, it will not be able to phosphorylate all Ub moieties in a chain due to steric hindrance. Nevertheless, PINK1/Parkin form a positive feedback loop, wherein PINK1 recruits and activates Parkin while Parkin provides more Ub for PINK1 to phosphorylate. This Ub/pUb decoration of the OMM recruits proteins such as Sequestome 1 (also known as p62), nuclear dot protein 52 (NDP52) (von Muhlinen et al, 2010) and optineurin (OPTN) (Pickles et al, 2018). Using their Ub-binding domains (UBDs), they physically connect these damaged mitochondria to microtubule-associated protein 1A/1B-light chain 3 (LC3) conjugated to phosphatidylethanolamine (PE-LC3) (Tanida et al, 2008). PE-LC3 is itself incorporated into the autophagosome, a double membrane structure which encapsulates doomed subcellular regions for lysosomal degradation. A parallel autophagosome-attracting pathway has also been reported in which RABGEF1, a guanosine nucleotide exchange factor (GEF) for Rab proteins, binds Ub/pUb chains and activates Rab5 to Rab5-GTP (Yamano et al, 2014; 2018). This enables Rab5 to wedge itself into the OMM and stimulate the MON1/CCZ1 complex, a Rab7 GEF, activating Rab7 to

Rab7-GTP. Rab7-GTP then recruits elements of the autophagosome in the process of maturation, thus establishing a redundant autophagosome recruitment mechanism.

The autophagosome requires a series of regulated maturation steps which mobilize several protein complexes. The details of autophagosomal maturation are discussed at length by Ivan Dikic (Dikic 2017). Briefly, the autophagosome originates as a phagophore whose growth depends on a multiprotein complex centered on unc-51-like autophagy activating kinase 1 (ULK1). Following ULK1 activation, recruitment of another complex containing vacuolar protein sorting 34 (VPS34), Beclin 1, and autophagy/Beclin-1 regulator 1 (AMBRA1) occurs. This other complex couples the autophagy-related proteins 12/5/16 (Atg12/5/16) to the Atg8/LC3/Gamma-aminobutyric acid receptor-associated protein (GABARAP) complex. This coupling nurtures phagophore expansion into the autophagosome. The final step of autophagy requires elements of the SNARE-like protein complex which orchestrate the autophagosome-lysosomal fusion. The contents of the fused structure are then degraded by hydrolases. The overarching PINK1/Parkin pathway, from PINK1 activation to autophagosome recruitment, are summarized in **Figure 5**.

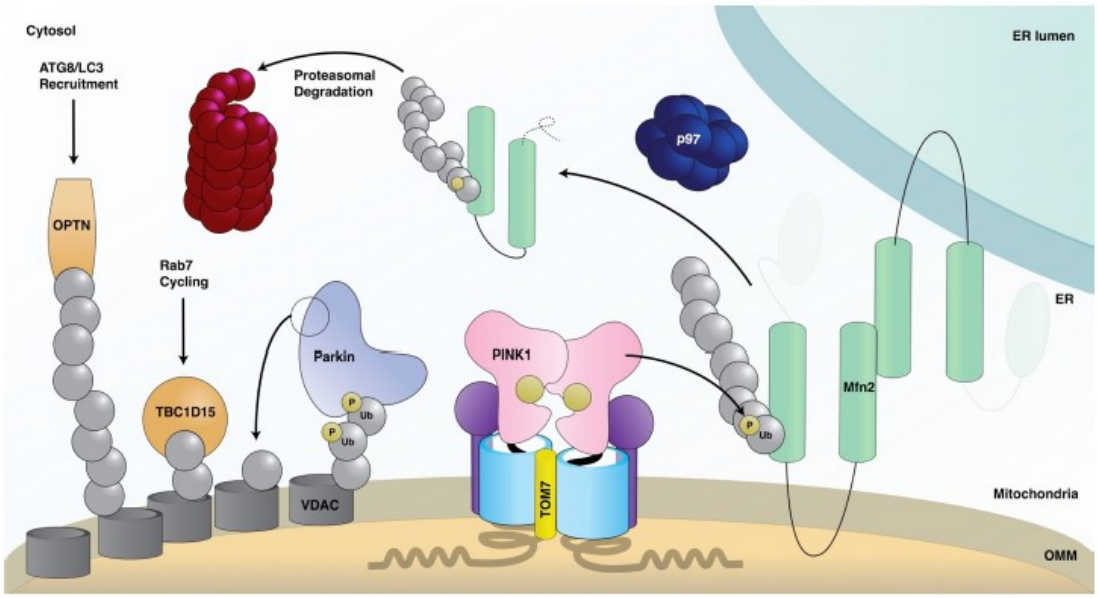

Figure 5: Overarching diagram of the PINK1/Parkin MQC pathway (Bayne and Trempe, 2019) in damaged mitochondria. Proteins names are annotated. Phosphorylation events are represented as gold spheres, and Ub moieties as gray spheres.

1.3. PINK1 and Parkin go beyond mitophagy

Thus, PINK1 and Parkin constitute two of the most upstream players in the MQC pathway: PINK1 acts as a damage sensor and Parkin acts as a signal broadcaster. However, the MQC pathway does not necessarily end with mitophagy. It has been shown that MQC via PINK1/Parkin can have less sweeping consequences than the total destruction of a damaged mitochondrion. Indeed, protein turnover measurements in Drosophila show that Parkin/PINK1 affect the turnover of only a subset of mitochondrial proteins (Vincow et al, 2013). PINK1/Parkin signaling is also required for the formation of mitochondrially-derived vesicles (MDVs) (Sugiura et al, 2014; McLelland et al, 2016), which are small portions of the mitochondria containing misfolded protein aggregates or other such harmful focal points. These MDVs merge with late endosomes/lysosomes in a syntaxin-17-dependent manner, leading to their degradation. Independent of Drp1 (putatively involved in larger fission events) and macroautophagy adaptors, MDV budding is thought to be a less drastic approach to mitochondrial damage, where selected regions of damaged mitochondria are removed.

It has also been reported that PINK1/Parkin suppress the formation of a different subset of MDVs involved in mitochondrial antigen presentation (MitAP) (Matheoud et al, 2016). Upon extraction, isolation, and breakdown of mitochondrial contents, certain MDVs can be trafficked to the cell surface and transfer their cargo to major histo-compatibility class I (MHC I) proteins. These cell surface proteins can present the mitochondrially-derived contents as antigens. Subsequently, recognition of MitAP by patrolling T-cells could unleash an immune response towards these neurons (Cebrian et al, 2014). Indeed, certain mitochondrial elements are highly reminiscent of bacteria, and excessive MitAP could trigger an autoimmune-like response. The MDVs responsible for MitAP are formed by the action of Sorting nexin 9 (Snx9), a dynamin binding partner involved in vesicular trafficking (Lundmark and Carlsson, 2009). Following activation by PINK1, Parkin ubiquitinates and targets Snx9 for degradation, preventing MitAP. The details regarding the differentiation between MDVs induced by PINK1/Parkin and those suppressed by PINK1/Parkin are still under investigation.

PINK1/Parkin have also been implication in the neuroinflammation response. Serum taken from individuals with mono- or bi-allelic Parkin mutations contained increased levels of inflammatory cytokines. In a recent study (Sliter et al, 2018), Parkin and PINK1 homozygous KO mice were found to also have significantly higher levels of the inflammatory cytokines Interleukin-6 (IL-6)

and Interferon β1 (IFNβ1) following exhaustive exercise. Interestingly, these mutant mice also had higher levels of circulating mtDNA post-exercise. Cytosolic DNA is recognized by STING (Stimulator of Interferon Genes), an adaptor protein in the type I interferon response which orchestrates the secretion of those cytokines (Chen et al, 2016). Indeed, homozygous KO of STING returned the cytokine and mtDNA levels to WT. These data provide evidence that PINK1/Parkin are necessary for the regulated and prompt removal of damaged mitochondria before their DNA leaks into the cytosol and triggers a STING-mediated inflammatory response.

1.4. PINK1 activation as a potential disease-modifying treatment for PD

In summary, the past three decades of research have established mitochondrial dysfunction as a primordial factor in both genetic and sporadic PD pathogenesis. In parallel, the elucidation of the PINK1/Parkin MQC pathway has brought many potential therapeutic targets to the forefront of the field. We now understand that the role of PINK1 as a mitochondrial damage sensor and a Parkin activator is indispensable for MQC. Thus, a pharmacological intervention aimed at positively modulating PINK1 activity constitutes an ideal strategy to treat PD for several reasons. Firstly, PD-associated mutations that decrease PINK1 activity could be remedied by pharmacological positive modulation. Secondly, mutations in other proteins downstream of PINK1 in the MQC pathway could be compensated for by PINK1 activation, since its activity is upstream of them all. Most importantly, we believe that the accumulation of mitochondrial damage observed in idiopathic or sporadic cases of PD could be mitigated by a PINK1-mediated MQC boost. Exogenous PINK1 activation was achieved using a PINK1-specific neo-substrate, kinetin triphosphate (KTP), which increased PINK1 activity in cell-based experiments (Hertz et al, 2013). However, KTP failed to rescue PD phenotypes in rat models (Orr et al, 2017). The challenge currently lies in how PINK1, the only known ubiquitin kinase, can be positively modulated.

1.4.1 Kinases are complex pharmacological targets

Kinases are among the most studied enzymes in the human proteome (Roskoski 2019). It is estimated that 1 in 40 genes encodes a kinase, giving rise to a human kinase family of 518 members (Manning et al, 2002). Mutant, dysregulated, and overexpressed kinases are involved in numerous

illnesses including cardiovascular and nervous diseases, autoimmune and inflammatory disorders, and most notably, cancers (Cohen 2002; Roskoski 2015). It follows that 20 to 33% of all drug discovery efforts in the world are focused on kinase modulation, and the US FDA has approved 48 small-molecule kinase inhibitors primarily against 20 kinases (Carles et al, 2018). These inhibitors represent the tip of the kinase pharmacology iceberg: countless other compounds have been tested, and over 6,000 kinase X-ray crystal structures have been published (Roskoski 2019). Our understanding of kinases is built on the characterization of their inhibitors (Shen et al, 2005). It is thus necessary to briefly review the different modes of kinase inhibition in order to, paradoxically, substantiate our strategy for kinase activation.

Kinases have highly dynamic structures which enable efficient yet subtle tertiary structure changes in response to the cellular situation (Dar and Shokat, 2011; Taylor and Kornev, 2011; Roskoski 2015). Kinases are understood to have inner networks of residue interactions that activate and prepare them for catalysis. The R-spine is a columnar network spanning the catalytic region built with at least 4 residue interactions that are consistently observed in active kinase structures (Hu et al, 2015). The first R-spine residue (RS1) is the His in the HRD motif (His335 in TcPINK1); RS2 is the Phe in the DFG motif (Phe360 in TcPINK1); RS3 is an aliphatic residue on the αC-helix (Pro220 in TcPINK1); and RS4 is an aliphatic residue on the β4 strand (Ile243 in PhPINK1) (Okatsu et al, 2018). In addition to participating in the R-spine, the DFG Asp must face inward (a position known as DFG-in, the opposite being DFG-out) to coordinate the magnesium ion cofactor; as well, the αC helix must also rotate inwards such that the conserved glutamine (Glu214 in PhPINK1, Glu217 in TcPINK1) interacts with a lysine (Lys193 in PhPINK1, Lys 196 in TcPINK1) in the Gly-rich loop (known as αC helix-in) **(Figure 2)**. The C-spine is another network on the opposite side of the catalytic region which is always formed when ATP, binding to its pocket next to the kinase hinge **(Figures 1, 2)**, is on the verge of being consumed in a phosphorylation reaction. In fact, the C-spine is only complete with the binding of ATP. In PINK1, it is entirely made of 8 non-aromatic hydrophobic residues (see Schubert et al, 2018 for details). These two spine networks, or at least their chemical properties, are conserved across kinases.

Based on crystal structures and mutagenesis studies, small-molecule kinase inhibitors have been shown to disrupt the R-spine and C-spine networks, as well as the orientations of the DFG motif and αC helix. The classification of kinase inhibitors has thus been as a function of their effects on

this conserved architecture (Dar and Shokat, 2011; Roskoski 2019). Type I inhibitors are molecules that bind to active-form kinases; that is, DFG-in/αC helix-in kinases **(Figure 2)**, with only the C-spine disrupted by replacing ATP with the inhibitor. Type I½ inhibitors bind to semi-inactive kinases, in that they are DFG-in but αC helix-out (Zuccotto et al, 2010). Type II inhibitors bind to DFG-out kinases. Type III inhibitors bind inside the catalytic region but not the ATP binding site *per se*, thus without the displacement of ATP (Gavrin and Saiah, 2013). This creates a situation in which both ATP and the inhibitor bind the kinase in its catalytic cleft. Type IV inhibitors bind outside of the catalytic region altogether. Type V inhibitors span two distinct binding sites; for example, they could be large enough to bind part of the catalytic region and part of a non-catalytic domain (Lamba and Ghosh, 2012). Finally, Type VI inhibitors are covalent inhibitors.

When reviewing the literature on kinase pharmacology, it is quickly apparent that the precedent for kinase activators is meager. One study of pharmacological kinase activation reported PS48 as a PDK1 activator (Hindie et al, 2009). Phosphoinositide-dependent kinase 1, or PDK1, is a kinase upstream of several growth- and metabolism-regulating pathways. It is an AGC kinase (named after the well-studied kinases PKA, PKG, and PKC); as such, it bears a hydrophobic motif (HM) within its C-terminal extension (Arencibia et al, 2013). To achieve the correct configuration for activation, it must translocate to the membrane where it binds phosphatidylinositol-1,4,5-trisphosphate (PIP3) produced by phosphoinositide 3-kinase (PI3K). There, PDK1 is phosphorylated by membrane-bound kinases on its activation segment and its HM. PDK1 becomes activated when the phosphorylated HM wraps around and binds its N-terminal region in the so-called PIF pocket (Newton 2003; Biondi 2004). To mimic the phosphorylated HM, a group synthesized a bi-arylic compound joint by a carboxylic acid moiety, thus creating a surrogate binding partner for the PIF pocket (Hindie et al, 2009). The binding was confirmed by X-ray crystallography, and PS48 was shown to increase PDK1 activity in vitro. This result confirmed the standing model of AGC kinase activation and proved that structure-based kinase activator design was possible.

More recently, the kinase PKCδ has been targeted for activation (Bessa et al, 2018). Although the upregulation of the PKC kinase family has been linked to intestinal and colon carcinogenesis, these phenotypes are reported to be paralleled with downregulation of the specific isozyme PKCδ (Cerda

et al, 2001; Hernandez-Maqueda et al, 2015). A yeast-based screening assay produced a molecule called Roy-Bz which displayed PKCδ-dependent anticancer activity, such as inhibition of tumor cell migration and apoptotic cell death. No crystal structure was published alongside these findings, but molecular docking simulations suggest that Roy-Bz binds the C1 domain of PKCδ. This domain is involved in sensing diacylglycerol (DAG), and perhaps Roy-Bz binding has analogous effects to PS48 binding the PDK1 PIF pocket.

1.4.2. Kinases can be paradoxically activated by inhibitors

Amidst the efforts to pharmacologically inhibit oncogenic kinases, some studies have reported that certain ATP-competitive small-molecule kinase inhibitors unexpectedly activate the kinase pathways they are meant to inhibit. This is a highly problematic side effect in anticancer therapy as it can induce the growth of new tumors (Dar and Shokat, 2011). The consensus regarding this phenomenon, called "paradoxical kinase activation", is that it occurs via conformational rearrangements in non-catalytic regions of the targeted kinase. Since the paradoxical activators are ATP-competitive, it is thought that these structural consequences originate from the ATP binding pocket. These changes are able to compensate for the catalytic inhibition caused by the ligand binding, ultimately leading to the upregulation of the oncogenic pathway. The following section of the introduction provides examples of such paradoxical kinase activation.

Example 1: Inositol-requiring enzyme 1, or Ire1, is a bifunctional transmembrane ER enzyme involved in the initiation of the unfolded protein response (UPR). It contains an ER-lumenal stress-sensing domain connected to a kinase domain on one end, and a cytosolic RNAse domain on the other. When increases in unfolded protein are detected in the ER lumen, chaperones normally bound to the stress-sensing domain abandon Ire1 in order to assist protein folding (Patil and Walter, 2001). This was observed to trigger kinase domain oligomerization, followed by its transphosphorylation, leading to a conformational change that activates its cytosolic RNAse domain, which cleaves the HAC^u messenger RNA (mRNA) in yeast, or *Xbp1* in mammals. Cleavage of this mRNA causes excision of a translation-inhibitory intron (Ruegsegger et al, 2001) and re-ligation into its active form, HAC^i (Cox and Walter, 1996; Sidrauski and Walter, 1997). The active mRNA jumpstarts a program that upregulates several proteins aimed at ER-stress relief, including chaperones, oxido-reductases, and degradation and secretory pathway components. To

study how the Ire1 kinase domain oligomerization and transphosphorylation communicates ER stress to the Ire1 RNAse domain, an Ala and a Gly gatekeeper mutation were introduced in its catalytic region to sensitize Ire1 to a particular inhibitor, 1-tertbutyl-3-naphthalen-1-ylmethyl-1H-pyrazolo[3,4-d]pyrimidin-4-ylemine, or 1NM-PP1 (Papa et al, 2003). Since almost every known kinase harbors gatekeeper residues larger than Ala or Gly, this "chemical genetics" approach is commonly used to study kinases as only the mutated kinase will be inhibited, thus isolating the function of the kinase in question (Bishop et al, 2000; Dar and Shokat, 2011). The 1NM-PP1-sensitizing mutations themselves crippled Ire1 kinase activity and UPR signaling, but paradoxically, addition of 1NM-PP1 increased, rather than inhibited, UPR signaling. While mutations of the transphosphorylation serines (S840A/S841A) abrogated UPR signaling, Ire1 with both 1NM-PP1-sensitizing mutations and the double S840A/S841A rescued UPR signaling upon addition of 1NM-PP1. These results indicated that paradoxically, the ATP-pocket-binding inhibitor 1NM-PP1 was activating Ire1 signaling by inducing oligomerization and bypassing the need to transphosphorylate (Papa et al, 2003).

Example 2: Akt (also known as PKB) is an AGC kinase which positively regulates cell growth and survival (Hennessy et al, 2005; Manning et al, 2007). Its activation requires two phosphorylation events by two kinases bound to the plasma membrane. To reach the plasma membrane, Akt employs its pleckstrin-homology (PH) domain to bind PIP3, the product of PI3K. There, its activation segment is phosphorylated by PDK1 at Thr308 (Alessi et al, 1997), and its HM is phosphorylated by mTORC2 (mammalian target of rapamycin 2) at Ser473 (Sarbossov et al, 2005). Active Akt then phosphorylates mTORC1 and glycogen synthase kinase 3 β (GSK3β). Many mutations along the PI3K-Akt-mTORC1 pathway are associated with carcinogenesis, and years of research have produced several Akt inhibitors. One such inhibitor, A-443654, was reported to unexpectedly induce increased phosphorylation of Akt Thr308/Ser473 (Okuzumi et al, 2009). It was initially proposed that A-443654 was nonselectively inhibiting other kinases playing negative feedback roles on Akt activation. To address this hypothesis, a chemical genetics approach was used, in which Akt had its gatekeeper residue mutated and sensitized to specific inhibitors. This specific inhibition still led to Akt hyperphosphorylation, implying that the paradoxical phosphorylation was drug-binding induced. The current model explaining this phenomenon involves conformational changes beyond the site of drug binding. These changes could increase the ease of Akt phosphorylation by PDK1 and mTORC2 by modulating the PH

domain affinity for the membrane PIP3 such as to increase the rate of localization. As well, the adopted conformations could decrease Akt susceptibility to phosphatases, thereby decreasing the rate of dephosphorylation (Okuzumi et al, 2009). Termed "Akt activation hijacking", small-molecule inhibitors could impart conformational changes such as to overcome the catalytic inhibition they display *in vitro*, resulting in net activation of the targeted kinase population.

Example 3: RAF kinases participate in a kinase cascade that ultimately leads to a wide array of growth factor signaling via ERK (Wemmer and Baccarini, 2010). Following activation of growth factor receptors, Ras proteins exchange GTP for GDP, recruiting and activating RAF by elusive mechanisms. RAF then primes itself for catalysis through dimerization, in which one protomer allosterically alters the conformation of the other. Active RAF phosphorylates MEK, and MEK phosphorylates ERK. Although the V600E mutant form of the BRAF isozyme has been intensively targeted for its heavy involvement in carcinogenesis (Niault and Baccarini, 2010), efforts have been marred by reports of paradoxical MEK/ERK activation despite treatment with *in vitro* BRAF-specific inhibitors (Tse and Verkhivker, 2016). It was initially hypothesized that Type I½ inhibitors would have more specificity to RAFs since inactive (αC helix-out) kinases are more structurally divergent than their active forms (Roskoski 2019). However, X-ray co-crystal structures of BRAF with its Type I½ inhibitors PLX4720, Dabrafenib, and Vemurafenib have shown that these ATP-competitive small-molecules promote the homodimerization and heterodimerization of BRAFs and CRAFs. This dimerization induction is accompanied with negative cooperativity effects, in which the binding of an inhibitor to one protomer discourages the binding of another inhibitor to the other protomer (Tse and Verkhivker, 2016). The drug-induced dimerization is also believed to promote the formation of BRAF R- and C-spines. As a result, partial inhibition of RAF dimers is thought to lead to hyper-transactivation of the unbound protomer, causing net activation of RAF signaling. Indeed, engineered mutations to the CRAF dimerization interface abrogate paradoxical CRAF activation (Poulikakos et al, 2010). As well, molecular dynamics (MD) simulations of drug-binding dimerization induction support a model in which the ability of a compound to promote dimerization is correlated with RAF paradoxical activation (Tse and Verkhivker, 2016). This model is also supported by dose-response studies with respect to MEK phosphorylation which trace a bell-shaped curve: inhibition is achieved at low doses, but at intermediate doses, paradoxical activation leads to increased MEK phosphorylation

(Dar and Shokat, 2011). At high doses, RAF signaling inhibition is achieved by full inhibitor saturation of RAF dimers.

1.5. Hypothesis: PINK1 can be paradoxically activated

Thus, despite some catalytic inhibition, these paradoxical activators cause conformation changes that result in net kinase activation through promotion of oligomerization, subcellular localization, and dimer hyperactivation. In many of these cases, there exists a dose window in which this paradoxical activation overcomes the catalytic inhibition, and we believe that this can be exploited to intentionally activate PINK1 to bolster incompetent MQC for PD treatment. Indeed, other avenues for PINK1 activation are scarce. The only PINK1 binding pockets are the ATP binding site and the Ub/Ubl binding interface (Kumar et al, 2017; Schubert et al, 2018; Okatsu et al, 2018). Targeting the Ub/Ubl interface is difficult because of its large area and because interfering with the region might negatively affect normal substrate binding. The ATP binding site therefore constitutes the only druggable area for pharmacological efforts. Although all ATP binding site interactors have been designed to inhibit kinases, the discovery of paradoxical kinase activation provides a novel strategy to positively modulate PINK1. Such a project would be the first to attempt intentional paradoxical kinase activation, as well as the first to attempt pharmacological activation of PINK1 for PD treatment. In doing so, we will deepen our understanding of paradoxical kinase activation, providing new insights on how to evade it in cancer while opening new doors for kinase activation.

1.6. Research objectives

Hence, the goal of this project was to use an ATP-competitive small-molecule kinase inhibitor to paradoxically activate PINK1. This goal was pursued by first screening a library of known small-molecule kinase inhibitors against recombinantly expressed TcPINK1 to search for thermal stabilizers, as a proxy for their ability to impart a conformational change that may be necessary for paradoxical activation in cells. The most potent thermal stabilizers were then characterized *in vitro* in order to assess their effects on TcPINK1 and HsPINK1 auto- and substrate phosphorylation, and in mammalian cell lines to gauge their effect on MQC. *In silico* docking simulations were also performed to predict binding interactions between the compounds and PINK1, and collaborations with medicinal chemistry groups have been established to synthesize and test analogs of the most promising molecules.

We discovered several TcPINK1 thermal stabilizers that were able to increase the TcPINK1 melting temperature (T_m) by up to roughly 5°C. Two of the top six thermal stabilizers (CYC116 and PRT062607) were shown by *in vitro* phosphorylation assays to be bona fide TcPINK1 autophosphorylation and substrate phosphorylation inhibitors with IC_{50}s of roughly 28.09 μM and 18.02 μM, respectively. NMR experiments demonstrated that these inhibitors are directly inhibiting ATP hydrolysis, and *in silico* simulations predicted that they are Type I inhibitors. Treatment of mammalian cell lines with the strongest inhibitor, PRT062607, inhibited pUb production in the context of CCCP treatment. However, high concentrations of PRT062607 increased CCCP-induced mitophagy in Parkin-overexpressing U2OS cells. This manuscript therefore reports that PRT062607 was discovered to be an inhibitor of both TcPINK1 and HsPINK1, and preliminary studies in cells suggest that it may act as paradoxical mitophagy activator under specific conditions. Chemical derivatives of PRT062607 are currently being synthesized in order to increase its potency and selectivity.

2. Methods

2.1. Thermal Shift Assay screening (performed by Nathalie Croteau)

TcPINK1 D337N (kinase dead TcPINK1, or "TcPINK1 KD") previously purified by Shafqat Rasool and donated to Nathalie Croteau was used for the Thermal Shift Assay screening. Each of the 430 compounds from a SelleckChem Kinase Inhibitor Library were combined at 100 μM in wells of a polypropylene 96-Well Tube Plates (Agilent) with TcPINK1 KD at 0.5 mg/mL (approximately 10 μM) and SYPRO Orange Protein Gel Stain 5,000X (Thermo Fisher Scientific) at 6X in a 300 mM NaCl, 20 mM Tris-HCl pH 8, 5 mM DTT, 5% DMSO buffer. The reaction mixtures were heated from 10°C to 70°C for approximately 1 hr by a QuantStudio 7 Pro Real-Time PCR System (Thermo Fisher Scientific). Approximately 770 evenly spaced measurements of fluorescence against the temperature gradient were recorded and processed by QuantStudio V1.3 (Thermo Fisher Scientific), and then further analyzed by Protein Thermal Shift Software v1.3 (Thermo Fisher Scientific). Thermal shift (ΔT_m) was calculated by subtracting the TcPINK1 KD T_m in the presence of a compound to the plate- and column-specific buffer control.

2.2. Protein expression and purification of Ub and Ubl

Full length Ub and Ubl N-terminally tagged with Glutathione S-Transferase (GST) were recombinantly expressed from BL21 DE3 *E. coli* for *in vitro* assays using the same purification protocol. 20 μL of homemade BL21 DE3 *E. coli* were transformed with approximately 50 ng of either GST-Ub or GST-Ubl in pGEX6p1 vectors **(Figures 6, 7)** following the standard transformation protocol by the New England Biolabs (NEB). A small frozen piece of a 50% glycerol stock of the successfully transformed BL21 cells was used to inoculate a 5 mL starter culture at 37°C, 170 rpm in autoclaved LB with 0.1 mg/mL ampicillin. 5mL of the starter culture was then used to inoculate 1 L of autoclaved LB with 0.1 mg/mL ampicillin and the cultures were grown at 37°C, 170 rpm until OD_{600} reached 1.0. 300 μM isopropyl-β-D-1-thiogalactopyranoside (IPTG; Bio Basic Canada Inc.) was added to the cultures for 16°C, 170 rpm overnight induction of GST-Ub/Ubl expression. The following day, cells were pelleted by low-speed centrifugation (approximately 2,000 g). Cell pellets were resuspended in a bacterial lysis buffer (0.025 mg/mL DNAse (Bio Basic Canada Inc.); 5 mM $MgSO_4$ (Fisher Scientific); 1 mM DTT (Fisher

BioReagents); 1 mM PMSF (Roche); 0.1 mg/mL lysozyme (Bio Basic Canada Inc.); 0.5% Tween 20 (Fischer BioReagents); in 100 mM NaCl, 50 mM Tris-HCl pH 7.4, 3 mM DTT, hereon referred to as "Ub/Ubl buffer"). The resuspended pellets were vortexed, and then sonicated on ice at 6.0 W for 20 s for 8 cycles. Total lysates were centrifuged at high speed for clarification (approximately 17,600 g). Clarified lysates (i.e. the supernatants) were incubated with 1.5 mL glutathione-Sepharose beads (GE Healthcare Life Sciences) in Ub/Ubl buffer at 4°C for 3 hr, and then passed through gravity columns to allow non-GST proteins in the clarified lysates to flow-through. GST-Ub/Ubl was eluted using a Ub/Ubl buffer with 20 mM glutathione (Bio Basic Canada Inc.), and concentrated by centrifugation using 3,000 Da Centrifugal Filter Units (Millipore). For cleavage of GST, 5 to 10 µg of HRV-3C (recombinantly expressed by Nathalie Croteau) was added to concentrated GST-Ub/Ubl for an overnight reaction at 4°C. Free GST and HRV-3C were separated from Ub/Ubl by size-exclusion chromatography (SEC) with a HiLoad Superdex 75 10/300 GL (GE Healthcare Life Sciences) connected to an AKTA Pure chromatography system (GE Healthcare Life Sciences) over an elution volume of 105 mL. Chromatography results were processed and analyzed by UNICORN 6 (GE Healthcare Life Sciences). Fractions containing Ub/Ubl were pooled and concentrated using 3,000 Da Centrifugal Filter Units. Final protein concentrations were taken both before storing at -80°C and upon thawing for reactions by a Denovix DS-11 spectrophotometer using nanodrop absorption at 280 nm with theoretical extinction coefficients and molar masses calculated by Uniprot.

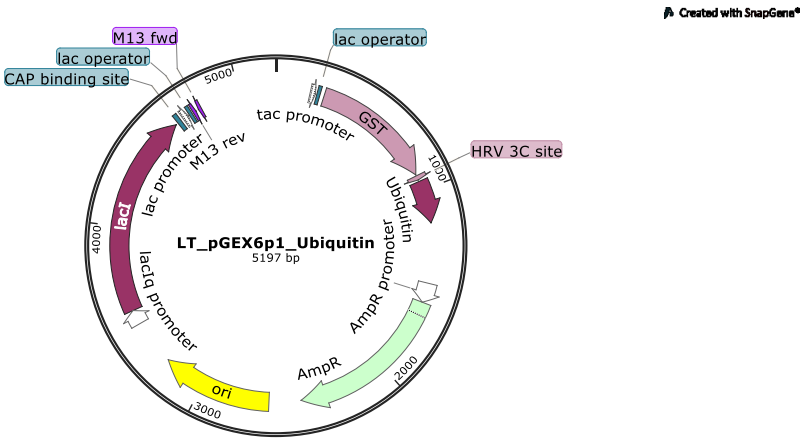

Figure 6: pGEX6p1 vector containing GST-Ub in the Multiple Cloning Site. An HRV-3C cleavage site was engineered between the GST tag and Ub.

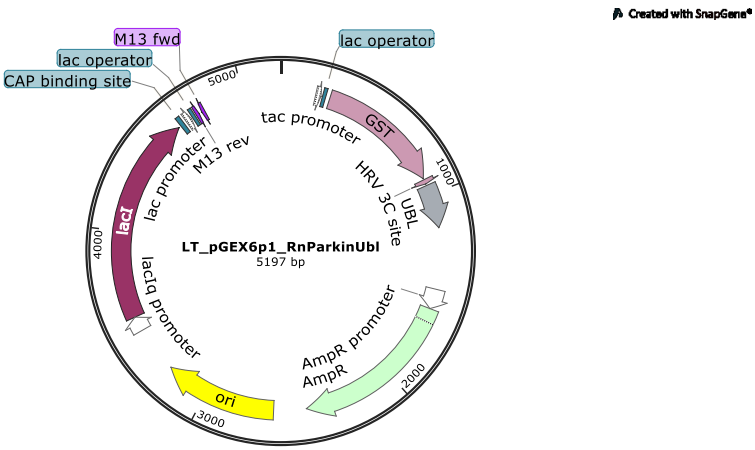

Figure 7: pGEX6p1 vector containing GST-Ubl in the Multiple Cloning Site. An HRV-3C cleavage site was engineered between the GST tag and Ub.

2.3. Protein expression and purification of ^{15}N-TcPINK1

Approximately 50 ng of GST-TcPINK1 (121-570) in a pGEX6p1 vector **(Figure 8)** was used to transform 20 µL of BL21 DE3 *E. coli* as per NEB protocol. A small frozen piece of a 50% glycerol stock of the successfully transformed BL21 cells was used to inoculate a 5 mL starter culture grown at 37°C, 170 rpm in autoclaved LB with 0.1 mg/mL ampicillin. The starter culture was centrifuged to pellet down the cells, and the cell pellet was resuspended in 3 mL of autoclaved 1X M9 minimal medium (42.2 mM Na_2HPO_4 (Fisher Scientific), 22.0 mM KH_2PO_4 (Fisher Scientific), 8.56 mM NaCl). 1 L of 1X M9 minimal medium with 0.1 mg/mL ampicillin was inoculated with these 3 mL of resuspended cells, in addition to final concentrations of the following: 20% w/v D-glucose (Sigma-Aldrich); 20% w/v $^{15}NH_4Cl$ (Sigma-Aldrich); 1.0 M $MgSO_4$ (Fisher Scientific); 0.1 M $CaCl_2$ (Fisher Scientific); 0.5% w/v thiamine (Sigma-Aldrich); 0.01 M $FeSO_4$ (Sigma-Aldrich); and 0.01 M $ZnCl_2$ (Fisher Scientific). The culture was grown at 37°C at 170 rpm until OD_{600} reached 1.5. 100 µM IPTG was added to the cultures for 16°C, 170 rpm overnight induction of ^{15}N-GST-TcPINK1 expression. The following day, cells were pelleted by low-speed centrifugation (approximately 2,000 g). Cell pellets were resuspended in a bacterial lysis buffer (0.025 mg/mL DNAse; 5 mM $MgSO_4$; 1 mM DTT; 1 mM PMSF; 0.1 mg/mL lysozyme; 0.5% Tween 20; in 300 mM NaCl, 50 mM Tris-HCl pH 8, 2 mM DTT, hereon referred to as "PINK1 buffer"). The remainder of the purification is identical to the Ub/Ubl protocol up

until protein concentration. 10,000 Da Centrifugal Filter Units (Millipore) were used to concentrate ^{15}N-GST-TcPINK1. For cleavage of GST, 5 to 10 µg of HRV-3C (recombinantly expressed by Nathalie Croteau) was added to concentrated ^{15}N-GST-TcPINK1 for an overnight reaction at 4°C. Free GST and HRV-3C were separated from ^{15}N-TcPINK1 by SEC with a Superdex 200 Increase 10/300 GL (GE Healthcare Life Sciences) and a GSTrap HP Column (GE Healthcare Life Sciences) connected to an AKTA Pure chromatography system over an elution volume of 105 mL. Chromatography data was processed and analyzed by UNICORN 6. Fractions containing ^{15}N-TcPINK1 were pooled and concentrated by 10,000 Da Centrifugal Filter Units. Final protein concentrations were taken both before storing at -80°C and upon thawing for reactions in the same way as was performed for Ub/Ubl.

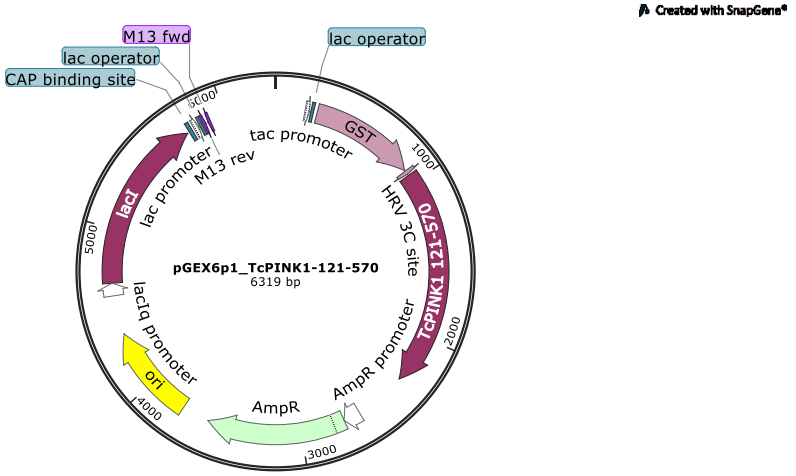

Figure 8: pGEX6p1 vector containing GST-TcPINK1 (121-570) in the Multiple Cloning Site. An HRV-3C cleavage site was engineered between the GST tag and Ub.

2.4. Dephosphorylation of ^{15}N-TcPINK1 and CIP separation

Purified and concentrated ^{15}N-TcPINK1 at roughly 5 mg/mL was dephosphorylation by addition of excess (approximately 500 units) of CIP (Alkaline Phosphatase, Calf Intestinal; NEB) treatment at 30°C for 30 min. The reaction was spun down by high-speed centrifugation (16,000 g) to pellet precipitated protein and the supernatant was purified by anion exchange chromatography using a Mono Q anion exchange chromatography 5/50 GL column (GE Healthcare Life Sciences) and a 0

to 500 mM NaCl salt gradient over 20 mL. Dephosphorylation of ^{15}N-TcPINK1 was confirmed by intact protein MS using a Bruker Impact II ESI-QTOF, as described in this section. Hereon, it is implied that all ^{15}N-TcPINK1 was dephosphorylated by and separated from CIP.

2.5. Intact protein MS (adapted from Trempe et al, 2016)

Proteins in question were diluted to 0.1 mg/mL in 0.05% TFA and 2% acetonitrile (ACN) and 20 µL was injected on a Dionex C4 Acclaim 1.0/15 mm column followed by a 10 minute 4-50% gradient of ACN in 0.1% formic acid with a flow rate of 40 µL/min. The eluate was analyzed on a Bruker Impact II Q-TOF mass spectrometer equipped with an Apollo II ion funnel ESI source. The multiply charged ions were deconvoluted at 10,000 resolution to yield the isotopically-resolved mass spectra. Peak assignment was performed using the SNAP algorithm, which takes into account natural abundance isotope distribution to assign monoisotopic mass.

2.6. Kinase inhibition assays

5 µM ^{15}N-TcPINK1 was combined with 50 µM Ub or Ubl, 100 µM compound of interest, 1 mM ATP, 2 mM $MgSO_4$ in 150 mM NaCl, 50 mM Tris-HCl pH 7.5, 1 mM DTT, 2% DMSO at 30°C for 2 min for Ub phosphorylation reactions, and 1 min for Ubl phosphorylation reactions (unless otherwise specified). Reactions were stopped by addition of a final concentration of 1X Laemmli buffer (2% SDS, 0.1% bromophenol blue (Sigma-Aldrich), 10% glycerol, 100 mM DTT), followed by boiling at 85°C for 5 min. 14 µL of the stopped reactions were loaded into a Tris-Tricine gel (1 M Tris-HCl pH 8.45, 15% acrylamide, 0.1% SDS, 0.1% APS, 0.04% TEMED) doped with 20 µM Phostag (APExBIO) and 40 µM $ZnSO_4$ (Fisher Scientific). The gels were run at 140 V for approximately 1 hr with cathode buffer (100 mM Tris-HCl pH 8.25, 100 mM Tricine, 0.1% SDS) inside the gasket and anode buffer (1 M Tris-HCl pH 8.9) outside the gasket.

2.7. Gel staining and Coomassie/Western Blot band quantification

Poly-acrylamide gels were stained overnight using 0.125% w/v Coomassie G250 (Bio Basic Canada Inc.) in 45% methanol, 10% acetic acid. Gels were then destained using 25% methanol,

0.75% acetic acid for at least 24 hr or until the gel background was as translucent as possible. Band intensities for destained poly-acrylamide gels and immunoblot membranes were quantified using ImageJ. A rectangle drawn to fit the bands of interest with minimal inclusion of background were used to record integrated density values. Background integrated density was systematically subtracted from these recorded values. Non-linear regression (least squares curve fit) of the small molecule concentrations versus response was calculated using GraphPad Prism 7.

2.8. Transphosphorylation inhibition assays

5 μM ^{15}N-TcPINK1 was combined with 5 μM TcPINK1 D337N, 100 μM compound of interest, 1 mM ATP, 2 mM $MgSO_4$ in TcPINK1 buffer with 2% DMSO at 30°C for transphosphorylation reactions with timepoints of 0 s, 30 s, 60 s, and 120 s. Timepoint reactions were stopped by addition of 0.05% TFA and 2% ACN (final concentrations). Reactions were analyzed by intact protein MS using the ESI-QTOF, as previously described.

2.9. ^{1}H-^{13}C HSQC-NMR of ATP

1 μM ^{15}N-TcPINK1 was combined with 100 μM ^{13}C-ATP (Sigma-Aldrich), 0.1 mM compound of interest, 500 μM $MgSO_4$, 5% D_2O (Sigma-Aldrich), and 5% DMSO in TcPINK1 buffer. For the ADP control, knowing that the natural abundance of ^{13}C is 1.1%, 1 μM ^{15}N-TcPINK1 was combined with 10 mM ADP (Sigma-Aldrich) in the same buffer in order to re-create a ^{13}C signal equivalent to 100 μM ^{13}C-ADP. 20 Standard 2D ^{1}H-^{13}C correlation HSQC (Heteronuclear single quantum coherence)-NMR spectra via double inept transfer using sensitivity improvements (Palmer et al, 1991; Kay et al, 1992; Schleucher et al, 1994) was acquired at 298K every 5 minutes for approximately 1.5 hr on a 600 MHz Bruker Avance spectrometer equipped with a triple resonance (^{15}N/^{13}C/^{1}H) cryoprobe. The spectrum was acquired with a carrier frequency of 600.3328216 MHz (4.7 ppm) for F2 (^{1}H) and 150.9697038 MHz (110 ppm) for F1 (^{13}C); a sweep width of 13.0136 ppm for F2 (^{1}H) and 36.0000 ppm for F1 (^{13}C); 42 increments; 16 dummy scans; and 2 scans. Spectra were processed using TopSpin 4.0.6 (Bruker).

2.10. Homology modeling of HsPINK1

Homology modeling of HsPINK1 was computed by MOE 2018.01 (Chemical Computing Group). The HsPINK1 (112-581) sequence was modeled using TcPINK1^{DDEE} (PDB: 5yj9) as a template. Outgaps were not modeled but disulfide bonds were automatically detected. 10 models were generated with 1 sidechain sample at 300K. The level of intermediate model refinement was Medium with an RMS gradient of 1. The final scoring was based on the Generalized Born/Volume Integral (GB/VI) methodology. The level of final model refinement was Medium with an RMS gradient of 0.5. The final model was protonated prior to refining. The homology modeling of HsPINK1 produced a construct spanning residues 147-581. Algorithm details and references supporting models can be found in the MOE User Guide.

2.11. Molecular docking simulations

Docking simulations were computed by MOE 2018.01. The ligands were modeled based on two PDB files: 2uue, a crystal structure of Cyclin-dependent kinase 2 bound to CYC116, and 5ut2, a crystal structure of Janus kinase 2 bound to PRT062607. 2uue, 5ut2, and the TcPINK1^{DDEE} structure (PDB: 5yj9) underwent a "QuickPrep" operation. Within the QuickPrep operation, structures were prepared, their sequences were preserved and neutralized, sidechains were protonated, and charged sidechains were allowed to flip upon protonation. QuickPrepped 2uue, 5ut2, and 5yj9 were then aligned and superimposed. After superposition, all objects within the ligand-containing crystal structures were inactivated except for the ligand of interest (CYC116 or PRT062607). An "F1 Acc" (hydrogen-bond acceptor) pharmacophore was defined as the center of the AMP-PNP adenine N7 nitrogen which putatively makes hydrogen-bond interactions with the kinase hinge. The general-type docking between the ligand (CYC116 or PRT062607) and TcPINK1^{DDEE} within the AMP-PNP binding site was then computed. The placement method was set to Pharmacophore with the scoring set to London dG, generating 30 poses. The refinement method was set to either Rigid Receptor or Induced Fit (data not shown in this thesis) with the scoring set to GBVI/WSA dG, generating 5 poses. These 5 top-scoring conformers were saved, and those which formed contacts with the kinase hinge are shown, superimposed, in **Figures 27 and 29**. This process was repeated with the previously computed HsPINK1 model, and the

conformers which formed contacts with the kinase hinge are shown, superimposed, in **Figures 28 and 30**. Algorithm details and references supporting models can be found in the MOE User Guide.

2.12. HeLa and U2OS cell culture

Frozen stocks of HeLa, U2OS, and U2OS PINK1 KO cells in 90% FBS (Fetal Bovine Serum; Invitrogen) and 10% DMSO were generously gifted by Yang (Sophie) Lu. Stocks were rapidly (<1 min) thawed by water bath and seeded in 10 cm cell culture dishes (TC Dishes 100, Standard; Sarstedt) with pre-warmed 10 mL DMEM (Dulbecco's Modified Eagle Medium; Invitrogen) with 10% FBS and 1% pen/strep (hereon referred to as "DMEM" unless otherwise specified). Cells were grown in a Napco 6000 Water-Jacketed CO2 Incubator, with replacement of old media with fresh DMEM every 3 days or passaging when reaching high confluency (>85%). Passaging was done by washing twice with 7 mL pre-warmed PBS (Phosphate Buffer Solution; Invitrogen), followed by treatment with 2 mL Trypsin-EDTA (Invitrogen). Trypsinization was quenched by adding 7 mL DMEM and cells were spun down at 1200 rpm for 3 min. Cell pellets were resuspended with 10 mL DMEM and 1 mL was used to seed a new 10 cm cell culture dish containing 9 mL DMEM.

2.13. Mitochondrial extraction from HeLa cells (Adapted from Tang et al, 2017)

HeLa cells grown to high confluency (>85%) on 10 cm or 15 cm cell culture plates were treated with DMSO (Sigma-Aldrich) or CCCP (Sigma-Aldrich) to a final concentration of 10 μM and left in the CO2 cell incubators for 3 hours. Cells were then washed twice with 10 or 20 mL mitochondrial isolation buffer (20 mM HEPES (with pH 7.4 by incremental addition of KOH), 220 mM mannitol (Fisher Scientific), 70 mM sucrose (Fisher Scientific), 10 mM Potassium acetate; hereon referred to as "MIB"). Cells were harvested in a volume of 2 mL of MIB and subjected to Nitrogen cavitation at 500 psi on ice for 5 min. Cells were then spun at 500 g for 5 min at 4°C. The supernatant was spun at 12,000 g for 15 min. The resulting pellet was resuspended in 1 mL MIB to wash, and spun again at 12,000 g for 15 min. The resulting pellet was resuspended in 200 μL MIB.

2.14. In organello assays

20 µL of HeLa mitochondria extracted by previously described methods were combined with 20 nM E1 activating enzyme, 100 nM His-UbcH7 E2 conjugation enzyme, 100 nM *Rattus norvegicus* Parkin (RnParkin; generously donated by Yang (Sophie) Lu), 5 µM Ub, 1 mM ATP, 50 µM TCEP in a total of 40 µL MIB with 2% DMSO or compounds in equal DMSO concentrations. Reactions were incubated at 37°C for 20 min and stopped using a final concentration of 1X Laemmli buffer (previously described). 14 µL of the reactions were loaded onto 15-well 4-20% Mini-PROTEAN TGX Precast Protein Gels (Bio-Rad) and run at 120 V for approximately 1 hr. Specific proteins were then detected and visualized by Western Blot as described later in this section.

2.15. Inhibitor assays in cells

Highly confluent (>85%) cells in 6-well cell culture plates were treated with either DMSO or compounds at various final concentrations (but equal DMSO concentrations) for 3 hr at 37°C in the CO2 cell incubator. The treatment was stopped by aspiration of the media and wells were washed twice with cold PBS. Cells were scraped off the bottom of the wells using a chopped pipette tip, transferred into Eppendorf tubes in 1 mL cold PBS, and spun down at 500 g. Cell pellets were resuspended in 100 µL cell lysis buffer (0.2% SDS, 1% Triton-X, 1% Halt Protease Cocktail 100X (Thermo Fisher Scientific), 1 crushed tablet per 10 mL buffer of PhosSTOP EASYpack (Roche), in 20 mM HEPES pH 7.5, 120 mM NaCl, 1 mM DTT; hereon referred to as “cell lysis buffer”) and spun down at 16,000 g for 40 min. The supernatant lysate was transferred to another Eppendorf tube and stored at -80°C until the day of Western Blotting, as described later in this section. Prior to Western Blotting, protein concentrations were measured by BCA assay (as per the Thermo Scientific Pierce™ BCA Protein Assay Kit protocol) in order to normalize loaded amounts of total protein to the least concentrated sample.

2.16. Western Blotting

Proteins were transferred onto Immuno-Blot PVDF membranes (Bio-Rad) from poly-acrylamide gels by a Mini Trans-Blot Cell set (Bio-Rad) at 250 mA for 90 min at 4°C. Area-wise consistent

transfer was confirmed by Ponceau-S (Bio Basic Canada Inc.) staining. Membranes were blocked with 5% BSA (Wisent Bioproducts) in PBS with 0.1% Tween 20 (PBS-T) for 1 hr at room temperature. Membranes were then cut to isolate particular molecular weight regions of interest and these sections were incubated overnight with primary antibodies against specific proteins diluted in PBS-T as follows: against PINK1, a rabbit monoclonal antibody (mAb; Cell Signaling #6946) diluted 1:2,000 in 5% BSA; against Parkin, a mouse mAb (Cell Signaling #4211P) diluted 1:40,000 in 3% BSA; against Mfn2, a rabbit mAb (Cell Signaling #9482) diluted 1:2,000 in 3% BSA; against VDAC, a rabbit mAb (Cell Signaling #4661) diluted 1:5000 in 3% BSA; against pUb, a rabbit mAb (Cell Signaling #62802) diluted 1:2,000 in 5% BSA. Membrane sections were washed three times with 5 to 10 mL PBS-T for a total of 30 min. Membrane sections were then incubated with secondary antibodies (mouse (Cell Signaling #7076P2) and rabbit (Cell Signaling #70745)) against corresponding primary antibodies at a 1:10,000 dilution in PBS-T with 3% BSA for 1 hr at room temperature. Membrane sections were washed three times with 5 to 10 mL of PBS-T for a total of 30 min again. Finally, membrane sections were incubated with Clarity Western ECL Blotting Substrates (peroxide solution and luminol/enhancer solution) and imaged by ImageQuant LAS 500 (GE Healthcare Life Sciences) in Chemiluminescence mode.

2.17. Mitophagy assays (performed by Mohamed Eldeeb)

Mitophagy was examined using a FACS-based analysis of mitochondrially targeted Keima (mKeima). This protocol is based on previously described procedure in Tang et al, 2017, and Wei et al, 2019. Briefly, U2OS cells stably expressing an ecdysone-inducible mKeima were induced with 10 μM ponasterone A. After 24 h, the cells that stably expressing wild-type GFP-Parkin were either left untreated or pretreated with PRT (1uM, 2uM or 10uM) for 2 hr then treated with 10 μM CCCP for 18 h. For FACS analysis, cells were trypsinized, washed and resuspended in PBS prior to their analysis on an LSR Fortessa (BD Bioscience) equipped with 405 and 561 nm lasers and 610/20 filters (Department of Microbiology and Immunology Flow Cytometry Facility, McGill University). Measurement of lysosomal mKeima was made using a dual excitation ratiometric pH measurement where pH 7 was detected through the excitation at 405 nm and pH 4 at 561 nm. For each sample, at least 20,000 events were collected, and single, GFP-Parkin-positive cells were subsequently gated for m-Keima. Data were analyzed using

FlowJo v10.1 (Tree Star). For statistical analysis, the data represent the average percentage of mitophagy from three independent experiments, and *P* values were determined by one-way ANOVA with Dunnett's post-hoc tests were performed. * $P<0.05$.

3. Research findings

3.1. Screening kinase inhibitors for TcPINK1 KD thermal stabilizers (performed by Nathalie Croteau)

A thermal shift assay was performed to screen 430 kinase inhibitors for thermal stabilizers as a proxy for their ability to impart a conformational change to PINK1. Despite their nature as ATP-competitive inhibitors, we hypothesized that the conformational changes inferred by thermal stabilization could compensate for catalytic inhibition and cause paradoxical PINK1 activation in cells. For this screen, catalytically inactive TcPINK1 D337N (TcPINK1 KD) was used as it is homogenously unphosphorylated, unlike TcPINK1 WT. Thus, thermal stabilizers were identified based on their ability to increase the melting temperature (T_m) of TcPINK1 KD. The screening strategy employed previously described methodologies (Lo et al, 2004), which rely on the fluorescence activity of SYPRO Orange. In solution, SYPRO orange fluoresces as it dissociates from the fluorescence-quenching water molecules and preferentially associates with hydrophobic protein cores. These cores are exposed when proteins are unfolded by gradually increasing the solution temperature using a qPCR machine. As such, the fluorescence continues to increase until proteins begin to aggregate. This deprives the dye of binding partners, ending the increase in fluorescence. The point at which the rate of fluorescence increase is maximal is considered to be the T_m of the protein. TcPINK1 KD T_m was compared to its T_m in the presence of each of the 430 kinase inhibitor library compounds. The top 4 thermal stabilizers were (in order of best to worst): CYC116, CYT387, VE822, and PRT062607 **(Table 1; Appendix Figures 1, 2, 3)**. All 4 of these compounds were selected for further characterization.

Compound added	Compound structure	TcPINK1 KD T_m	ΔT_m
CYC116 MW: 363.46	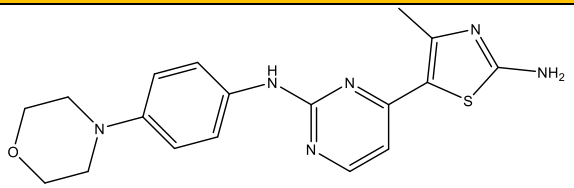	54.08°C	+5.17°C
CYT387 MW: 414.47	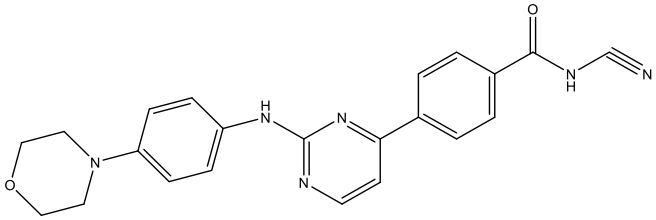	53.40°C	+4.49°C
VE822 MW: 463.55	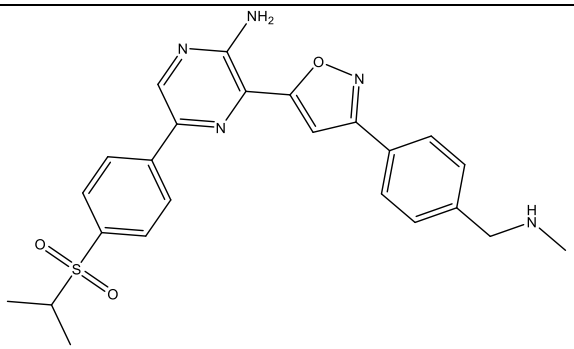	52.01°C	+3.88°C
PRT062607 MW: 393.45	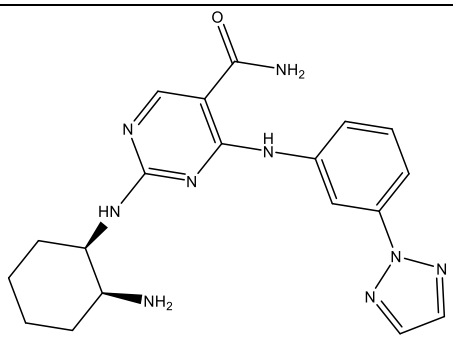	51.26°C	+2.38°C

Table 1: Summary of kinase inhibitor effects on thermal stability of TcPINK1. ΔT_m: difference in T_m between TcPINK1 KD in the presence and absence of the kinase inhibitor.

3.2. Heterologously expressing and purifying recombinant Ub and Ubl

As reagents for *in vitro* TcPINK1 kinase assays, Ub and Ubl were heterologously expressed in BL21 DE3 *E. coli* and purified using an N-terminal GST tag. The GST-tag was subsequently removed by treatment with HRV-3C which exploited an engineered cleavage site connecting GST to Ub (and Ubl). In this section, for purposes of succinctness, only data from the Ub purification are shown, as it is nearly identical to that of Ubl. Following incubation with glutathione-Sepharose beads, gravity column purification, HRV-3C cleavage, and SEC **(Figure 9)**, a 4-20% poly-acrylamide gel was run to confirm the purification of Ub **(Figure 10)**.

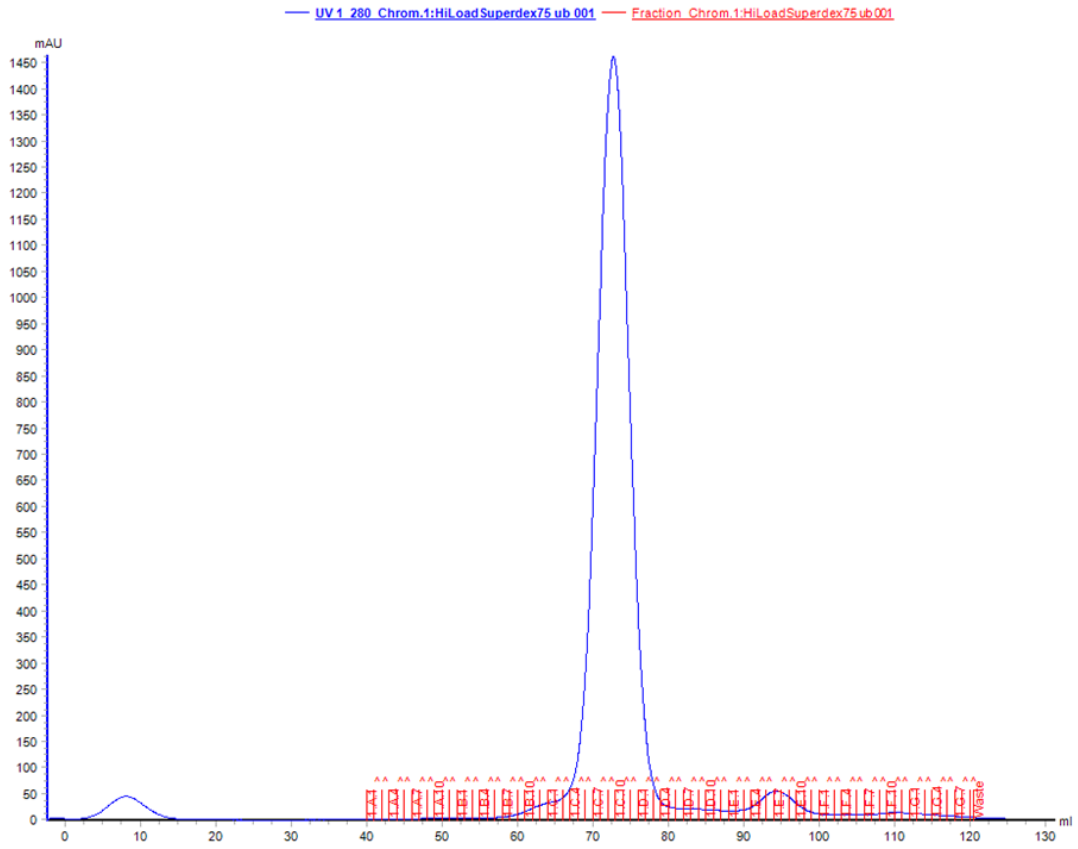

Figure 9: Ub is separated from GST and HRV-3C by SEC after HRV-3C cleavage. The SEC fractions and the elution volume are shown on the x axis, and the UV absorbance (280 nm) is shown on the y-axis. The 50 mAU peak at approximately 8 mL most likely corresponds to large protein aggregates eluting in the void volume of the column. The 1450 mAU peak at approximately 75 mL corresponds to monomeric GST (26 kDa). The 50 mAU peak at approximately 95 mL corresponds to Ub (9 kDa). mAU: milli-absorbance units.

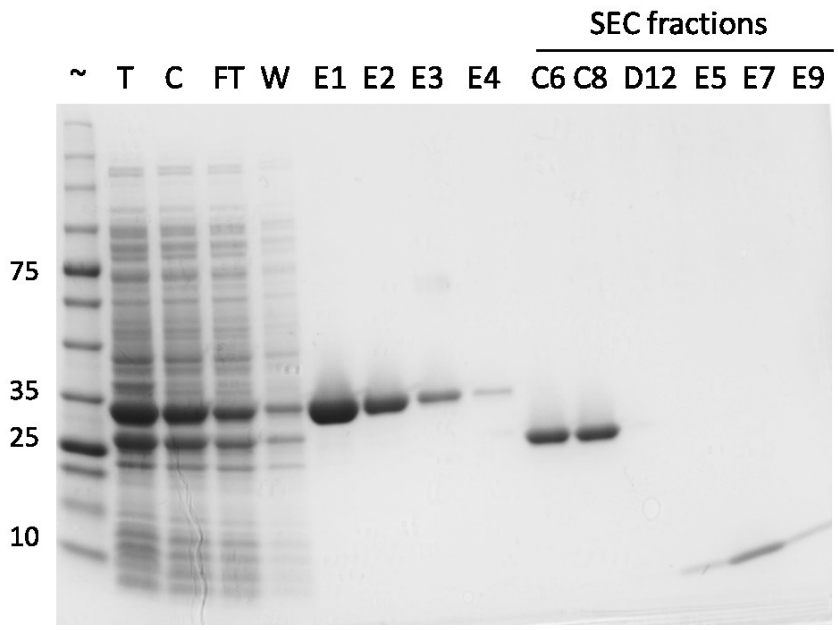

Figure 10: Ub is successfully purified. A Coomassie-stained diagnostic 4-20% poly-acrylamide gel was used to evaluate the quality of GST-Ub gravity column and subsequent SEC purification. The following volumes were loading in 1X Laemmli buffer: 0.7 µL of total lysate (T), clarified lysate (C), and clarified lysate flow-through (FT); 10 µL glutathione-Sepharose bead wash (W); 1 µL gravity column-eluted fractions 1, 2, 3, and 4 (E1, E2, E3, E4), and SEC fractions C6, C8, D12, E5, E7, and E9 **(see Figure 9)**. In T, C, FT, W, E1, E2, E3, and E4, the band situated at 35 kDa corresponds to GST-Ub. In the SEC fractions C6 and C8, the band situated at 25 kDa corresponds to GST monomer. In the SEC fractions E5, E7, E9, the band roughly situated at 10 kDa corresponds to cleaved Ub. ~: molecular weight marker, with relevant weights shown vertically in kDa.

3.3. Heterologously expressing and purifying recombinant ^{15}N-TcPINK1 and CIP-mediated dephosphorylation

As mentioned in the Introduction, it was not possible to recombinantly purify usable or active amounts of HsPINK1. Hence, we decided to purify its well-characterized insect ortholog, TcPINK1. A TcPINK1 construct spanning residue 121 to its C-terminus (denoted as "TcPINK1" unless otherwise specified) was recombinantly expressed in BL21 DE3 *E. coli* and purified using an N-terminal GST tag. Problematically, heterologously expressed TcPINK1 is

autophosphorylated up to 8 times **(Figure 11)** while HsPINK1 is autophosphorylated only at Ser228 and Ser402 (Ser205 and Ser375 in TcPINK1) (Okatsu et al, 2012). It was necessary to devise a strategy to decrease the number of non-physiological autophosphorylation events in TcPINK1. During transphosphorylation experiments requiring ^{15}N-labeled TcPINK1 (Rasool et al, 2018), we discovered that the minimal media necessary for ^{15}N incorporation reduced the number of autophosphorylations to a maximum of 4, and that the most abundant form of ^{15}N-TcPINK1 had 2 autophosphorylations **(Figure 12)**. Subsequent CIP treatment of ^{15}N-TcPINK1 reduced the number of autophosphorylations to a maximum of 2 with mono-autophosphorylated ^{15}N-TcPINK1 being the most abundant form **(Figure 12)**. By tryptic-digest LC-MS/MS, Thr530 autophosphorylation was discovered to be the remaining autophosphorylation site (data not shown). It is unclear what role (if any) Thr530 autophosphorylation plays in TcPINK1 activity, but its resistance to dephosphorylation is believed to be due to limited CIP phosphatase accessibility. Nonetheless, we settled with CIP-treated ^{15}N-TcPINK1 as our best approximation of HsPINK1 *in vitro*; consequently, it was used for all subsequent kinase assays. Our strategy was thus to treat SEC-purified ^{15}N-TcPINK1 **(Figures 13, 14, 15)** with CIP, and then remove the CIP by anion exchange chromatography **(Figure 16)**. The number of autophosphorylations was confirmed by intact protein MS **(Figures 12, 13)**.

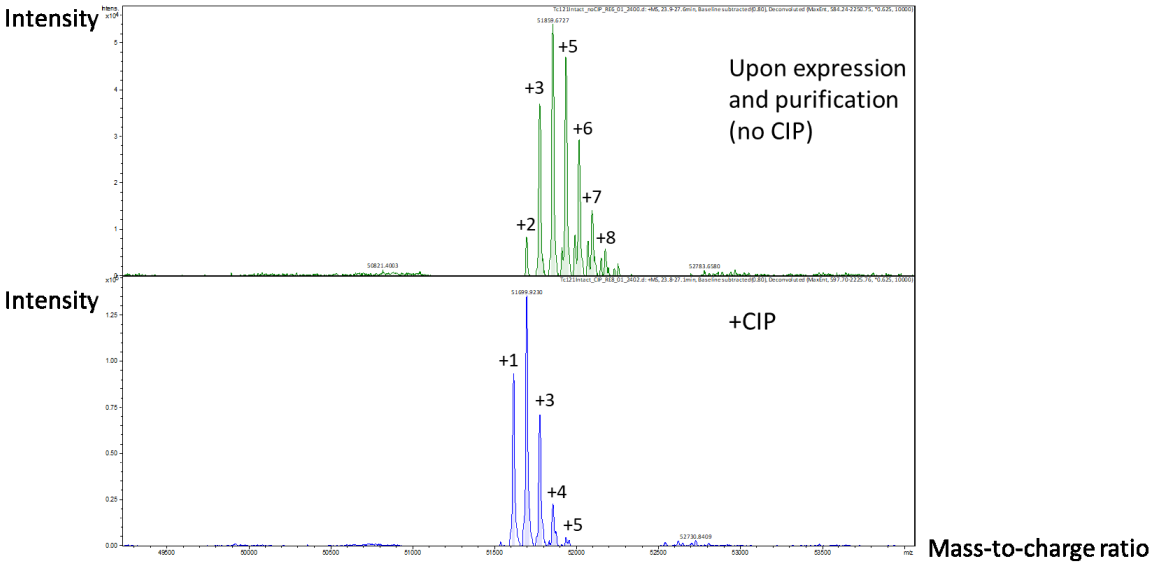

Figure 11: TcPINK1 is spuriously autophosphorylated when heterologously expressed in *E. coli*. Deconvoluted spectra (see Methods section for details) shows molecular mass on the x-axis and intensity on the y-axis. Regular ^{14}N-TcPINK1 bears at least 8 autophosphorylation phosphoryls (upper spectrum). Addition of CIP reduces this number to 5 (lower spectrum). +Numbers represent an additional 80 Da corresponding to covalent phosphoryl additions to TcPINK1.

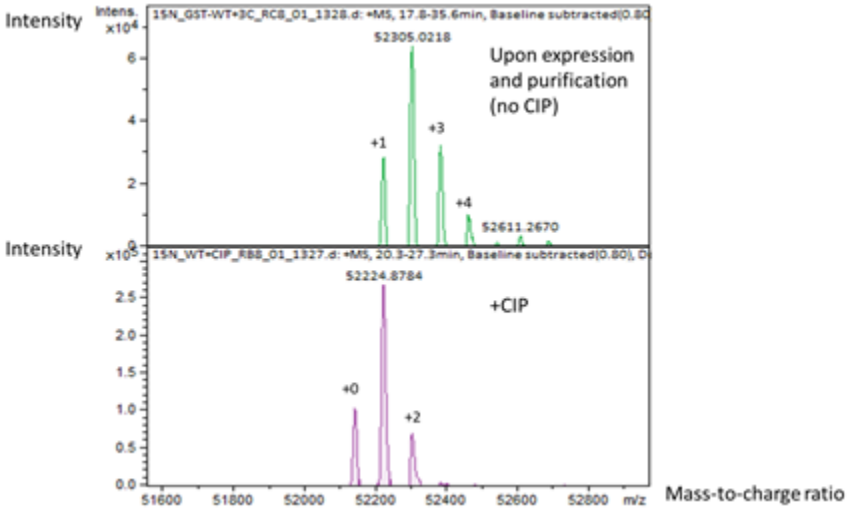

Figure 12: ^{15}N-TcPINK1 is less autophosphorylated than regular ^{14}N-TcPINK1. Deconvoluted spectra (see Methods section for details) shows molecular mass on the x-axis and

intensity on the y-axis. Expressed in minimal media, ^{15}N-TcPINK1 only bears a maximum of 4 autophosphorylation phosphates (upper spectrum). Addition of CIP reduces this number to 2 (lower spectrum). +Numbers represent an additional 80 Da corresponding to covalent phosphoryl additions to TcPINK1. Hereon, CIP-dephosphorylated ^{15}N-TcPINK1 will be referred to as simply "^{15}N-TcPINK1".

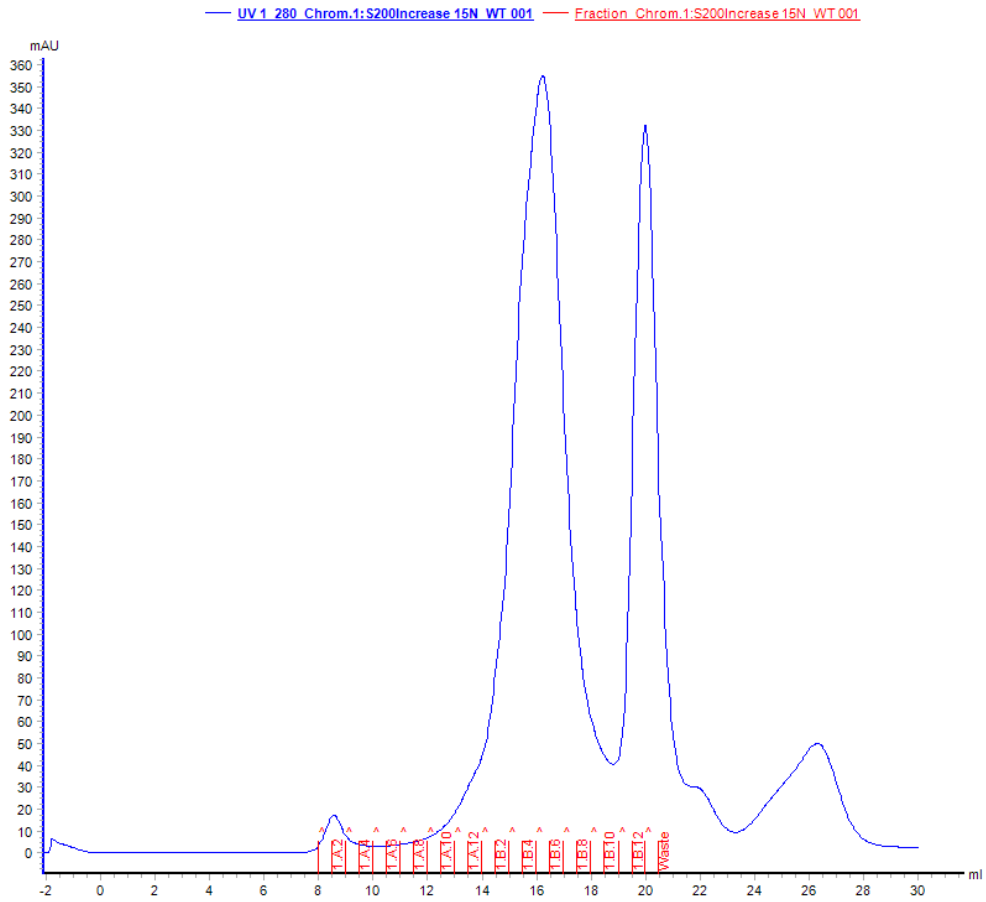

Figure 13: ^{15}N-TcPINK1 is separated from GST and HRV-3C by SEC after HRV-3C cleavage. The SEC fractions and the elution volume are shown along the x axis, and the UV absorbance (280 nm) is shown on the y-axis. The 350 mAU peak at approximately 16 mL corresponds to monomeric ^{15}N-TcPINK1 (52 kDa). The 330 mAU peak at approximately 20 mL corresponds to GST (bound by the GSTrap and eluted by glutathione flow-through). The 50 mAU peak at approximately 26 mL most likely corresponds to small protein fragments resulting from protein degradation. mAU: milli-absorbance units.

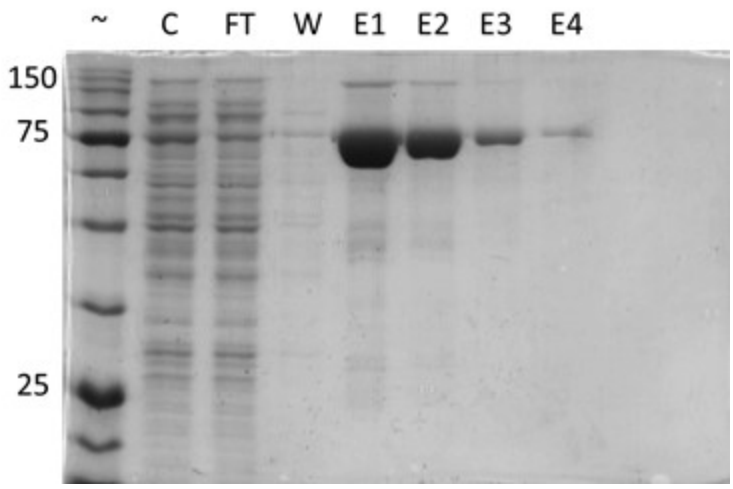

Figure 14: ^{15}N-GST-TcPINK1 is successfully purified. A Coomassie-stained diagnostic 12% poly-acrylamide gel was used to evaluate the quality of ^{15}N-GST-TcPINK1 purification. The following volumes were loaded in 1X Laemmli buffer: 0.7 µL of clarified lysate (C), and clarified lysate flow-through (FT); 10 µL glutathione-Sepharose bead wash (W); and 1 µL gravity column-eluted fractions 1, 2, 3, and 4 (E1, E2, E3, E4). In E1, E2, E3, and E4, the band at 75 kDa corresponds to ^{15}N-GST-TcPINK1. The faint band at around 150 kDa most likely corresponds to ^{15}N-TcPINK1 dimers. ~: molecular weight marker, with relevant weights shown vertically in kDa.

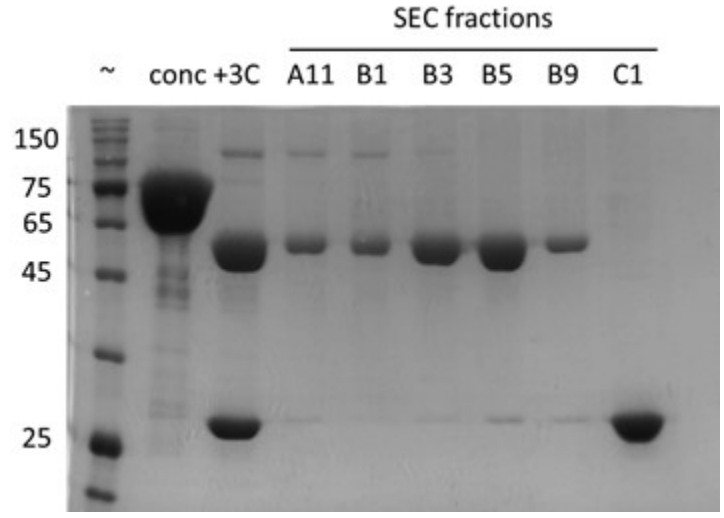

Figure 15: ^{15}N-TcPINK1 is successfully purified by SEC. A Coomassie-stained 12% poly-acrylamide gel was used to evaluate the quality of ^{15}N-TcPINK1 SEC purification **(Figure 13)**. The following volumes were loaded in 1X Laemmli buffer: 2 µL of gravity column-eluted and

10,000 Da Centrifugal Filter Unit-concentrated ^{15}N-GST-TcPINK1 (“conc”); 1 µL of the cleavage reaction between HRV-3C and ^{15}N-GST-TcPINK1 (“+3C”), and 1 µL of SEC fractions A11, B1, B3, B5, B9, and C1. The 75 kDa band in the “conc” lane corresponds to ^{15}N-GST-TcPINK1. In “+3C”, A11, B1, B3, B5, and B9, the band between 65 kDa and 45 kDa corresponds to cleaved ^{15}N-TcPINK1. In “+3C” and C1 the 25 kDa band corresponds to monomeric GST. ~: molecular weight marker with relevant weights shown vertically in kDa.

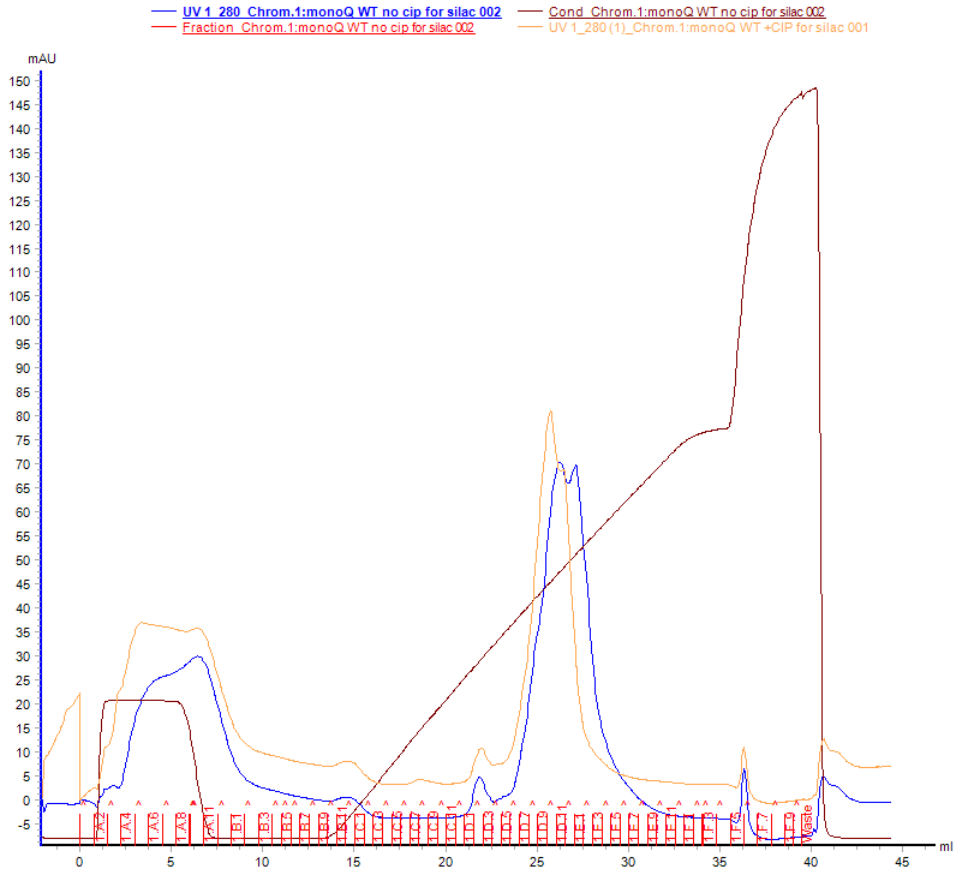

Figure 16: CIP is separated from ^{15}N-TcPINK1 by anion exchange chromatography. Elution volume and fractions are shown on the x-axis and UV absorbance (280 nm) is shown on the y-axis. This figure overlays chromatograms of ^{15}N-TcPINK1 with (orange trace) and without (blue trace) CIP. The orange trace is translated upwards from the baseline because of inaccurate zeroing of UV280 values by the chromatography system during that run. The brown trace corresponds to conductivity, showing the NaCl gradient used to elute ^{15}N-TcPINK1. The elongated 30 to 35 mAU UV trace peaks at approximately 2 to 7 mL correspond to UV-active peptides in the initial injection

that failed to bind the column. The 5 mAU UV trace peaks at approximately 15 mL most likely corresponds to CIP. The 75 mAU UV trace peaks at approximately 26 mL (eluting at 300 mM NaCl) correspond to ^{15}N-TcPINK1. Of note, the CIP-treated ^{15}N-TcPINK1 elutes earlier along the salt gradient because the CIP-mediated dephosphorylation decreases its overall charge.

3.4. Testing the thermal stabilizers in kinase assays

The effect of the thermal stabilizers VE822, CYC116, CYT387, and PRT062607 on ^{15}N-TcPINK1 substrate phosphorylation was assessed using Phostag gels. Foretinib served as a non-thermally stabilizing control **(Appendix Figure 4)**. Phostag gels are poly-acrylamide gels that incorporate Phostag, a divalent metallic cation-coordinating molecule. This Phostag-metal complex interacts with phosphate groups, causing a decrease in the rate of migration of phosphorylated proteins. Upon Coomassie staining, phosphorylated proteins are visualized as an upward shifted band compared to a non-phosphorylated control. Specifically, the intensity of the pUbl or pUb band produced during an *in vitro* reaction with ^{15}N-TcPINK1 was compared to that produced in the presence of the previously discovered thermal stabilizers (and Foretinib) **(Figures 17, 18, 19)**. These gels demonstrate that among the thermal stabilizers, CYC116 and PRT062607 are ^{15}N-TcPINK1 Ub and Ubl phosphorylation inhibitors. IC_{50} values were obtained by quantifying Ub phosphorylation against increasing concentrations of the inhibitors and performing a non-linear fit **(Figure 20)**. VE822, CYT387, and Foretinib have no detectable effect on ^{15}N-TcPINK1 Ub or Ubl phosphorylation.

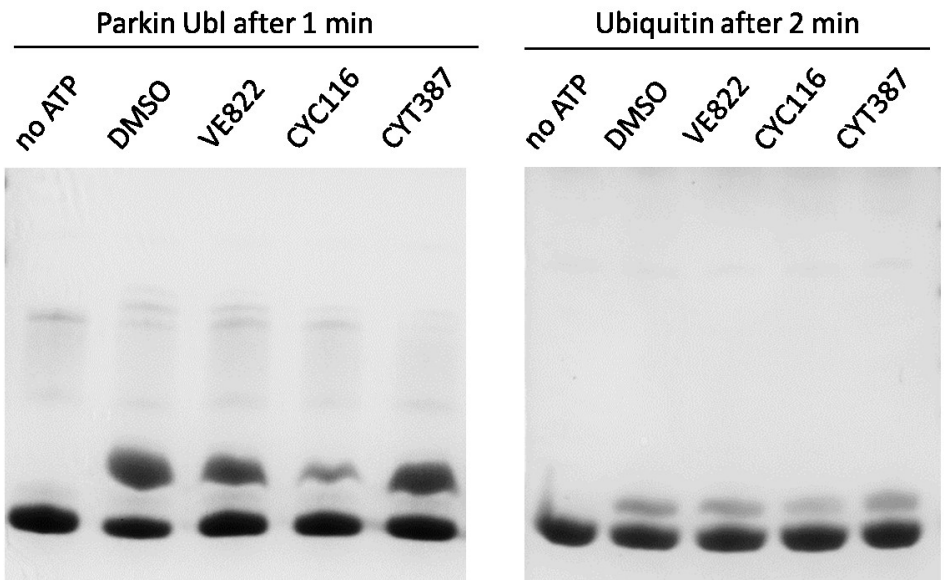

Figure 17: CYC116 inhibits ^{15}N-TcPINK1 Ubl and Ub phosphorylation. The first lane in both gels serves as a control for the location of the non-phosphorylated Ub band. Small molecules were tested at 100 μM in 2% DMSO. The decreased intensity of the upward-shifted pUbl and pUb bands in the CYC116 lane in both gels indicates a decreased rate of Ubl and Ub phosphorylation.

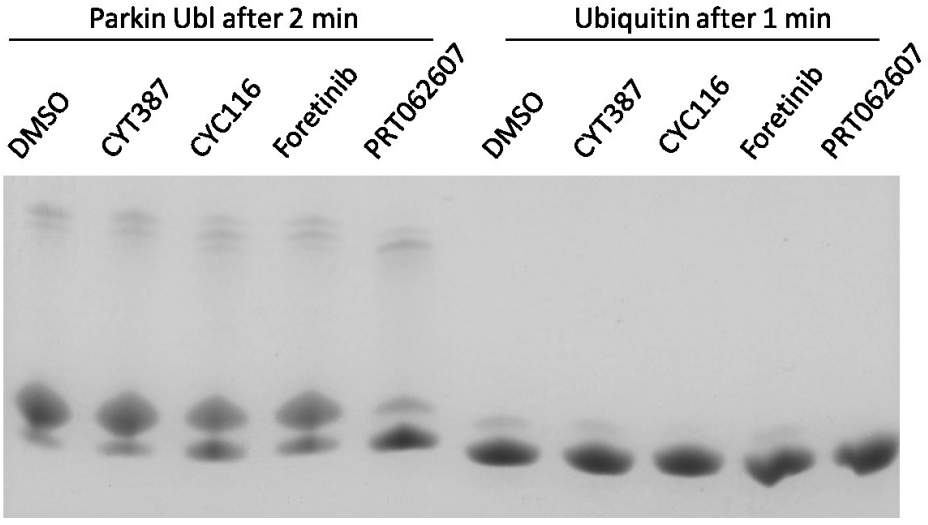

Figure 18: PRT062607 inhibits ^{15}N-TcPINK1 Ubl and Ub phosphorylation. Small molecules were tested at 100 μM in 2% DMSO. The decreased intensity of the upward-shifted pUbl and pUb band in the PRT062607 lane in both gels indicates a decreased rate of Ubl and Ub phosphorylation.

Equivalently, the more intense non-phosphorylated Ubl and Ub bands also indicate less phosphorylation. This is apparent in both the CYC116 and the PRT062607 lanes.

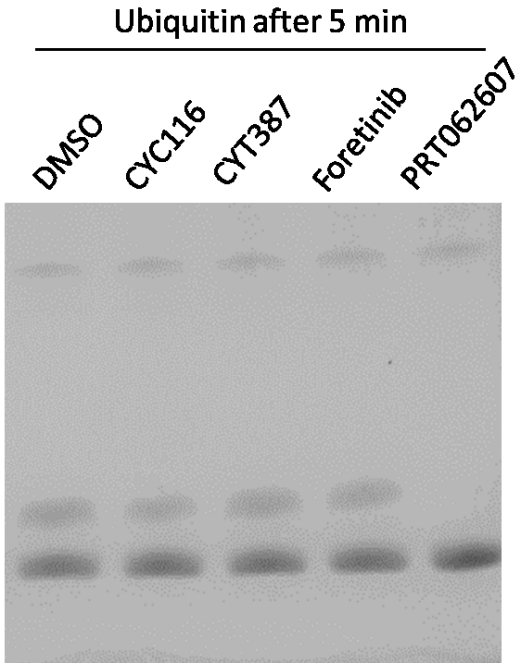

Figure 19: PRT062607 is a better ^{15}N-TcPINK1 Ub phosphorylation inhibitor than CYC116. Small molecules were tested at 100 μM in 2% DMSO. After 5 min, despite the presence of CYC116, ^{15}N-TcPINK1 manages to produce amounts of pUb that are comparable to the non-inhibiting thermal stabilizers and DMSO. However, ^{15}N-TcPINK1 still fails to phosphorylate Ub in the presence of PRT062607.

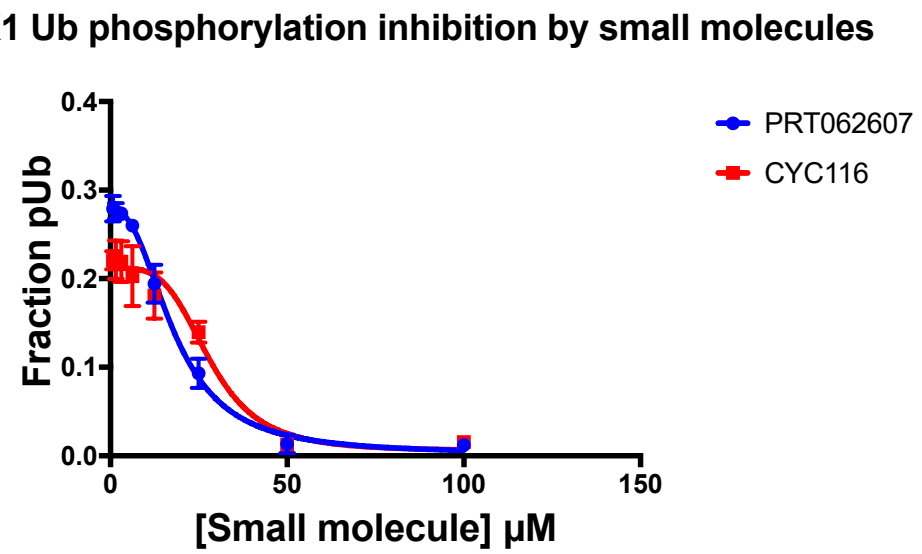

Figure 20: PRT062607 causes ^{15}N-TcPINK1 inhibition with a lower IC_{50} than CYC116. The quantified pUb based on Phostag gel band intensity were plotted against PRT062607 and CYC116 concentrations. Non-linear fit of inhibitor concentration vs. pUb levels indicates that PRT062607 has an IC_{50} of 18.02 ± 1.305 µM, while CYC116 has an IC_{50} of 28.09 ± 3.565 µM **(Appendix Figure 5)**. 2 biological replicates were performed. Error bars show ±SEM.

3.5. Testing the thermal stabilizers in transphosphorylation assays

As mentioned previously, PINK1 phosphorylates itself, and we showed that this autophosphorylation occurs in *trans*. To assess the effect of the thermal stabilizers on ^{15}N-TcPINK1 transphosphorylation, intact protein MS was used to monitor transphosphorylation of TcPINK1 KD by ^{15}N-TcPINK1. The conducted timecourses consisted of combining recombinantly expressed and purified ^{15}N-TcPINK1 and TcPINK1 KD. The latter construct bears no autophosphorylation phosphoryls upon heterologous expression and purification **(Figure 21)**; consequently, it was used as a monitor of PINK1 transphosphorylation, serving as a substrate for the active WT ^{15}N-TcPINK1. Additionally, since the WT TcPINK1 is ^{15}N-labelled, the mass spectra of the two constructs could be resolved following maximum entropy deconvolution **(Figure 21)**. These data show that CYC116 and PRT062607 are TcPINK1 transphosphorylation inhibitors. As well, despite their ability to confer thermal stability, CYT387 and VE822 do not

appear to affect TcPINK1 transphosphorylation activity. Foretinib, which did not affect TcPINK1 thermal stability, does not affect transphosphorylation activity either.

$$Fraction\ transphosphorylated = \frac{S/N_{TcPINK1\ KD\ mass+80}}{S/N_{TcPINK1\ KD\ mass+80} + S/N_{TcPINK1\ KD\ mass}}$$

Equation 1: Calculation of transphosphorylated TcPINK1 KD fraction. S/N symbolizes signal-to-noise ratio of the subscript protein's signal. This equation calculates the fraction of phosphorylated TcPINK1 KD to total TcPINK1 KD as measured by S/N by the MS.

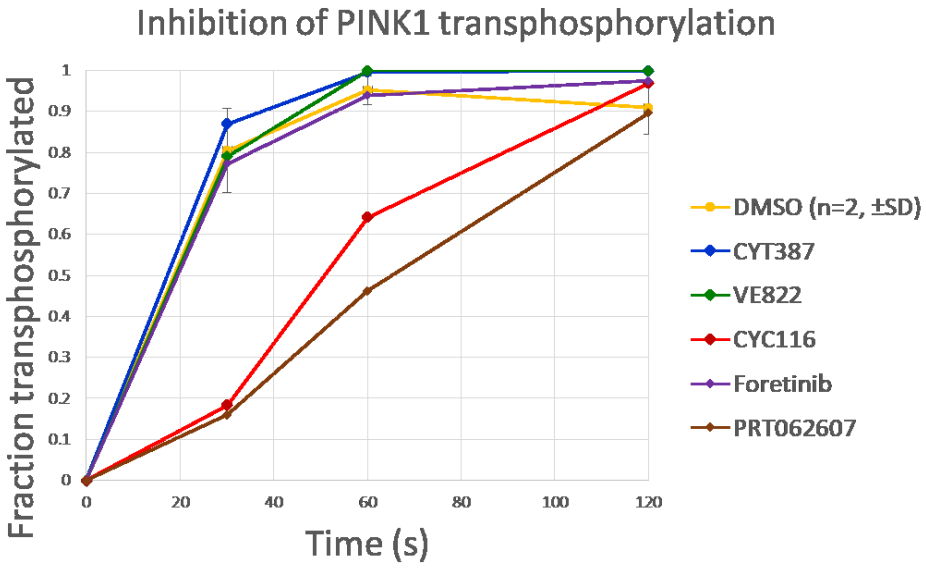

Figure 21: CYC116 and PRT062607 inhibit ^{15}N-TcPINK1 transphosphorylation of TcPINK1 KD. The fractions of transphosphorylated TcPINK1 KD were calculated by **Equation 1** and plotted against time points 0 s, 30 s, 60 s, and 120 s. The DMSO control was performed twice, and its average is plotted ±SD per time point.

3.6. Monitoring the effect of CYC116 and PRT062607 on TcPINK1 ATP hydrolysis by NMR

In order to assess the effect of the two inhibiting thermal stabilizers (CYC116 and PRT062607) on TcPINK1 ATP hydrolysis *in vitro*, we exploited the ability of ^{1}H-^{13}C HSQC NMR to monitor

the chemical environment surrounding ^{1}H-^{13}C bonds. Indeed, ^{13}C-ATP and ^{13}C-ADP ^{1}H-^{13}C HSQC NMR spectra differ in the coordinates of their cross-peaks (especially those corresponding to the 4' and 5' CH bonds; **Figures 22, 23**). This was employed to follow ATP hydrolysis into ADP by ^{15}N-TcPINK1. We had previously observed that TcPINK1 hydrolyzes ATP in the absence of substrate (data not shown), a phenomenon hereon referred to as "futile hydrolysis". As such, ^{15}N-TcPINK1 was incubated with ^{13}C-ATP in the presence of CYC116 and PRT062607 in order to observe their effects on TcPINK1 ATP futile hydrolysis **(Figures 25, 26)**, using differences in the ATP and ADP spectra as controls **(Figure 23)**. Thus, we reproduced the previously observed TcPINK1 futile hydrolysis **(Figure 24)** with a catalytic turnover rate of 0.83 min^{-1} **(Equation 2)** and show that CYC116 and PRT062607 both inhibit ^{15}N-TcPINK1 ATP hydrolysis *in vitro*.

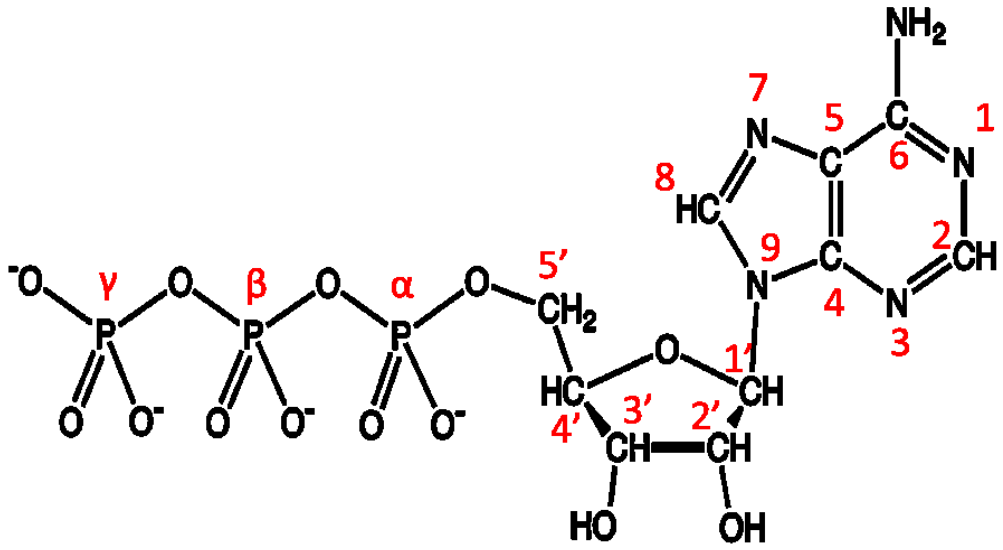

Figure 22: Structure and IUPAC numbering of ATP.

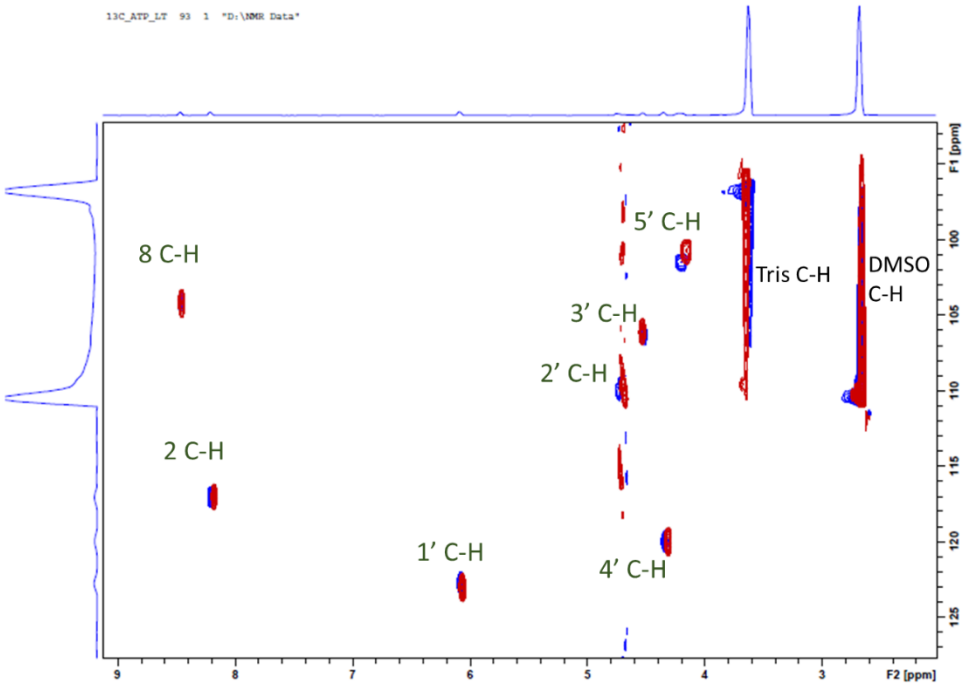

Figure 23: Differences in ^{1}H-^{13}C cross-peak position between ATP and ADP. Overlay of full ^{1}H-^{13}C HSQC NMR spectra of ATP (blue spectrum) and ADP (red spectrum) in buffer reveal differences in the coordinates of cross-peaks which are exploited in monitoring the hydrolytic activity of TcPINK1. The 4' and 5' CH peaks display the most noticeable differences. The vertically smeared signals at 3.7 ppm and 2.7 ppm correspond to Tris and DMSO CH bonds, respectively. They appear on the ^{1}H-^{13}C HSQC spectra due to their relatively high concentrations and the natural 1.1% abundance of ^{13}C. F2: ^{1}H; F1: ^{13}C.

$$k_{cat} = \frac{V_{max}}{[E]} = \frac{50\ \mu M\ ATP / 60\ min}{1\ \mu M\ TcPINK1} = 0.83\ min^{-1}$$

Equation 2: Calculation of TcPINK1 futile hydrolysis rate. Given that 1 µM TcPINK1 hydrolyzed half of the 100 µM ^{13}C-ATP in 60 min (spectrum not shown), the ATP turnover rate during futile hydrolysis is approximately 0.83 min^{-1}.

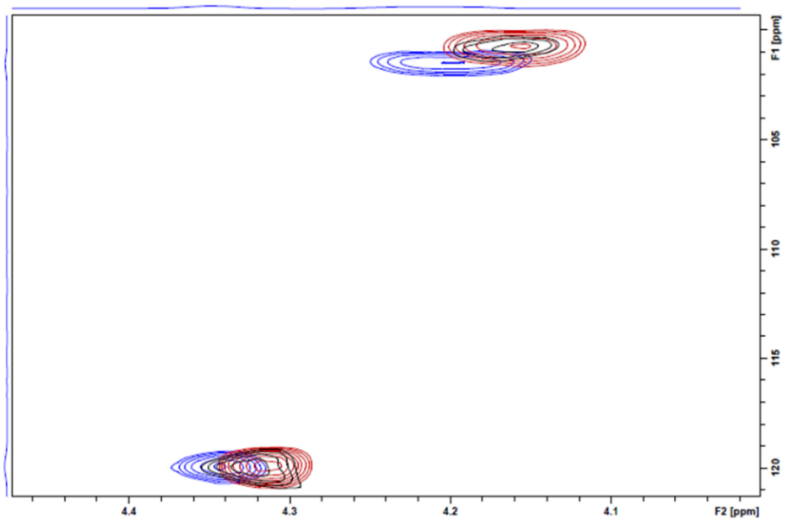

Figure 24: ^{15}N-TcPINK1 hydrolyzes ATP in the absence of Ub or Ubl. Overlay of 4' and 5' CH peaks from 3 ^{1}H-^{13}C HSQC NMR spectra: ATP (blue spectrum), ADP (red spectrum), and ATP + ^{15}N-TcPINK1 + DMSO (black spectrum). The black spectrum overlaps with the ADP peaks, indicating the presence of ADP in solution. This means that ^{15}N-TcPINK1 produces ADP from the ATP in the presence of DMSO alone. F2: ^{1}H; F1: ^{13}C.

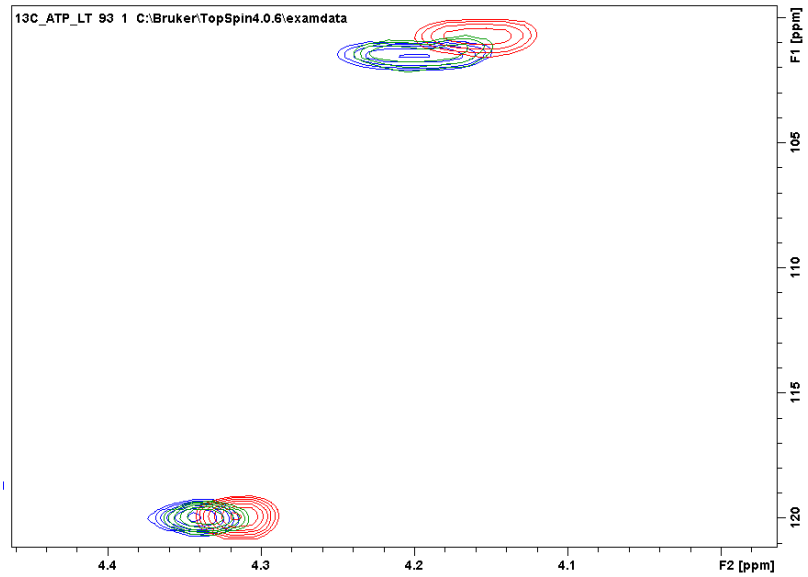

Figure 25: CYC116 inhibits ^{15}N-TcPINK1 ATP hydrolysis *in vitro*. Overlay of 4' and 5' CH peaks from 3 ^{1}H-^{13}C HSQC NMR spectra: ATP (blue spectrum), ADP (red spectrum), and ATP + ^{15}N-TcPINK1 + 100 µM CYC116 (green spectrum). The green spectrum overlaps with the ATP

peaks, indicating the presence of only ATP in solution. This means that the ATP is unhydrolyzed despite the presence of active ^{15}N-TcPINK1; its hydrolytic activity is therefore inhibited by CYC116. F2: ^{1}H; F1: ^{13}C.

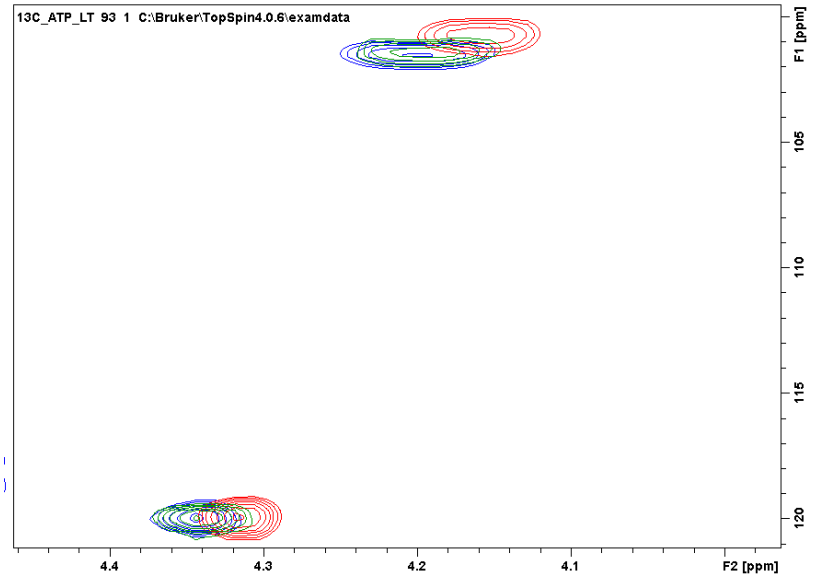

Figure 26: PRT062607 inhibits ^{15}N-TcPINK1 ATP hydrolysis *in vitro*. Overlay of 4' and 5' CH peaks from 3 ^{1}H-^{13}C HSQC NMR spectra: ATP (blue spectrum), ADP (red spectrum), and ATP + ^{15}N-TcPINK1 + 100 µM PRT062607 (green spectrum). The green spectrum overlaps with the ATP peaks, indicating the presence of only ATP in solution. This means that the ATP is unhydrolyzed despite the presence of active ^{15}N-TcPINK1; its hydrolytic activity is therefore inhibited by PRT062607. F2: ^{1}H; F1: ^{13}C.

3.7. Modeling CYC116 and PRT062607 TcPINK1 and HsPINK1 binding

Computer-based modeling was performed using MOE 2018.01 (see Methods for details) to characterize the binding site of the two inhibiting thermal stabilizers, CYC116 and PRT062607, on TcPINK1 and HsPINK1. The compounds effectively occupy the space normally dedicated to the ATP ribose and purine rings **(Figures 27, 28, 29, 30)**. Moreover, they bind TcPINK1 and HsPINK1 in the ATP binding pocket without affecting the DFG-in and αC helix-in active conformation of neither TcPINK1 nor HsPINK1 when free-moving induced fit simulations were

performed (data not shown). These docking simulations suggest that CYC116 and PRT062607 are Type I inhibitors of PINK1. The detailed interactions mediated by each inhibitor is described in the figure legends below.

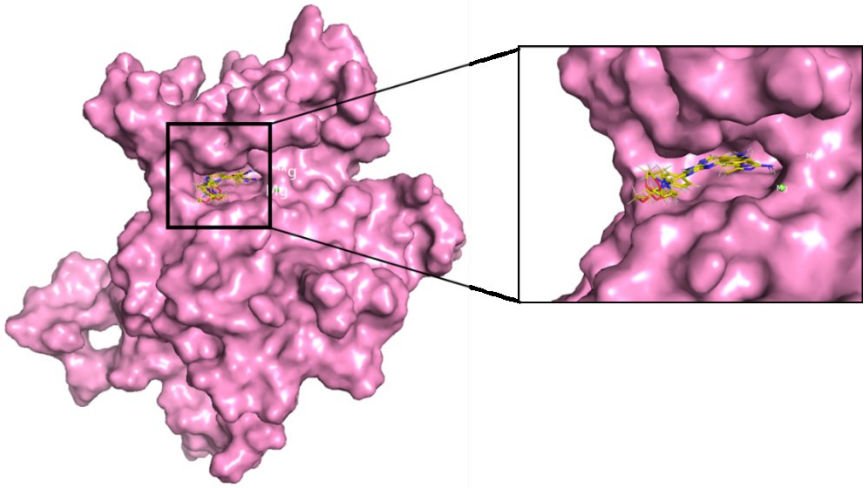

Figure 27: Four superimposed CYC116 conformers binding to TcPINK1. The 4 selected conformers made interactions with the kinase hinge. The pink surface map, modeling TcPINK1^{DDEE}, was rendered by PyMol.

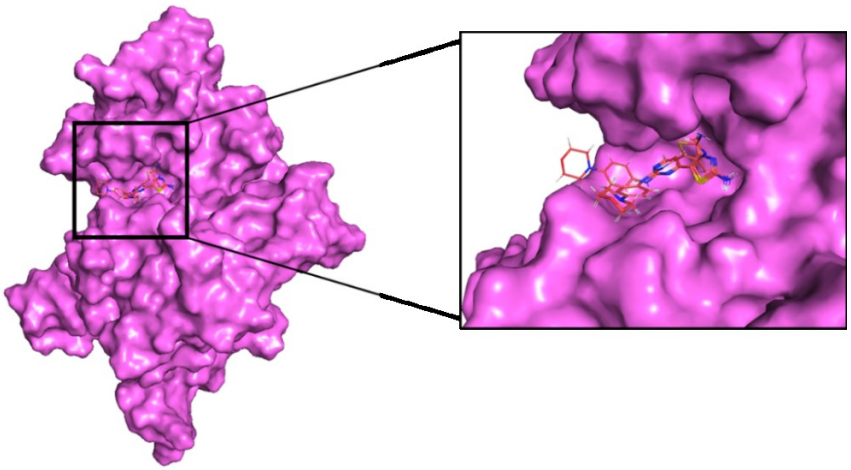

Figure 28: Four superimposed CYC116 conformers binding to HsPINK1. The 4 selected conformers made interactions with the kinase hinge. The violet surface map, modeling HsPINK1, was rendered by PyMol.

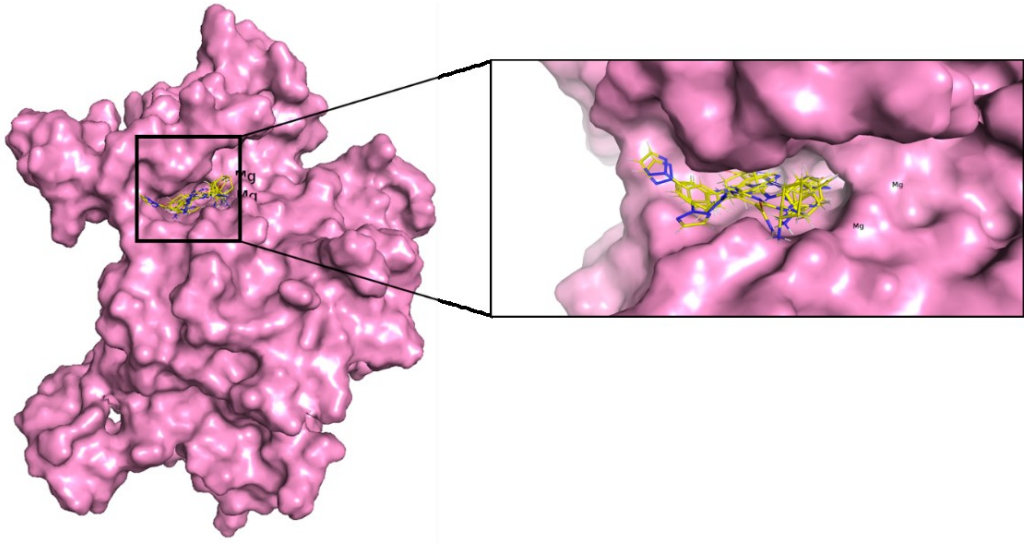

Figure 29: Five superimposed PRT062607 conformers binding to TcPINK1. The 5 selected conformers made interactions with the kinase hinge. The pink surface map, modeling TcPINK1^{DDEE}, was rendered by PyMol.

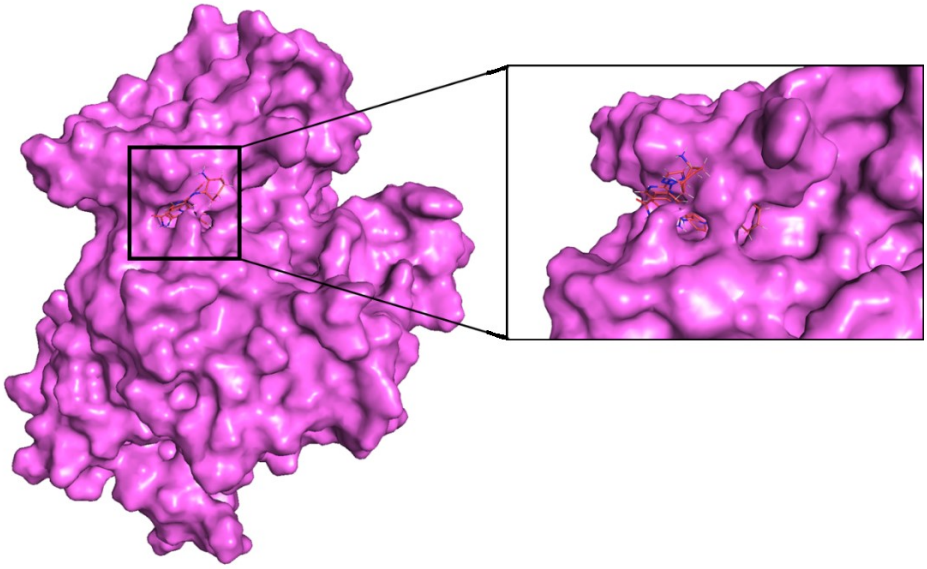

Figure 30: Two superimposed PRT062607 conformers binding to HsPINK1. The 2 selected conformers made interactions with the kinase hinge. The pink surface map, modeling HsPINK1, was rendered by PyMol.

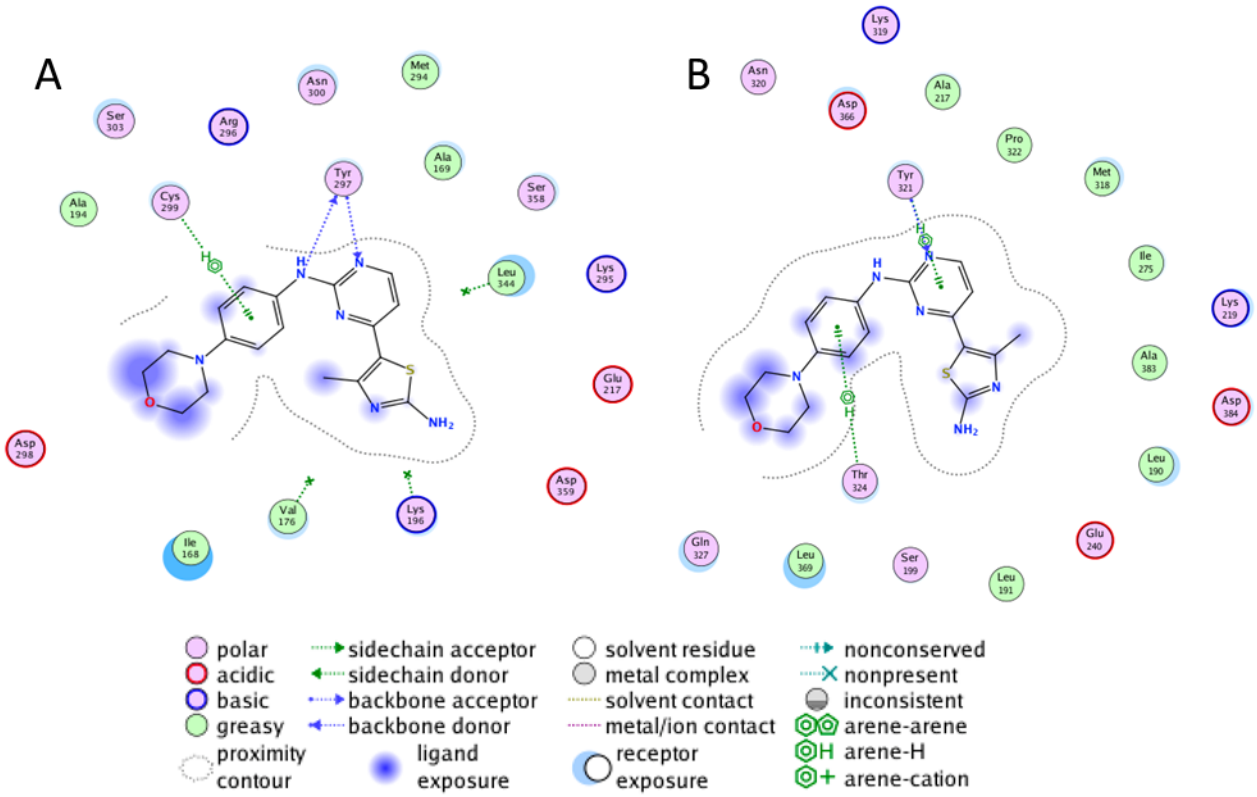

Figure 31: CYC116 is predicted to bind PINK1 at the kinase hinge. Schematic representation of predicted interactions averaged over the 4 CYC116 conformers in **Figure 27 (A)** and the 4 conformers in **Figure 28 (B)**. **(A)** With TcPINK1, poses that CYC116 were predicted to adopt make hydrogen-bonds with the main chain of Tyr297 via the pyrimidine moiety and its adjacent amino moiety. CYC116 also forms an arene-H interaction with Cys299. Val176, Lys196, and Leu344 make interactions that are not conserved across all conformers. **(B)** With HsPINK1, poses that CYC116 were predicted to adopt make arene-H interactions between the pyrimidine ring and Tyr321 (the equivalent to Tyr197 in PhPINK1), as well as between the phenyl ring and Thr324. CYC116 also makes a hydrogen-bond with the backbone of Tyr321 using its pyrimidine ring.

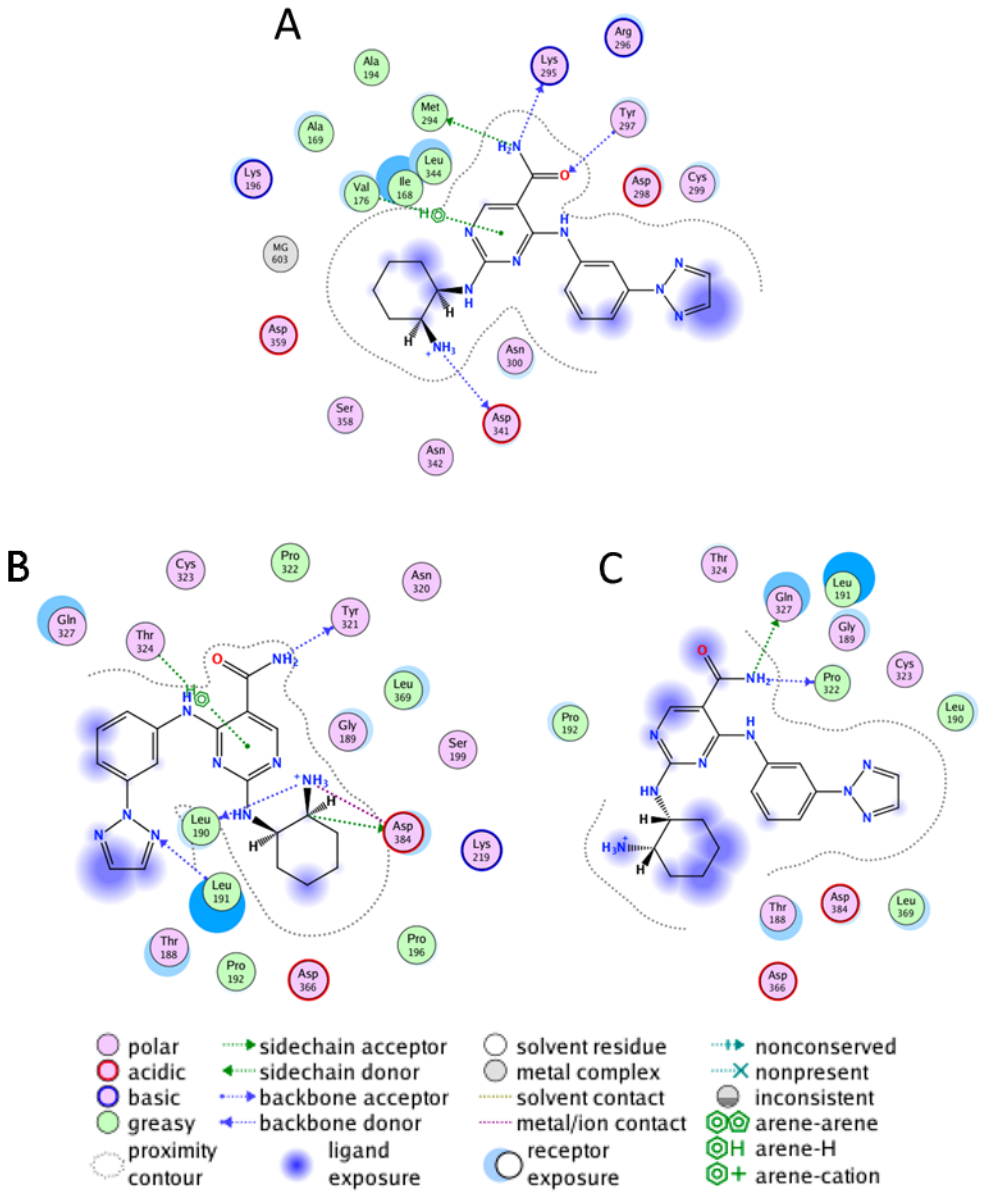

Figure 32: PRT062607 is predicted to bind PINK1 at the kinase hinge. Schematic representation of predicted interactions averaged over the 5 PRT062607 conformers in **Figure 29 (A)** and the 2 conformers in **Figure 30 (B, C)**. **(A)** With TcPINK1, poses that PRT062607 were predicted to adopt make arene-H interactions between the pyrimidine ring and Val176. PRT062607 also uses its amide group to make hydrogen-bond interactions with the Met294 sidechain, and with the Lys295 and Tyr297 main chains. **(B, C)** Here, the two poses are shown individually because of the stark contrast in their manner of interacting with HsPINK1. **(B)** PRT062607 is predicted to make arene-H interactions between the pyrimidine ring and Thr324.

The amide is predicted to make hydrogen-bond interactions with the Tyr321 main chain. The amino group attached to the cyclohexane is predicted to make hydrogen-bond interactions with the Leu190 main chain and a salt-bridge with the DFG Asp384. The carbon it is connected to is also predicted to make direct interactions with the DFG Asp384 sidechain. The 1,2,3-triazole is predicted to make hydrogen-bonds with the Leu191 main chain. **(C)** The second pose is predicted to only make a hydrogen-bond with the Glu327 sidechain and the Pro322 main chain.

3.8. Testing the effect of CYC116 and PRT062607 on HsPINK1 *in organello*

After discovering that CYC116 and PRT062607 are TcPINK1 Type I inhibitors, we sought to translate our findings to HsPINK1. As previously mentioned, it was not possible to heterologously express and purify usable nor active HsPINK1 for kinase assays. However, our group had optimized a method to test HsPINK1 *in vitro* without the need to express and purify it (Tang et al, 2017). This method, known as the *in organello assay*, uses purified mitochondria from CCCP-treated HeLa cells. Accumulated on the OMM, HsPINK1 is extracted along with the mitochondria. DMSO-treated mitochondria from the same cell lines are used as HsPINK1-devoid controls. The mitochondria are then used as a reagent in *in vitro* ubiquitination assays with recombinant Parkin (see Methods for details), and the ubiquitination of Parkin substrates such as Mfn2 are assessed by Western Blot **(Figures 33, 34, 35)**. Parkin activity is thus used as an indirect measure of the effect of the thermal stabilizers on HsPINK1. Our results indicate that PRT062607 inhibits HsPINK1 *in organello* with an IC_{50} of 192.3 ± 87.44 μM **(Figure 36; Appendix Figure 6)** while Foretinib and the other thermal stabilizers, including CYC116, do not.

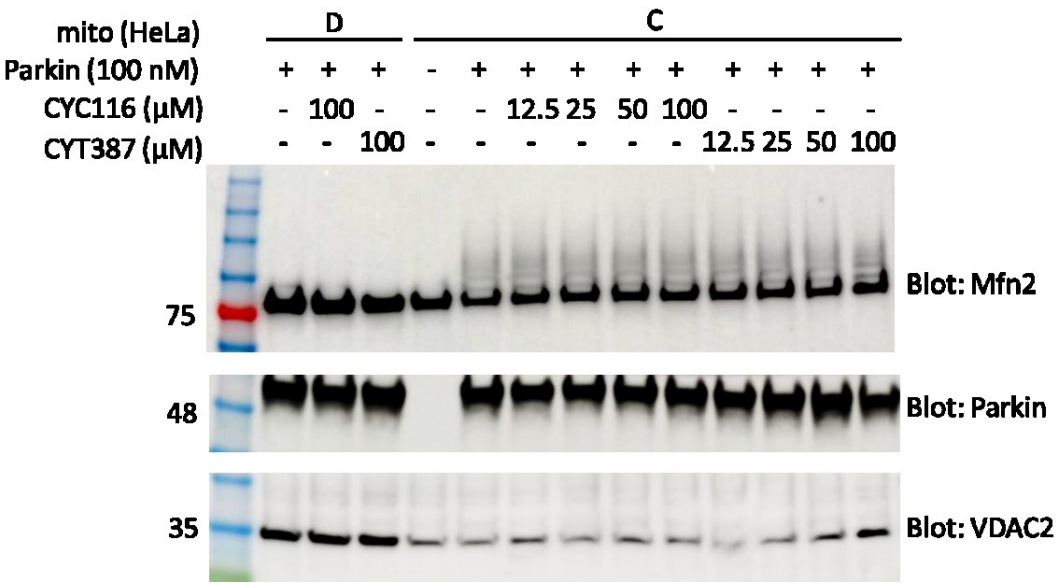

Figure 33: CYC116 and CYT387 do not inhibit HsPINK1 *in organello*. HsPINK1 activity was indirectly assessed by immunoblotting for Mfn2. Its Parkin-mediated ubiquitination is evinced by upward-shifted smears caused by varying levels of covalent Ub moiety additions. The smearing does not decrease in the presence of CYC116 and CYT387, thus ruling them out as HsPINK1 inhibitors. The VDAC2 immunoblot serves as a mitochondrial loading control. D, C: DMSO- and CCCP-treated HeLa mitochondria, respectively. Molecular weight in kDa are shown on the left.

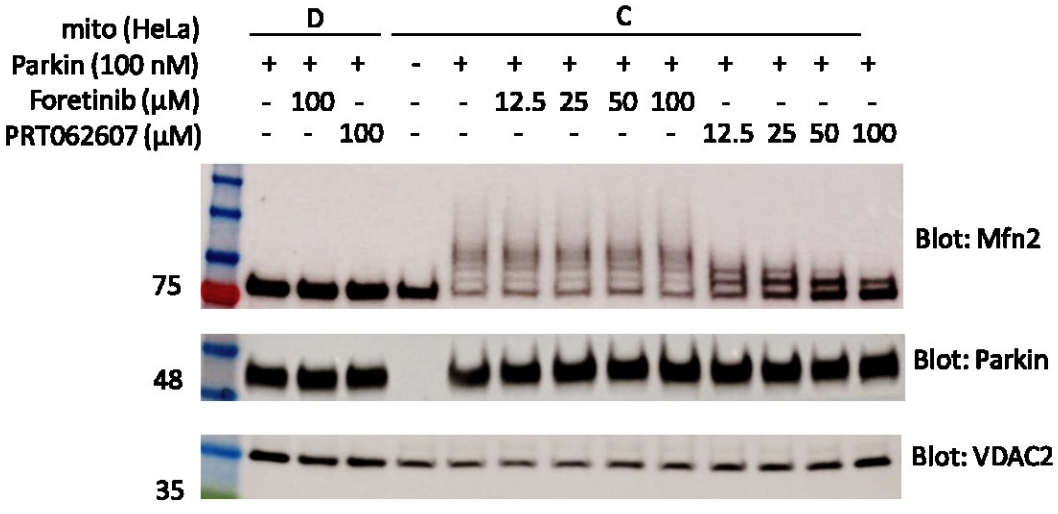

Figure 34: PRT062607, but not Foretinib, inhibits HsPINK1 *in organello*. HsPINK1 activity was indirectly assessed by immunoblotting for Mfn2. The ubiquitination-dependent smearing

decreases in the presence of PRT062607, demonstrating its indirect Parkin inhibition via HsPINK1 inhibition. Foretinib does not affect Mfn2 ubiquitination. The VDAC2 immunoblot serves as a mitochondrial loading control. D, C: DMSO- and CCCP-treated HeLa mitochondria, respectively. Molecular weight in kDa are shown on the left.

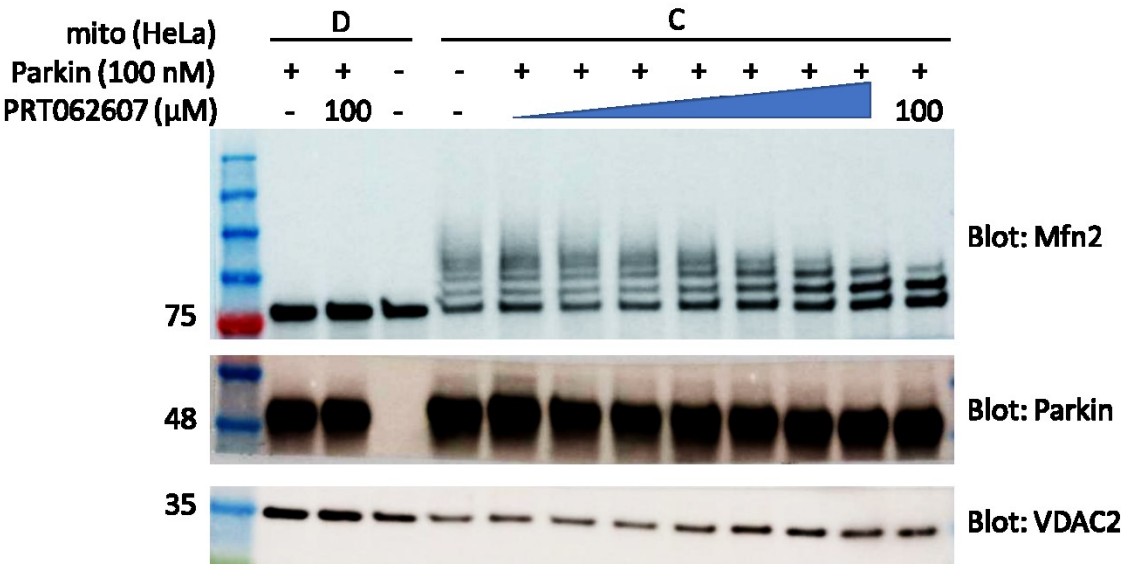

Figure 35: PRT062607 inhibits HsPINK1 dose-dependently *in organello*. Each lane from right to left of the blue triangle is a 2-fold dilution of the PRT062607 concentration, beginning at 100 µM. The VDAC2 immunoblot serves as a mitochondrial loading control. D, C: DMSO- and CCCP-treated HeLa mitochondria, respectively. Molecular weight in kDa are shown on the left.

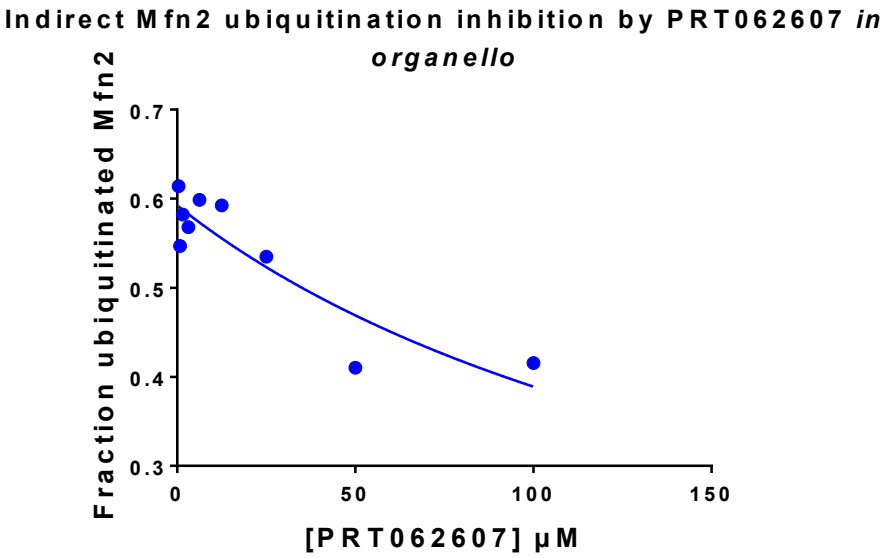

Figure 36: Quantification of indirect Mfn2 ubiquitin inhibition by PRT062607. Quantification of the integrated densities of the Mfn2 ubiquitination smears in the CCCP-treated HeLa mitochondria lanes in **Figure 35**, normalized to the integrated density of the unmodified Mfn2 band. The Non-linear fit (with curve bottom set to 0) of inhibitor concentration vs. Mfn2 ubiquitination indicates that PRT062607 has an IC_{50} of approximately 192.3 ± 87.44 µM **(Appendix Figure 6)**.

3.9. Testing the effect of PRT062607 on HsPINK1 activity in cells

The direct effect of the most potent thermally stabilizing kinase inhibitor, PRT062607, was tested in U2OS and HeLa cells. These cells provide a model system in which, unlike *in vitro* phosphorylation assays, HsPINK1 expression and mitochondrial localization occurs in an endogenous manner. As well, U2OS cells express endogenous levels of Parkin, while HeLa cells do not. The effects of PRT062607 on HsPINK1 accumulation in these two cell lines were compared to assess the Parkin-dependence of PRT062607 activity. We predicted that paradoxical HsPINK1 activation by PRT062607 may cause conformational changes that could sensitize HsPINK1 to lower levels of CCCP-induced damage. Concretely, we expected to detect increased pUb production and/or HsPINK1 accumulation at lower CCCP concentrations. Instead, we observed PRT062607-dependent inhibition of CCCP-induced pUb production in U2OS cells

(Figures 37, 38). We also observed that HsPINK1 levels were unaffected by PRT062607 in neither U2OS nor HeLa cells **(Figures 39, 40; Appendix Figure 7)**. These results show that in cells expressing endogenous levels of PINK1 and Parkin, PRT062607 is an HsPINK1 inhibitor rather than a paradoxical activator.

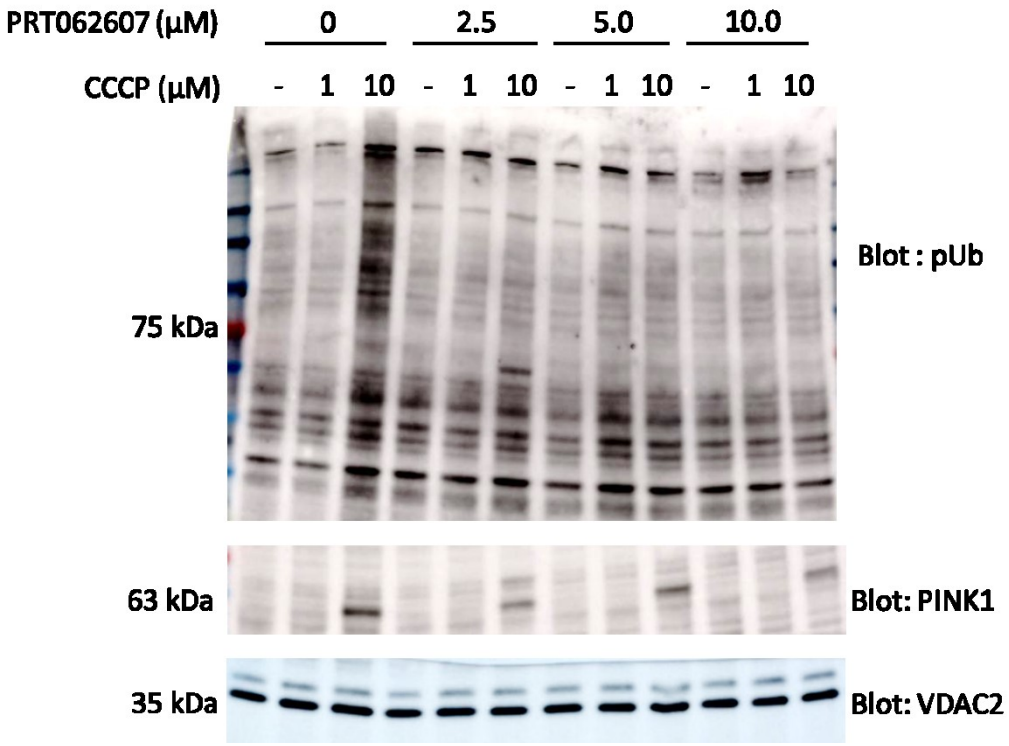

Figure 37: PRT062607 inhibits HsPINK1 pUb production in U2OS cells. 10 μM CCCP treatment causes pUb production (in the form of large (>75 kDa) chains) and HsPINK1 accumulation, which is abrogated by simultaneous treatment with PRT062607. The PINK1 immunoblot shows that PRT062607 does not increase HsPINK1 levels. The VDAC2 immunoblot serves as a mitochondrial loading control. Molecular weights are shown on the left.

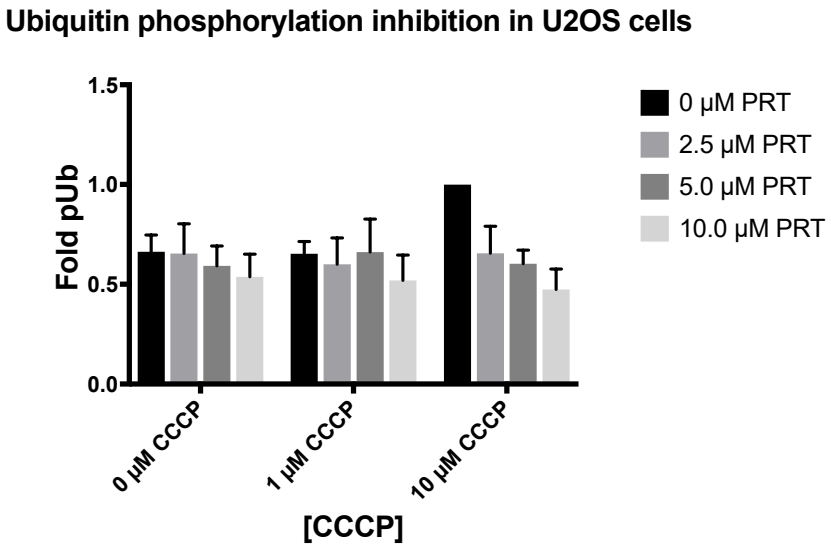

Figure 38: Quantification of pUb levels against different CCCP and PRT062607 concentrations. Quantification of pUb signals between 75 and 150 kDa in **Figure 37**, normalized to 0 µM PRT062607/10 µM CCCP pUb levels. PRT062607 decreases CCCP-dependent HsPINK1 pUb production. 3 biological replicates were performed. Error bars show ±SEM. PRT: PRT062607.

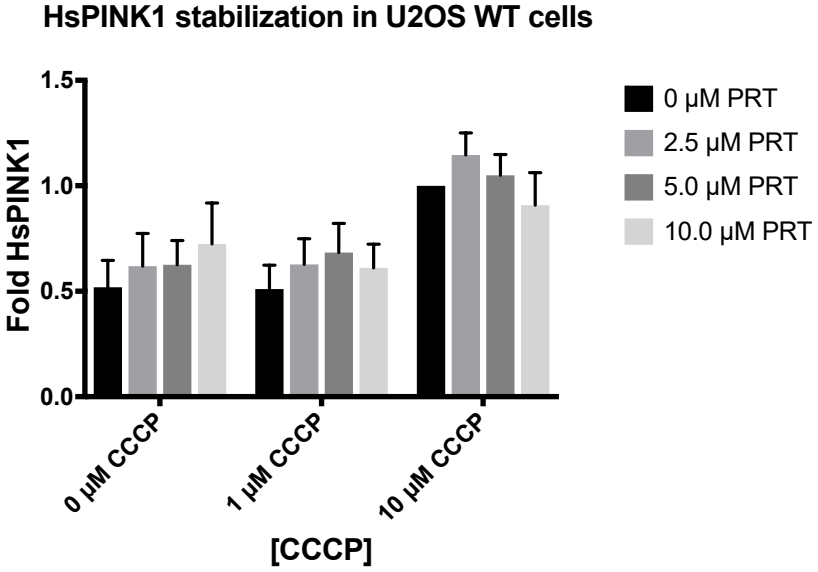

Figure 39: PRT062607 does not increase HsPINK1 levels in U2OS cells. Quantification of the HsPINK1 63 kDa band in **Figure 37**, normalized to 0 µM PRT062607/10 µM CCCP pUb levels.

PRT062607 does not noticeably affect HsPINK1 levels in U2OS cells. 3 biological replicates were performed. Error bars show ±SEM. PRT: PRT062607.

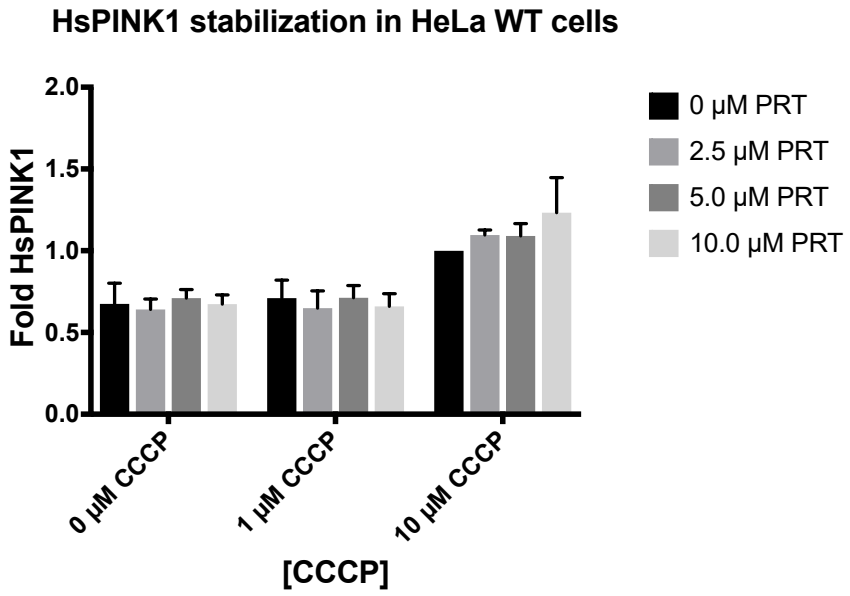

Figure 40: PRT062607 does not increase HsPINK1 levels in HeLa cells. Quantification of HsPINK1 63 kDa band in **Appendix Figure 7**, normalized to 0 µM PRT062607/10 µM CCCP pUb levels. PRT062607 does not increase HsPINK1 levels in Parkin-devoid HeLa cells. 3 biological replicates were performed. Error bars show ±SEM. PRT: PRT062607.

3.10. Testing the effect of PRT062607 on mitophagy in Parkin-overexpressing U2OS cells using FACS (performed by Mohamed Eldeeb)

We sought to test the effect of PRT062607 on mitophagy in cells. Given our data showing the PRT062607-dependent inhibition of PINK1 pUb production, we predicted that a PRT062607 treatment would decrease CCCP-induced mitophagy in cells. To monitor mitophagy, we used a fluorescence-activated cell sorting (FACS) assay with cells stably expressing mt-Keima, a mitochondrially-localized fluorescent protein which displays a pH-dependent shift in excitation profile. As such, mt-Keima acts as a mitophagy reporter, shifting its excitation spectrum to longer wavelengths as mitochondria fuse to acidic lysosomes. Upon cell sorting, the ratio of shifted to unshifted spectra is used to quantify the percentage of mitochondria undergoing mitophagy. Unlike

previously performed assays, these cells stably overexpress GFP-Parkin and are treated with 10 μM CCCP during an 18 hr timeframe in order to build up a sufficient mt-Keima signal for FACS. Our data indicate that 1 μM PRT062607 decreases CCCP-induced mitophagy, but that 10 μM PRT062607 increases CCCP-induced mitophagy.

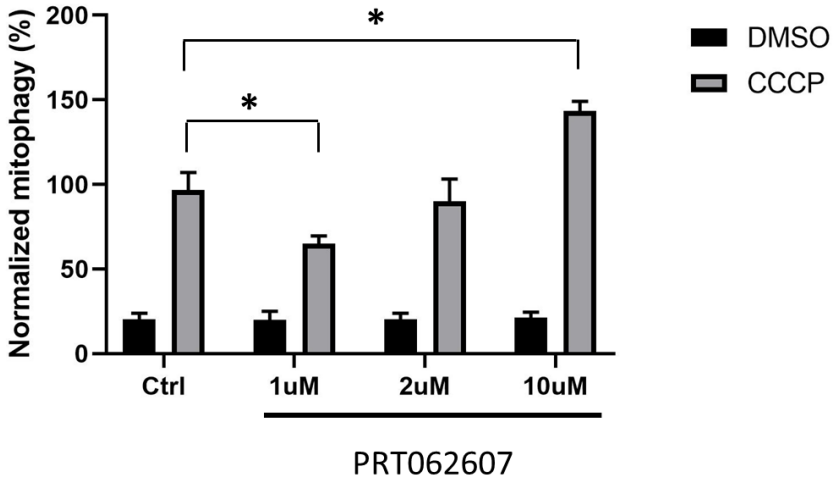

Figure 41: PRT062607 inhibits mitophagy at low concentrations, but increases it at high concentrations. Bars showing mitophagy percentage of DMSO-treated or 10 μM CCCP-treated U2OS cells stably overexpressing wild-type GFP-Parkin pre-treated 2 hr prior with different concentrations of PRT. The data from 3 independent experiments were quantified from the mt-Keima signal, normalized to CCCP-treated cells ("Ctrl."). *P*-values were determined by one-way ANOVA with Dunnett's post-hoc. * $P < 0.05$.

4. Discussion

It has been reported that several kinase inhibitors paradoxically activate kinase-centric oncogenic pathways by unexpectedly accelerating kinase subcellular localization, inducing kinase oligomerization, or hyperactivating kinase dimers. These phenomena constitute a serious obstacle in the development of anti-cancer treatments, but provide a novel strategy to activate PINK1. Coincidentally, PINK1 has been shown to exhibit the very biochemical behavior during mitochondrial stress that is thought to cause paradoxical activation: it requires localization and accumulation on the OMM, as well as transactivation by transient dimerization and autophosphorylation. Thus, the goal of this project was to exploit the phenomenon of paradoxical kinase activation to increase PINK1 activity using small-molecule kinase inhibitors. To this end, we screened known kinase inhibitors for TcPINK1 KD thermal stabilizers, as a proxy for their ability to impart a conformational change that may be necessary for the paradoxical activation of PINK1 in cells. Selected thermal stabilizers were characterized *in vitro* and in cellular culture to assess their effects on PINK1. It was discovered that CYC116 and PRT062607 are both Type I TcPINK1 auto- and substrate phosphorylation inhibitors, but that only PRT062607 is capable of inhibiting HsPINK1 *in organello* and in cells. Intriguingly, 10 μM PRT062607 managed to increase CCCP-induced mitophagy in Parkin-overexpressing cells. Thus, this project revealed that in combination with Parkin overexpression, PRT062607 is a paradoxical mitophagy activator. The remainder of this section discusses the major issues arising from the Results section and presents an outlook on the future of pharmacological PINK1 activation.

The TcPINK1 thermal stabilizers selected for further characterization were CYC116, CYT387, VE822, and PRT062607 **(Table 1)**. All of these molecules had been previously identified as *in vitro* inhibitors of other kinases: CYC116 inhibits Cyclin dependent kinase 2, Aurora kinases A, B, and C, and vascular endothelial growth factor receptor 2 (Andrews et al, 2006; Wang et al, 2010; Jayanthan et al, 2014); CYT387 inhibits Janus kinases (JAK) 1 and 2 (Pardanani et al, 2009); VE822 inhibits ATM-Rad3-related kinase (Fokas et al, 2012); and PRT062607 inhibits Spleen tyrosine kinase (Coffey et al, 2017) and JAK2 (Puleo et al, 2017). Clearly, if any of these compounds were to be used as PINK1 paradoxical activators, they would need to be modified to decrease their affinity for these other kinases to minimize off-target effects. The *in vitro* characterization of these compounds was thus useful in two ways: it revealed the effects of the

compounds beyond thermal stabilization on the activity of TcPINK1 and HsPINK1, and it simplified the issue of target-selectivity by singling out an optimal molecular scaffold.

In vitro characterization of the TcPINK1 thermal stabilizers led us to several discoveries. Despite their effects on thermal stability, CYT387 and VE822 do not positively nor negatively modulate TcPINK1 activity *in vitro*. It is possible that their binding to TcPINK1 KD is sufficient for a significant right-ward T_m shift at 100 μM, but that their affinity for TcPINK1 WT is too weak to cause inhibition of phosphorylation. On the other hand, both CYC116 and PRT062607 inhibit TcPINK1 phosphorylation activity. The chemical similarity between CYT387 and CYC116 provides an opportunity to understand the structure-activity relationship of TcPINK1 inhibitors. CYT387 and CYC116 share the same morpholino-phenyl-amino core, but diverge elsewhere: CYT387 has a phenyl ring with an amide-nitrile substituent, and CYC116 has a substituted thiazole group **(Table 1)**. Computer-based docking simulations indicate that the thiazole group is important for interactions with the conserved β sheet lysine (Lys196 in TcPINK1; **Figure 31**) and that the phenyl-amide-nitrile group in CYT387 might be too large for the ATP binding pocket to accommodate. This size restriction could also explain the inability of VE822 **(Table 1)** to inhibit TcPINK1: if it were to bind the ATP binding pocket via its amino-pyrimidine group, its oxazole-phenyl-amine group would be too large to fit into TcPINK1. The largeness of CYT387 and VE822 would cause those molecules to extend outside of the catalytic region and be highly solvent exposed, reducing their affinity for TcPINK1. Interestingly, they still managed to thermally stabilize TcPINK1 KD; this suggests that the TcPINK1 KD and TcPINK1 WT ATP binding pockets are different. Specifically, due to the mutation of the catalytic Asp337 to an Asn, TcPINK1 KD might either have a larger ATP binding pocket than TcPINK1 WT, or have a more flexible binding site which could stretch itself to fit a larger ligand.

HSQC-NMR was used to monitor the effect of CYC116 and PRT062607 on TcPINK1 ATP hydrolysis in the absence of Ub or Ubl. It is clear that TcPINK1 binds ATP in its catalytically active conformation without assistance from substrate binding (Okatsu et al, 2018), unlike other kinases (Wang and Cole, 2014). Whether HsPINK1 also hydrolyzes ATP in the absence of Ub or Ubl, and the physiological role of PINK1 futile hydrolysis in cells, remain to be elucidated. Regardless, we found that in the DMSO control, the rate of TcPINK1 futile hydrolysis is approximately 0.83 min^{-1} **(Equation 2; Figure 24)**. This approximate turnover rate is slower than

that of the phosphorylation of Ub (18.0 min^{-1}) and Ubl (7.8 min^{-1}) (Rasool et al, 2018). HSQC-NMR also revealed that CYC116 and PRT062607 inhibit TcPINK1 ATP hydrolysis *in vitro* **(Figures 25, 26)**, suggesting that they either allosterically affect the ATP binding site or that they outcompete ATP binding. The latter effect is more likely given that the only small-molecule binding pocket on the surface of PINK1 is its ATP binding site. It is possible that CYC116 or PRT062607 also perform their inhibitory function by indirectly interfering with the PINK1:Ub/Ubl binding interface via remodeling of the catalytic region which could by extension affect the folding of Insert 3. To test this hypothesis, we will employ an ^{15}N-SH3-Ubl competition assay. This experiment exploits the Ubl Ile44-centric binding site shared by both the Endophilin-A1 SH3 domain (hereon referred to as simply "SH3") and PINK1 (Trempe et al, 2009; Rasool et al, 2018). Briefly, HSQC-NMR is used to monitor chemical shifts induced by Ubl binding to ^{15}N-SH3. Addition of PINK1 reduces the pool of available Ubl to bind the ^{15}N-SH3, decreasing the binding-induced chemical shifts. Such experiments were performed to obtain the dissociation constant of the PINK1-Ubl interaction (Rasool et al, 2018), and will be repeated in the presence of CYC116 and PRT062607 to test their effect on PINK1 Ubl binding.

In silico docking simulations indicate that CYC116 and PRT062607 are Type I ATP-competitive inhibitors. The schematic diagrams of the docking results shown in **Figures 31 and 32** were performed using a rigid receptor model of TcPINK1 and a homology model of HsPINK1 to show possible interactions between residues and CYC116/PRT062607 moieties. It is important to note that the simulations are only useful in creating a visual representation of how a compound might be interacting with a receptor protein, and are of no use in determining other binding parameters such as affinity or residence time. The induced-fit refinement modeling of TcPINK1 and HsPINK1 with free-moving sidechains suggests that CYC116/PRT062607 binding does not disturb the orientation of the DFG Asp and the αC helix (data not shown). From this we infer that they are Type I inhibitors, binding to PINK1 in its active conformation. That being said, the induced-fit free-moving models only compute the movement of residues up to 10 Å from the defined binding pocket; this precludes more complex modeling of larger conformational rearrangements that may underpin paradoxical PINK1 activation. For this reason, we were compelled to complement these simulations with assays testing the effect of CYC116 and PRT062607 on HsPINK1 *in organello* and in cells.

We discovered that PRT062607, but not CYC116, inhibits HsPINK1 activity *in organello*. This *in organello* technique is used to obtain HeLa mitochondria with HsPINK1 accumulated on their surface. The mitochondria are then used as a reagent in an *in vitro* ubiquitination reaction using recombinant Parkin (see Methods and Results for details). At the time of these *in organello* experiments, our pUb antibody was cross-reacting excessively with non-pUb epitopes. Consequently, we monitored the effect of CYC116, CYT387, Foretinib, and PRT062607 on HsPINK1 indirectly via Parkin ubiquitination activity **(Figures 33 and 34)**. We show that only PRT062607 inhibits Parkin Mfn2 ubiquitination in a dose-dependent manner *in organello* **(Figures 35 and 36)**. None of the other thermal stabilizers (and Foretinib) positively nor negatively affect PINK1/Parkin activity. These data highlight PRT062607 as the only compound from the initial screen capable of interacting with both TcPINK1 and HsPINK1, but that PRT062607 failed to paradoxically activate HsPINK1 *in organello*. However, we believe that *in organello* experiments insufficiently recapitulate the physiological setting in which HsPINK1 would respond to mitochondrial damage. The pre-treatment of CCCP prior to the mitochondrial harvest causes HsPINK1 to accumulate before the Parkin ubiquitination assay is performed. This means that any possible effect of PRT062607 on HsPINK1 import, stabilization in the TOM complex, and even dimerization could not be measured in a system where HsPINK1 is already accumulated and transactivated. Since PRT062607 was the only confirmed HsPINK1 inhibitor, we decided to test the effect of PRT062607 on HsPINK1 in mammalian cells.

We expected that PRT062607-induced paradoxical activation of PINK1 would sensitize PINK1 to lower levels of mitochondrial damage by "tuning" its OMM stabilization or promoting dimerization and transactivation. One, or a combination of these effects would cause the accumulation of HsPINK1 or an appreciable production of pUb in the absence of CCCP or at lower CCCP concentration in the presence of PRT062607. Our initial experiments in cells expressing endogenous levels of PINK1/Parkin show that PRT062607 alone does not cause pUb production nor increase the accumulation of HsPINK1 following 1 nor 10 μM CCCP treatment in neither U2OS nor HeLa cells **(Figures 37, 38, 39, 40)**. It is possible that PRT062607 is sensitizing endogenous HsPINK1 to a degree which is not observable given our experimental design. Specifically, it may be sensitizing HsPINK1 to an amount of mitochondrial damage induced by greater than 1 μM CCCP but still less than 10 μM CCCP. To address this lapse, CCCP concentrations in this intermediate range will have to be tested. Nonetheless, our central finding is

that PRT062607 inhibits HsPINK1 Ub phosphorylation despite CCCP treatment in U2OS cells expressing endogenous levels of PINK1/Parkin. HeLa cells do not express Parkin (Denison et al, 2003; Lutz et al, 2009); therefore, pUb was not probed in HeLa cell lysates. These data suggest that PRT062607 is directly inhibiting HsPINK1. Indeed, the pUb signal is CCCP-dependent, and inhibition of pUb production is only seen when PINK1 is accumulated and PRT062607 is added.

Follow-up FACS experiments were performed with U2OS cells overexpressing Parkin pre-treated with PRT062607 prior to an 18 hr treatment of CCCP. The data indicate that PRT062607 pre-treatment decreases CCCP-induced mitophagy at lower concentration (1 μM), but increases it at higher concentration (10 μM) **(Figure 41)**.These findings suggest that despite catalytic inhibition of HsPINK1, PRT062607 can potentially act as a paradoxical mitophagy activator under certain conditions. The high concentration requirement is probably owed to the low affinity of PRT062607 for HsPINK1. It is possible and likely that PRT062607 is inhibiting off-target kinases, such as Syk and JAK2. The effects of the off-target binding were not possible to measure in our paradigm because we were only concerned with pUb production, PINK1 accumulation, and mitophagy percentage. It is not impossible, however, that off-target inhibition of Syk or JAK2 can indirectly affect MQC signaling, knowing that both of these kinases are involved in the regulation of numerous pathways. From our viewpoint, it is difficult to predict what indirect interaction (if any) may connect Syk or JAK2 inhibition to PINK1/Parkin activity. Nevertheless, we hypothesize that a concentrated PRT062607 pre-treatment could jumpstart mitophagy by increasing the initial (steady-state) concentration of HsPINK1 prior to CCCP administration. This will be tested by pre-treating cells with PRT062607 prior to CCCP treatment and blotting for HsPINK1. Augmented steady-state levels of HsPINK1 would compensate for the catalytic inhibition, most likely by increasing the probability of HsPINK1 dimerization and transphosphorylation on the OMM. Any subsequent increase in pUb signal, however small, could be detected in a Parkin overexpression background, leading to mitophagy. As such, we propose that a combination of Parkin activators and PRT062607 could be used as a viable therapeutic strategy to rescue incompetent MQC.

Given these data, we report the discovery of a TcPINK1 and HsPINK1 inhibitor, PRT062607, which acts as a paradoxical CCCP-induced mitophagy activator at high concentrations under Parkin overexpression. However, the characterization of PRT062607, as well as the other TcPINK1 KD thermal stabilizers, is still ongoing. We are planning to perform Isothermal

Calorimetry (ITC) to measure their affinity for TcPINK1. Furthermore, HDX-MS data will enable the monitoring of the thermal stabilizers' effects on the structural dynamics of TcPINK1. It would also be interesting to see what structural consequences result from the binding of a thermal *destabilizer*, such as Rapamycin (ΔT_m = -1.66°C), Ibrutinib (ΔT_m = -2.94°C), or Ponatinib (ΔT_m = -2.97°C) (data not shown). However, ITC and HDX require a homogenous sample of TcPINK1 WT. At the time of these experiments, we had not developed a strategy to overcome the tendency of TcPINK1 to autophosphorylate spuriously during heterologous expression **(Figure 11)**; the CIP-treated ^{15}N-labelled TcPINK1 was our best approximation of lowly-phosphorylated homogenous PINK1 **(Figure 12)**. Recently, our group developed a strategy to obtain homogenously mono-autophosphorylated TcPINK1 using a heterologous co-expression system with Lambda Phosphatase (data not shown; obtained from Shafqat Rasool). This homogenous TcPINK1 will be used to complete the characterization of the thermal stabilizers. Our group is also attempting to heterologously express and purify recombinant HsPINK1 for *in vitro* studies. Ultimately, our goal is to solve the structure of TcPINK1 and/or HsPINK1 bound to a thermal stabilizer to map the precise rearrangements occurring upon binding which correlate to thermal stabilization. Collected data would confirm or reject our *in silico* predictions and guide the development of optimized PINK1 ligands with increased affinity, selectivity, and potential as a paradoxical activator.

We have established that PRT062607 inhibits both TcPINK1 and HsPINK1, and preliminary data indicate that it can paradoxically activate CCCP-induced mitophagy under certain conditions. We are capitalizing on these discoveries by collaborating with a company (Mitokinin) to synthesize PRT062607 analogs in order to explore more of its chemical space. Indeed, its molecular weight is 393 g/mol, leaving room for chemical modifications and additions well within the 500 g/mol limit of the Lipinski rule of fives (Lipinski et al, 1997). Based on sequence and structure comparisons, these analogs (conceived by Dr. Trempe; not shown) are designed to decrease the affinity of PRT062607 for Syk and JAK2 while increasing its affinity for PINK1. Of note, certain compounds will be designed to test the effect of targeting the thiol sidechain of a conserved cysteine in the PINK1 catalytic region (Cys323 in HsPINK1) reversibly or irreversibly. These chemical modifications might improve PRT062607 as a paradoxical agonist or increase its potency as an inhibitor.

Indeed, PRT062607 could serve as a useful research tool in the study of the PINK1/Parkin MQC pathway if it turns out to be a potent inhibitor rather than an activator. Its administration would constitute a method to specifically inhibit the catalytic activity of PINK1 without affecting its expression (as is the case of a KO), translation (as is the case of a knockdown), import, or primary sequence. These hypothetical studies could also be performed *in vivo* since it has been shown that PRT062607 is well tolerated at very high plasma concentrations in rats and in humans (Coffey et al, 2017). In addition, PRT062607 has been shown to inhibit Syk, a kinase involved in autoimmunity and inflammation (Zhang et al, 2015). Treating PD patients with PRT062607 might be beneficial to target the recently elucidated autoimmune and neuroinflammatory aspects of PD (Matheoud et al, 2016; Sliter et al, 2018).

5. Summary and Conclusion

This project aimed to produce a disease-modifying pharmacological treatment for PD. It had been shown that accumulation of mitochondrial damage is central to the pathogenesis of PD; therefore, we chose to target PINK1, a kinase whose role is not only indispensable to, but also upstream of the MQC pathway. Recently published PINK1 structures reveal that its only small-molecule binding site is its ATP binding pocket, and problematically, all ATP-competitive compounds are designed as inhibitors. Incidentally, reports surfaced of kinase inhibitors which paradoxically activate the kinases they were meant to inhibit, by inducing their oligomerization, accelerating their subcellular localization, or hyperactivating kinase dimers. This phenomenon presents itself as a novel strategy to activate PINK1 for the treatment of PD. We screened known kinase inhibitors for TcPINK1 KD thermal stabilizers, as a proxy for their ability to impart a conformational change that may be necessary for PINK1 paradoxical activation. To study their effects on PINK1 activity, the top thermal stabilizers were characterized *in vitro*. CYC116 and PRT062607 were discovered to be Type I TcPINK1 auto- and substrate phosphorylation inhibitors. However, only PRT062607 was found to inhibit HsPINK1. Intriguingly, PRT062607 *increased* CCCP-induced mitophagy in Parkin overexpressing cells. The affinities of the thermal stabilizers, as well as the structural consequences conferred by their binding remain to be assessed by ITC and HDX, respectively. As well, PRT062607 derivatives, designed with increased affinity and selectivity for HsPINK1, remain to be tested. Finally, we aim to crystallize TcPINK1 or HsPINK1 bound to a thermal stabilizer to guide future PINK1 ligand design.

6. Reference list (in alphabetical order)

Alessi DR, Deak M, Casamayor A, Caudwell FB, Morrice N, Norman DG, Gaffney P, Reese CB, MacDougall CN, Harbison D, Ashworth A, Bownes M (1997) 3-Phosphoinositide-dependent protein kinase-1 (PDK1): structural and functional homology with the Drosophila DSTPK61 kinase. Curr Biol 7(10): 776-89

Andrews MJ, Kontopidis G, McInnes C, Plater A, Innes L, Cowan A, Jewsbury P, Fischer PM (2016) REPLACE: a strategy for iterative design of cyclin-binding groove inhibitors. Chembiochem 7(12): 1909-15

Arencibia JM1, Pastor-Flores D, Bauer AF, Schulze JO, Biondi RM (2013) AGC protein kinases: from structural mechanism of regulation to allosteric drug development for the treatment of human diseases. Biochim Biophys Acta 1843(7): 1302-21

Bausewein T, Mills DJ, Langer JD, Nitschke B, Nussberger S, Kühlbrandt W (2017) Cryo-EM Structure of the TOM Core Complex from Neurospora crassa. Cell 170(4): 693-700

Bayne AN, Trempe JF (2019) Mechanisms of PINK1, ubiquitin and Parkin interactions in mitochondrial quality control and beyond. Cell Mol Life Sci doi: 10.1007/s00018-019-03203-4

Beenstock J, Mooshayef N, Engelberg D (2016) How Do Protein Kinases Take a Selfie (Autophosphorylate)? Trends Biochem Sci 41(11): 938-953

Beilina A, Van Der Brug M, Ahmad R, Kesavapany S, Miller DW, Petsko GA, Cookson MR (2005) Mutations in PTEN-induced putative kinase 1 associated with recessive parkinsonism have differential effects on protein stability.Proc Natl Acad Sci U S A 102(16): 5703-8

Bender A, Krishnan KJ, Morris CM, Taylor GA, Reeve AK, Perry RH, Jaros E, Hersheson JS, Betts J, Klopstock T, Taylor RW, Turnbull DM (2006) High levels of mitochondrial DNA deletions in substantia nigra neurons in aging and Parkinson disease. Nat Genet 38(5): 515-7

Bentivoglio AR, Cortelli P, Valente EM, Ialongo T, Ferraris A, Elia A, Montagna P, Albanese A (2001) Phenotypic characterisation of autosomal recessive PARK6-linked parkinsonism in three unrelated Italian families. Mov Disord 16(6): 999-1006

Bessa C, Soares J, Raimundo L, Loureiro JB, Gomes C, Reis F, Soares ML, Santos D, Dureja C, Chaudhuri SR, Lopez-Haber C, Kazanietz MG, Gonçalves J, Simões MF, Rijo P, Saraiva L (2018) Discovery of a small-molecule protein kinase Cδ-selective activator with promising application in colon cancer therapy. Cell Death Dis 9(2): 23

Biondie RM (2004) Phosphoinositide-dependent protein kinase 1, a sensor of protein conformation. Trends Biochem Sci 29(3): 136-42

Bishop AC, Ubersax JA, Petsch DT, Matheos DP, Gray NS, Blethrow J, Shimizu E, Tsien JZ, Schultz PG, Rose MD, Wood JL, Morgan DO, Shokat KM (2000) A chemical switch for inhibitor-sensitive alleles of any protein kinase. Nature 407(6802): 395-401

Buetow L, Huang DT (2016) Structural insights into the catalysis and regulation of E3 ubiquitin ligases. Nat Rev Mol Cell Biol 17(10): 626-42

Burns RS, Chiueh CC, Markey SP, Ebert MH, Jacobowitz DM, Kopin IJ (1983) A primate model of parkinsonism: selective destruction of dopaminergic neurons in the pars compacta of the substantia nigra by N-methyl-4-phenyl-1,2,3,6-tetrahydropyridine. Proc Natl Sci U S A 80(14): 4546-50

Burns RS, Markey SP, Phillips JM, Chiueh CC (1984) The Neurotoxicity of 1-Methyl-4-phenyl-1,2,3,6-tetrahydropyridine in the Monkey and Man. Can J Neurol Sci 11: 166-168

Carles F, Bourg S, Meyer C, Bonnet P (2018) PKIDB: A Curated, Annotated and Updated Database of Protein Kinase Inhibitors in Clinical Trials. Molecules 23(4): E908

Cebrián C, Zucca FA, Mauri P, Steinbeck JA, Studer L, Scherzer CR, Kanter E, Budhu S, Mandelbaum J, Vonsattel JP, Zecca L, Loike JD, Sulzer D (2014) MHC-I expression renders catecholaminergic neurons susceptible to T-cell-mediated degeneration. Nature Commun 5: 3633

Cerda SR, Bissonnette M, Scaglione-Sewell B, Lyons MR, Khare S, Mustafi R, Brasitus TA (2001) PKC-delta inhibits anchorage-dependent and -independent growth, enhances differentiation, and increases apoptosis in CaCo-2 cells. Gastroenterology 120(7): 1700-12

Chang D, Nalls MA, Hallgrismdottir IB, Hunkapiller J, van der Burg M, Cai F, International Parkinson's Disease Genetics Consortium, 23andMe ResearchTeam, Kerchner GA, Ayalon G, Bingol B, Sheng M, Hinds D, Behrens TW, Singleton AB, Bhangale TR, Graham RR (2017) A

meta-analysis of genome-wide association studies identifies 17 new Parkinson's disease risk loci. Nat Genet 49(10): 1511-1516

Chaugule VK, Burchell L, Barber KR, Sidhu A, Leslie SJ, Shaw GS, Walden H (2011) Autoregulation of Parkin activity through its ubiquitin-like domain. EMBO J 30: 2853-2867.

Chen Q, Sun L, Chen ZJ (2016) Regulation and function of the cGAS-STING pathway of cytosolic DNA sensing. Nat Immun 17: 1142-1149

Clark IE, Dodson MW, Jiang C, Cao JH, Huh JR, Seol JH, Yoo SJ, Hay BA, Guo M (2006) Drosophila pink1 is required for mitochondrial function and interacts genetically with parkin. Nature 441(7097): 1162-6

Coffey G, Rani A, Betz A, Pak Y, Haberstock-Debic H, Pandey A, Hollenbach S, Gretler DD, Mant T, Jurcevic S, Sinha U (2017) PRT062607 Achieves Complete Inhibition of the Spleen Tyrosine Kinase at Tolerated Exposures Following Oral Dosing in Healthy Volunteers. J Clin Pharmacol 57(2): 194-210

Cohen C, Zavala-Pompa A, Sequeira JH, Shoji M, Sexton DG, Cotsonis G, Cerimele F, Govindarajan B, Macaron N, Arbiser JL (2002) Mitogen-actived protein kinase activation is an early event in melanoma progression. Clin Cancer Res 8(12): 3728-33

Cox JS, Walter P (1996) A novel mechanism for regulating activity of a transcription factor that controls the unfolded protein response. Cell 87(3): 391-404

Dar AC, Shokat KM (2011) The evolution of protein kinase inhibitors from antagonists to agonists of cellular signaling. Annu Rev Biochem 80: 769-95

Deas E, Plun-Favreau H, Gandhi S, Desmond H, Kjaer S, Loh SH, Renton AE, Harvey RJ, Whitworth AJ, Martins LM, Abramov AY, Wood NW (2011) PINK1 cleavage at position A103 by the mitochondrial protease PARL. Hum Mol Genet 20(5): 867-79

Denison SR, Wang F, Becker NA, Schüle B, Kock N, Phillips LA, Klein C, Smith DI (2003) Alterations in the common fragile site gene Parkin in ovarian and other cancers. Oncogene 22(51): 8370-8

Dick FD, Palma GD, Ahmadi A, Scott NW, Prescott GJ, Bennet J, Semple S, Dick S, Counsell C, Mozzoni P, Haites N, Bezzina Wettinger S, Mutti A, Otelea M, Seaton A, Soderkvist P, Felice A (2007) Environmental risk factors for Parkinson's disease and parkinsonism: the Geoparkinson study. Occup Environ Med 64(10): 666-672

Dickson DW, Braak H, Duda JE, Duyckaerts C, Gasser T, Halliday GM, Hardy J, Leverenz JB, Del Tredici K, Wszolek ZK, Litvan I (2009) Neuropathological assessment of Parkinson's disease: refining diagnostic criteria. Lancet Neurol 8(12): 1150-7

Dikic I (2017) Proteasomal and Autophagic Degradation Systems. Anny Rev Biochem 86: 193-224

Dorsey ER, Constantinescu R, Thomson JP, Biglan KM, Holloway RG, Kieburtz K, Marshall FJ, Ravina BM, Schifitto G, Siderowf A, Tanner CM (2007) Projected number of people with Parkinson disease in the most populous nations, 2005 through 2030. Neurology 68(5): 384-386

Durcan TM, Tang MY, Pérusse JR, Dashti EA, Aguileta MA, McLelland GL, Gros P, Shaler TA, Faubert D, Coulombe B, Fon EA (2014) USP8 regulates mitophagy by removing K6-linked ubiquitin conjugates from parkin. EMBO J 33(21): 2473-91

Endicott JA, Noble ME, Johnson LN (2012) The structural basis for control of eukaryotic protein kinases. Annu Rev Biochem 81: 587-613

Fokas E, Prevo R, Pollard JR, Reaper PM, Charlton PA, Cornelissen B, Vallis KA, Hammond EM, Olcina MM, Gillies McKenna W, Muschel RJ, Brunner TB (2012) Targeting ATR in vivo using the novel inhibitor VE-822 results in selective sensitization of pancreatic tumors to radiation. Cell Death Dis 3: e441

Foltynie T, Sawcer S, Brayne C, Barker R (2002) The genetic basis of Parkinson's disease. J Neurol Neurosurg Psychiatry 73(4): 363-370

Gandhi S, Muqit MM, Stanyer L, Healy DG, Abou-Sleiman PM, Hargreaves I, Heales S, Ganguly M, Parsons L, Lees AJ, Latchman DS, Holton JL, Wood NW, Revesz T (2006) PINK1 protein in normal human brain and Parkinson's disease. Brain 129(Pt 7): 1720-31

Gasser T (2001) Genetics of Parkinson's disease. J Neurol 248(10): 833-840

Gavrin LK, Saiah E (2013) Approaches to discover non-ATP site kinase inhibitors. Med Chem Comm 4: 41-51

Geisler S, Holmström KM, Skujat D, Fiesel FC, Rothfuss OC, Kahle PJ, Springer W (2010) PINK1/Parkin-mediated mitophagy is dependent on VDAC1 and p62/SQSTM1. Nat Cell Biol 12(2): 119-31

Geldenhuys WJ, Leeper TC, Carroll RT (2014) mitoNEET as a novel drug target for mitochondrial dysfunction. Drug Discov Today 19(10): 1601-6

Gibb WRG, Lees AJ (1988) The relevance of Lewy body to the pathogenesis of idiopathic Parkinson's disease. J Neurol Neurosurg Psychiatry 51: 745-752

Gladkova C, Maslen SL, Skehel JM, Komander D (2018) Mechanism of Parkin activation by PINK1. Nature 559(7714): 410-414

Greene JC, Whitworth AJ, Kuo I, Andrews LA, Feany MB, Pallanck LJ (2003) Mitochondrial pathology and apoptotic muscle degeneration in Drosophila parkin mutants. Proc Natl Acad Sci U S A 100(7): 4078-83

Greene AW, Grenier K, Aguileta MA, Muise S, Farazifard R, Haque ME, McBride HM, Park DS, Fon EA (2012) Mitochondrial processing peptidase regulates PINK1 processing, import and Parkin recruitment. EMBO Rep 13(4): 378-85

Grimes D, Gordon J, Snelgrove B, Lim-Carter I, Fon E, Martin W, Wieler M, Suchowersky O, Rajput A, Lafontaine AL, Stoessl J, Moro E, Schoffer K, Miyasaki J, Hobson D, Mahmoudi M, Fox S, Postuma R, Kumar H, Jog M (2012) Canadian Guidelines on Parkinson's Disease Introduction. Can J Neurol Sci 39: Suppl 4: S1-S30

Guo C, Sun L, Chen X, Zhang D (2013) Oxidative stress, mitochondrial damage and neurodegenerative damage. Neural Regen Res 8(21): 2003-2014

Hasson SA, Kane LA, Yamano K, Huang CH, Sliter DA, Buehler E, Wang C, Heman-Ackah SM, Hessa T, Guha R, Martin SE, Youle RJ (2013) High-content genome-wide RNAi screens identify regulators of parkin upstream of mitophagy. Nature 504(7479): 291-5

Hennessy BT, Smith DL, Ram PT, Lu Y, Mills GB (2005) Exploiting the PI3K/AKT pathway for cancer drug discovery. Nat Rev Drug Discov 4(12): 988-1004

Hernández-Maqueda JG, Luna-Ulloa LB, Santoyo-Ramos P, Castañeda-Patlán MC, Robles-Flores M (2015) Protein kinase C delta negatively modulates canonical Wnt pathway and cell proliferation in colon tumor cell lines. PLoS One 8(3): e58540

Hershko A, Ciechanover A (1998) The ubiquitin system. Annu Rev Biochem 67: 425-79

Hertz NT, Berthet A, Sos ML, Thorn KS, Burlingame AL, Nakamura K, Shokat KM (2016) A neo-substrate that amplifies catalytic activity of parkinson's-disease-related kinase PINK1. Cell 154(4): 737-47

Hindie V, Stroba A, Zhang H, Lopez-Garcia LA, Idrissova L, Zeuzem S, Hirschberg D, Schaeffer F, Jørgensen TJ, Engel M, Alzari PM, Biondi RM (2009) Structure and allosteric effects of low-molecular-weight activators on the protein kinase PDK1. Nat Chem Biol 5(10): 758-64

Hu J, Ahuja LG, Meharena HS, Kannan N, Kornev AP, Taylor SS, Shaw AS (2015) Kinase regulation by hydrophobic spine assembly in cancer. Mol Cell Biol 35(1): 264-76

Jayanthan A, Ruan Y, Truong TH, Narendran A (2014) Aurora Kinases as Druggable Targets in Pediatric Leukemia: Heterogeneity in Target Modulation Activities and Cytotoxicity by Diverse Novel Therapeutic Agents. PLoS One 9(7): e102741

Jin SM, Youle RJ (2013) The accumulation of misfolded proteins in the mitochondrial matrix is sensed by PINK1 to induce PARK2/Parkin-mediated mitophagy of polarized mitochondria. Autophagy 9(11): 1750-7

Jin SM, Lazarou M, Wang C, Kane LA, Narendra DP, Youle RJ (2010) Mitochondrial membrane potential regulates PINK1 import and proteolytic destabilization by PARL. J Cell Biol 191(5): 933-42

Johnson LN, Noble ME, Owen DJ (1996) Active and inactive protein kinases: structural basis of regulation. Cell 85(2): 149-58

Kalia LV, Lang AE (2015) Parkinson’s disease. The Lancet 386(9996): 896-912

Kay LE, Keifer P, Saarinen T (1992) Pure absorption gradient enhanced heteronuclear single quantum correlation spectroscopy with improved sensitivity. J Am Chem Soc 114: 10663-5

Khan NL, Jain S, Lynch JM, Pavese N, Abou-Sleiman P, Holton JL, Healy DG, Gilks WP, Sweeney MG, Ganguly M, Gibbons V, Gandhi S, Vaughan J, Eunson LH, Katzenschlager R, Gayton J, Lennox G, Revesz T, Nicholl D, Bhatia KP, Quinn N, Brooks D, Lees AJ, Davis MB, Piccini P, Singleton AB, Wood NW. (2005) Mutations in the gene LRRK2 encoding dardarin (PARK8) cause familial Parkinson's disease: clinical, pathological, olfactory and functional imaging and genetic data. Brain 128(Pt 12): 2786-96

Kitada T, Asakawa S, Hattori N, Matsumine H, Yamamura Y, Minoshima S, Yokochi M, Mizuno Y, Shimizu N (1998) Mutations in the parkin gene cause autosomal recessive juvenile parkinsonism. Nature 392(6676): 605-8

Komander D, Rape M (2012) The Ubiquitin Code. Annu Rev Biochem 81: 203-229

Kondapalli C, Kazlauskaite A, Zhang N, Woodroof HI, Campbell DG, Gourlay R, Burchell L, Walden H, Macartney TJ, Deak M, Knebel A, Alessi DR, Muqit MM (2012) PINK1 is activated by mitochondrial membrane potential depolarization and stimulates Parkin E3 ligase activity by phosphorylating Serine 65. Open Biol 2(5): 120080

Konermann L, Pan J, Liu YH (2011) Hydrogen exchange mass spectrometry for studying protein structure and dynamics. Chem Soc Rev 40(3): 1224-34

Kumar A, Tamjar J, Waddell AD, Woodroof HI, Raimi OG, Shaw AM, Peggie M, Muqit MM, van Aalten DM (2017) Structure of PINK1 and mechanisms of Parkinson's disease-associated mutations. Elife 6 e29985

Lamba V, Ghosh I (2012) New directions in targeting protein kinases: focusing upon true allosteric and bivalent inhibitors. Curr Pharm Des 18(20): 2936-45

Lazarou M, Jin SM, Kane LA, Youle RJ (2012) Role of PINK1 binding to the TOM complex and alternate intracellular membranes in recruitment and activation of the E3 ligase Parkin. Dev Cell 22(2): 320-33

Lipinski CA, Lombardo F, Dominy BW, Feeney PJ (1997) Experimental and computational approaches to estimate solubility and permeability in drug discovery and development settings. Adv Drug Deliv Rev 46(1-3): 3-26

Lo MC, Aulabaugh A, Jin G, Cowling R, Bard J, Malamas M, Ellestad G (2004) Evaluation of fluorescence-based thermal shift assays for hit identification in drug discovery. Anal Biochem. 332(1): 153-9

Lundmark R, Carlsson SR (2009) SNX9 – a prelude to vesicle release. J Cell Sci 122(Pt 1): 5-11

Lutz AK, Exner N, Fett ME, Schlehe JS, Kloos K, Lämmermann K, Brunner B, Kurz-Drexler A, Vogel F, Reichert AS, Bouman L, Vogt-Weisenhorn D, Wurst W, Tatzelt J, Haass C, Winklhofer KF (2009) Loss of parkin or PINK1 function increases Drp1-dependent mitochondrial fragmentation. J Biol Chem 284(34): 22938-51

Manning G, Whyte DB, Martinez R, Hunter T, Sudarsanam S (2002) The protein kinase complement of the human genome. Science 298(5600): 1912-34

Manning BD, Cantley LC (2007) AKT/PKB signaling: navigating downstream. Cell 129(7): 1261-74

Martin I, Dawson VL, Dawson TM (2011) Recent advances in the genetics of Parkinson's disease. Annu Rev Genomics Hum Genet 12: 301-25

Martinez A, Lectez B, Ramirez J, Popp O, Sutherland JD, Urbé S, Dittmar G, Clague MJ, Mayor U (2017) Quantitative proteomic analysis of Parkin substrates in Drosophila neurons. Mol Neurodegener 12(1): 29

Matheoud D, Sugiura A, Bellemare-Pelletier A, Laplante A, Rondeau C, Chemali M, Fazel A, Bergeron JJ, Trudeau LE, Burelle Y, Gagnon E, McBride HM, Desjardins M (2016) Parkinson's Disease-Related Proteins PINK1 and Parkin Repress Mitochondrial Antigen Presentation. Cell 166(2): 314-327

McLelland GL, Lee SA, McBride HM, Fon EA (2016) Syntaxin-17 delivers PINK1/parkin-dependent mitochondrial vesicles to the endolysosomal system. J Cell Biol 214(3): 275-91

McLelland GL, Goiran T, Yi W, Dorval G, Chen CX, Lauinger ND, Krahn AI, Valimehr S, Rakovic A, Rouiller I, Durcan TM, Trempe JF, Fon EA (2018) Mfn2 ubiquitination by PINK1/parkin gates the p97-dependent release of ER from mitochondria to drive mitophagy. Elife 7 e32866

Meissner C, Lorenz H, Weihofen A, Selkoe DJ, Lemberg MK (2011) The mitochondrial intramembrane protease PARL cleaves human Pink1 to regulate Pink1 trafficking. J Neurochem 117(5): 856-67

Nakamura K, Bindokas VP, Marks JD, Wright DA, Frim DM, Miller RJ, Kang UJ (2000) The selective toxicity of 1-methyl-4-phenylpyridinium to dopaminergic neurons: the role of mitochondrial complex I and reactive oxygen species revisited. Mol Pharmacol 58(2): 271-8

Narendra D, Tanaka A, Suen DF, Youle RJ (2008) Parkin is recruited selectively to impaired mitochondria and promotes their autophagy. J Cell Biol 183(5): 795-803

Narendra DP, Wang C, Youle RJ, Walker JE (2013) PINK1 rendered temperature sensitive by disease-associated and engineered mutations. Hum Mol Genet 22(13): 2572-89

Neupert W, Hermann JM (2007) Translocation of proteins in mitochondria. Annu Rev Biochem 76: 723-49

Newton AC (2003) Regulation of the ABC kinases by phosphorylation: protein kinase C as a paradigm. Biochem J 370(Pt 2): 361-71

Niault TS, Baccarini M (2010) Targets of Raf in tumorigenesis. Carcinogenesis 31(7): 1165-74

Nolen B, Taylor S, Ghosh G (2004) Regulation of protein kinases; controlling activity through activation segment conformation. Mol Cell 15(5): 661-75

Okatsu K, Oka T, Iguchi M, Imamura K, Kosako H, Tani N, Kimura M, Go E, Koyano F, Funayama M, Shiba-Fukushima K, Sato S, Shimizu H, Fukunaga Y, Taniguchi H, Komatsu M, Hattori N, Mihara K, Tanaka K, Matsuda N (2012) PINK1 autophosphorylation upon membrane potential dissipation is essential for Parkin recruitment to damaged mitochondria. Nat Commun 3:1016

Okatsu K, Uno M, Koyano F, Go E, Kimura M, Oka T, Tanaka K, Matsuda N (2013) A dimeric PINK1-containing complex on depolarized mitochondria stimulates Parkin recruitment. J Biol Chem 288(51): 36372-84

Okatsu K, Kimura M, Oka T, Tanaka K, Matsuda N (2015) Unconventional PINK1 localization to the outer membrane of depolarized mitochondria drives Parkin recruitment. J Cell Sci 128(5): 964-78

Okatsu K, Koyano F, Kimura M, Kosako H, Saeki Y, Tanaka K, Matsuda N (2015) Phosphorylated ubiquitin chain is the genuine Parkin receptor. J Cell Biol 209(1): 111-128

Okatsu K, Sato Y, Yamano K, Matsuda N, Negishi L, Takahashi A, Yamagata A, Goto-Ito S, Mishima M, Ito Y, Oka T, Tanaka K, Fukai S (2018) Structural insights into ubiquitin phosphorylation by PINK1. Sci Rep 8(1): 10382

Okuzumi T, Fiedler D, Zhang C, Gray DC, Aizenstein B, Hoffman R, Shokat KM (2009) Inhibitor hijacking of Akt activation. Nat Chem Biol 5(7): 484-93

Ordureau A, Paulo JA, Zhang W, Ahfeldt T, Zhang J, Cohn EF, Hou Z, Heo JM, Rubin LL, Sidhu SS, Gygi SP, Harper JW (2018) Dynamics of PARKIN-Dependent Mitochondrial Ubiquitylation in Induced Neurons and Model Systems Revealed by Digital Snapshot Proteomics. Mol Cell 70(2): 211-227

Orr AL, Rutaganira FU, de Roulet D, Huang EJ, Hertz NT, Shokat KM, Nakamura K (2017) Long-term oral kinetin does not protect against α-synuclein-induced neurodegeneration in rodent models of Parkinson's disease. Neurochem Int 109: 106-116

Palmer AG III, Cavanagh J, Wright PE, Rance (1991) Sensitivity improvement in proton-detected two-dimensional heteronuclear correlation NMR spectroscopy. J Magn Reson 93: 151-170

Papa FR, Zhang C, Shokat K, Walter P (2003) Bypassing a kinase activity with an ATP-competitive drug. Science 302(5650): 1533-7

Pardanani A1, Lasho T, Smith G, Burns CJ, Fantino E, Tefferi A (2009) CYT387, a selective JAK1/JAK2 inhibitor: in vitro assessment of kinase selectivity and preclinical studies using cell lines and primary cells from polycythemia vera patients. Leukemia 23(8): 1441-5

Park J, Lee SB, Lee S, Kim Y, Song S, Kim S, Bae E, Kim J, Shong M, Kim JM, Chung J (2006) Mitochondrial dysfunction in Drosophila PINK1 mutants is complemented by parkin. Nature 441(7097): 1157-61

Patil C, Walter P (2001) Intracellular signaling from the endoplasmic reticulum to the nucleus: the unfolded protein response in yeast and mammals. Curr Opin Cell Biol 13(3): 349-55

Pickles S, Vigié P, Youle RJ (2018) Mitophagy and Quality Control Mechanisms in Mitochondrial Maintenance. Curr Biol 28(4): R170-R185

Pickrell AM, Youle RJ (2015) The roles of PINK1, parkin, and mitochondrial fidelity in Parkinson's disease. Neuron 85(2): 257-73.

Pickrell AM, Huang CH, Kennedy SR, Ordureau A, Sideris DP, Hoekstra JG, Harper JW, Youle RJ (2015) Endogenous Parkin Preserves Dopaminergic Substantia Nigral Neurons following Mitochondrial DNA Mutagenic Stress. Neuron 87(2): 371-81

Poewe W, Seppi K, Tanner CM, Halliday GM, Brundin P, Volkmann J, Schrag AE, Lang AE (2017) Parkinson disease. Nat Rev Dis Prim 3: 17013

Poulikakos PI, Zhang C, Bollag G, Shokat KM, Rosen N (2010) RAF inhibitors transactivate RAF dimers and ERK signalling in cells with wild-type BRAF. Nature 464(7287): 427-30

Puleo DE, Kucera K, Hammarén HM, Ungureanu D, Newton AS, Silvennoinen O, Jorgensen WL, Schlessinger J (2017) Identification and Characterization of JAK2 Pseudokinase Domain Small Molecule Binders. ACS Med Chem Lett 8(6): 618-621

Ransom BR, Kunis DM, Irwin I, Langston JW (1987) Astrocytes convert the parkinsonism inducing neurotoxin, MPTP, to its active metabolite, MPP+. Neurosci Lett 75(3): 323-8

Rasool S, Trempe JF (2019) New insights into the structure of PINK1 and the mechanism of ubiquitin phosphorylation. Crit Rev Biochem Mol Biol 53(5): 515-534

Rasool S, Soya N, Truong L, Croteau N, Lukacs GL, Trempe JF (2018) PINK1 autophosphorylation is required for ubiquitin recognition. EMBO Rep 19(4) e44981

Riley BE, Lougheed JC, Callaway K, Velasquez M, Brecht E, Nguyen L, Shaler T, Walker D,Yang Y, Regnstrom K, Diep L, Zhang Z, Chiou S, Bova M, Artis DR, Yao N, Baker J, YednockT,

Johnston JA (2013) Structure and function of Parkin E3 ubiquitin ligase reveals aspects of RING and HECT ligases. Nat Commun 4: 1982.

Roskoski R Jr (2016) Classification of small molecule protein kinase inhibitors based upon the structures of their drug-enzyme complexes. Pharmacol Res 103:26-48

Roskoski R Jr (2019) Properties of FDA-approved small molecule protein kinase inhibitors. Pharmacol Res 144: 19-50

Rüegsegger U, Leber JH, Walter P (2001) Block of HAC1 mRNA translation by long-range base pairing is released by cytoplasmic splicing upon induction of the unfolded protein response. Cell 107(1): 103-14

Santel A, Frank S, Gaume B, Herrler M, Youle RJ, Fuller MT (2003) Mitofusin-1 protein is a generally expressed mediator of mitochondrial fusion in mammalian cells. J Cell Sci 116(Pt 13): 2763-74

Sarbassov DD, Guertin DA, Ali SM, Sabatini DM (2005) Phosphorylation and regulation of Akt/PKB by the rictor-mTOR complex. Science 307(5712): 1098-101

Sauvé V, Lilov A, Seirafi M, Vranas M, Rasool S, Kozlov G, Sprules T, Wang J, Trempe JF, Gehring K (2015) A Ubl/ubiquitin switch in the activation of Parkin. EMBO J 34(20): 2492-505

Sauvé V, Sung G, Soya N, Kozlov G, Blaimschein N, Miotto LS, Trempe JF, Lukacs GL, Gehring K (2018) Mechanism of parkin activation by phosphorylation. Nat Struct Mol Biol 25(7): 623-630

Schapira AHV, Cooper JM, Dexter D, Jenner P, Clark JB, Mardsen CD (1989) Mitochondrial complex I deficiency in Parkinson's disease. The Lancet 333(8649): 1269

Schapira AH (2008) Mitochondria in the aetiology and pathogenesis of Parkinson's disease. Lancet Neurol 7(1): 97-109

Schleucher J, Schwendinger M, Sattler M, Schmidt P, Schedletzky O, Glaser SJ, Sorensen OW, Griesinger C (1994) A general enhancement scheme in heteronuclear multidimensional NMR employing pulsed field gradients. J Biomol NMR 4: 301-306

Schubert AF, Gladkova C, Pardon E, Wagstaff JL, Freund SMV, Steyaert J, Maslen SL, Komander D (2018) Structure of PINK1 in complex with its substrate ubiquitin. Nature 552(7683): 51-56

Seirafi M, Kozlov G, Gehring K (2015) Parkin structure and function. FEBS 282(11): 2076-88

Sekine S, Youle RJ (2018) PINK1 import regulation; a fine system to convey mitochondrial stress to the cytosol. BMC Biol 16:2

Sena LA, Chandel, NS (2012) Physiological roles of mitochondrial reactive oxygen species. Mol Cell 48(2): 158-167

Shen K, Hines AC, Schwarzer D, Pickin KA, Cole PA (2005) Protein kinase structure and function analysis with chemical tools. Biochim Biophys Acta 1754(1-2): 65-78

Sidrauski C, Walter P (1997) The transmembrane kinase Ire1p is a site-specific endonuclease that initiates mRNA splicing in the unfolded protein response. Cell 90(6): 1031-9

Silvestri L, Caputo V, Bellacchio E, Atorino L, Dallapiccola B, Valente EM, Casari G (2005) Mitochondrial import and enzymatic activity of PINK1 mutants associated to recessive parkinsonism. Hum Mol Genet 14(22): 3477-92

Sim CH, Lio DS, Mok SS, Masters CL, Hill AF, Culvenor JG, Cheng HC (2006) C-terminal truncation and Parkinson's disease-associated mutations down-regulate the protein serine/threonine kinase activity of PTEN-induced kinase-1. Hum Mol Genet 15(21): 3251-62

Singleton AB, Farrer M, Johnson J, Singleton A, Hague S, Kachergus J, Hulihan M, Peuralinna T, Dutra A, Nussbaum R, Lincoln S, Crawley A, Hanson M, Maraganore D, Adler C, Cookson MR, Muenter M, Baptista M, Miller D, Blancato J, Hardy J, Gwinn-Hardy K (2003) alpha-Synuclein locus triplication causes Parkinson’s disease. Science 302(5646): 841.

Sliter DA, Martinez J, Hao L, Chen X, Sun N, Fischer TD, Burman JL, Li Y, Zhang Z, Narendra DP, Cai H, Borsche M, Klein C, Youle RJ (2018) Parkin and PINK1 mitigate STING-induced inflammation. Nature 561(7722): 258-262

Sugiura A, McLelland GL, Fon EA, McBride HM (2014) A new pathway for mitochondrial quality control: mitochondrial-derived vesicles. EMBO J 33(19): 2142-56

Surmeier DJ, Guzman JN, Sanchez-Padilla J, Schumacker PT (2011) The role of calcium and mitochondrial oxidant stress in the loss of substantia nigra pars compacta dopaminergic neurons in Parkinson’s disease. Neuroscience 198: 221-31

Surmeier DJ, Carrillo-Reid L, Bargas J (2011) Dopaminergic modulation of striatal neurons, circuits and assemblies. Neuroscience 198: 3-18

Tanaka A, Cleland MM, Xu S, Narendra DP, Suen DF, Karbowski M, Youle RJ (2010) Proteasome and p97 mediate mitophagy and degradation of mitofusins induced by Parkin. J Cell Biol 191(7): 1367-80

Tang MY, Vranas M, Krahn AI, Pundlik S, Trempe JF, Fon EA (2017) Structure-guided mutagenesis reveals a hierarchical mechanism of Parkin activation. Nat Commun 8: 14697

Tanida I, Ueno T, Kominami E (2008) LC3 and Autophagy. Methods Mol Biol 445: 77-88

Tasaki T, Sriram SM, Park KS, Kwon YT (2005) The N-end rule pathway. Annu Rev Biochem 81: 261-89

Taylor SS, Kornev AP (2011) Protein kinases: evolution of dynamic regulatory proteins. Trends Biochem Sci 36(2): 65-77

Taylor SS, Radzio Andzelm E (1994) Three protein kinase structures define a common motif. Structure 2: 345-355

Trempe JF, Chen CX, Grenier K, Camacho EM, Kozlov G, McPherson PS, Gehring K, Fon EA (2009) SH3 domains from a subset of BAR proteins define a Ubl-binding domain and implicate parkin in synaptic ubiquitination. Molecular cell 36: 1034-1047

Trempe JF, Fon EA (2013) Structure and Function of Parkin, PINK1, and DJ-1, the Three Musketeers of Neuroprotection. Front Neurol 4: 38

Trempe JF, Saskova KG, Siva M, Ratcliffe CDH, Veverka V, Hoegl A, Menade M, Feng X, Shenker S, Svoboda M, Kozisek M, Konvalinka J, Gehring K (2016) Structural studies of the yeast DNA damage-inducible protein Ddi1 reveal domain architecture of this eukaryotic protein family. Sci Rep 6: 33671

Trempe JF, Sauvé V, Grenier K, Seirafi M, Tang MY, Menade M, Al-Abdul-Wahid S, Krett J, Wong K, Kozlov G, Nagar B, Fon EA, Gehring K (2013) Structure of parkin reveals mechanisms for ubiquitin ligase activation. Science 340: 1451-1455.

Tse A, Verkhivker GM (2016) Exploring Molecular Mechanisms of Paradoxical Activation in the BRAF Kinase Dimers: Atomistic Simulations of Conformational Dynamics and Modeling of Allosteric Communication Networks and Signaling Pathways. PLoS One 11(11): e0166583

Valente EM1, Brancati F, Caputo V, Graham EA, Davis MB, Ferraris A, Breteler MM, Gasser T, Bonifati V, Bentivoglio AR, De Michele G, Dürr A, Cortelli P, Filla A, Meco G, Oostra BA, Brice A, Albanese A, Dallapiccola B, Wood NW; European Consortium on Genetic Susceptibility in Parkinson's Disease (2002) PARK6 is a common cause of familial parkinsonism. Neurol Sci 23 Suppl 2: S117-8

Valente EM, Abou-Sleiman PM, Caputo V, Muqit MM, Harvey K, Gispert S, Ali Z, Del Turco D, Bentivoglio AR, Healy DG, Albanese A, Nussbaum R, González-Maldonado R, Deller T, Salvi S, Cortelli P, Gilks WP, Latchman DS, Harvey RJ, Dallapiccola B, Auburger G, Wood NW (2004) Hereditary early-onset Parkinson's disease caused by mutations in PINK1. Science 304(5674): 1158-60

Vincow ES, Merrihew G, Thomas RE, Shulman NJ, Beyer RP, MacCoss MJ, Pallanck LJ (2013) The PINK1-Parkin pathway promotes both mitophagy and selective respiratory chain turnover in vivo. Proc Natl Acad Sci U S A 110(16): 6400-5

von Muhlinen N, Thurston T, Ryzhakov G, Bloor S, Randow F (2010) NDP52, a novel autophagy receptor for ubiquitin-decorated cytosolic bacteria. Autophagy 6(2): 288-9

Wang Z, Cole PA (2014) Catalytic mechanisms and regulation of protein kinases. Methods Enzymol 548: 1-21

Wang S, Midgley CA, Scaërou F, Grabarek JB, Griffiths G, Jackson W, Kontopidis G, McClue SJ, McInnes C, Meades C, Mezna M, Plater A, Stuart I, Thomas MP, Wood G, Clarke RG, Blake DG, Zheleva DI, Lane DP, Jackson RC, Glover DM, Fischer PM (2010) Discovery of N-phenyl-4-(thiazol-5-yl)pyrimidin-2-amine aurora kinase inhibitors. J Med Chem 53(11): 4367-78

Wang X, Winter D, Ashrafi G, Schlehe J, Wong YL, Selkoe D, Rice S, Steen J, LaVoie MJ, Schwarz TL (2011) PINK1 and Parkin target Miro for phosphorylation and degradation to arrest mitochondrial motility. Cell 147(4): 893-906

Wauer T, Komander D (2013) Structure of the human Parkin ligase domain in an autoinhibited state. The EMBO journal 32: 2099-2112.

Wimmer R1, Baccarini M (2010) Partner exchange: protein-protein interactions in the Raf pathway. Trends Biochem Sci 35(12): 660-8

Wiedemann N, Frazier AE, Pfanner N (2017) The Protein Import Machinery of Mitochondria. J Biol Chem 279: 14473-14476

Woodroof HI, Pogson JH, Begley M, Cantley LC, Deak M, Campbell DG, van Aalten DM, Whitworth AJ, Alessi DR, Muqit MM (2011) Discovery of catalytically active orthologues of the Parkinson's disease kinase PINK1: analysis of substrate specificity and impact of mutations. Open Biol 1(3): 110012

Yamano K, Youle RJ (2013) PINK1 is degraded through the N-end rule pathway. Autophagy 9(11): 1758-1769

Yamano K, Fogel AI, Wang C, van der Bliek AM, Youle RJ (2014) Mitochondrial Rab GAPs govern autophagosome biogenesis during mitophagy. Elife 3: e01612

Yamano K, Wang C, Sarraf SA, Münch C, Kikuchi R, Noda NN, Hizukuri Y, Kanemaki MT, Harper W, Tanaka K, Matsuda N, Youle RJ (2018) Endosomal Rab cycles regulate Parkin-mediated mitophagy. Elife 7 e31326

Yi W, MacDougall EJ, Tang MY, Krahn AI, Gan-Or Z, Trempe JF, Fon EA (2019) The Landscape of *Parkin* Variants Reveals Pathogenic Mechanisms and Therapeutic Targets in Parkinson's Disease. Hum Mol Genet ddz080

Zhang Z1, Cao C2, Sun S1, Xu Q3 (2015) Selective spleen tyrosine kinase inhibition delays autoimmune arthritis in mice. Mol Med Rep 12(2): 2902-6

Zheng N, Shabek N (2017) Ubiquitin Ligases: Structure, Function, and Regulation. Annu Rev Biochem 86: 129-157

Zuccotto F, Ardini E, Casale E, Angiolini M (2010) Through the "gatekeeper door": exploiting the active kinase conformation. J Med Chem 53(7): 2681-94

7. Appendix

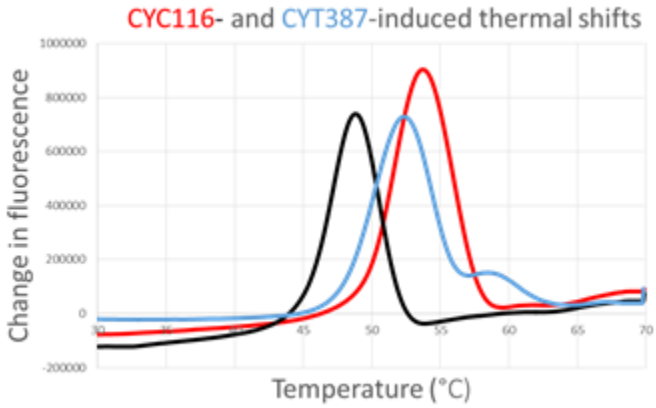

Figure 1: Thermal shift assay screening reveals CYC116 and CYT387 as TcPINK1 thermal stabilizers. Y-axis values represent values of the first temperature-wise derivative of measured fluorescence, and thus curve maxima are inflection points, or T_m.

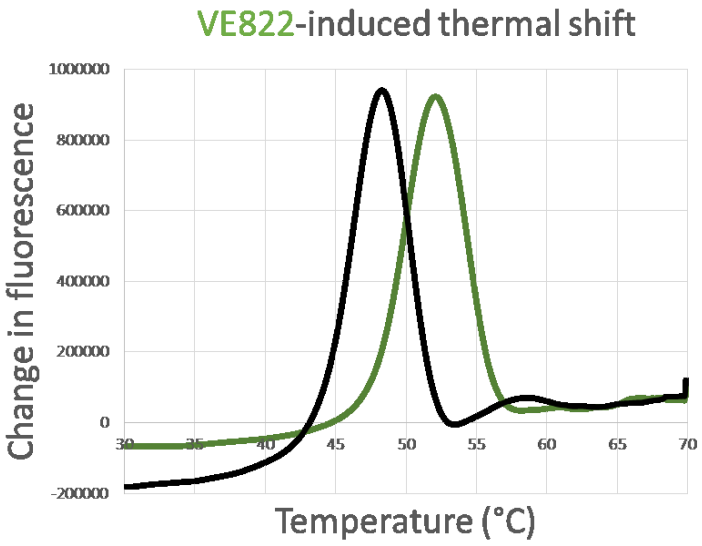

Figure 2: Thermal shift assay screening reveals VE822 as a TcPINK1 thermal stabilizer. Y-axis values represent values of the first temperature-wise derivative of measured fluorescence, and thus curve maxima are inflection points, or T_m.

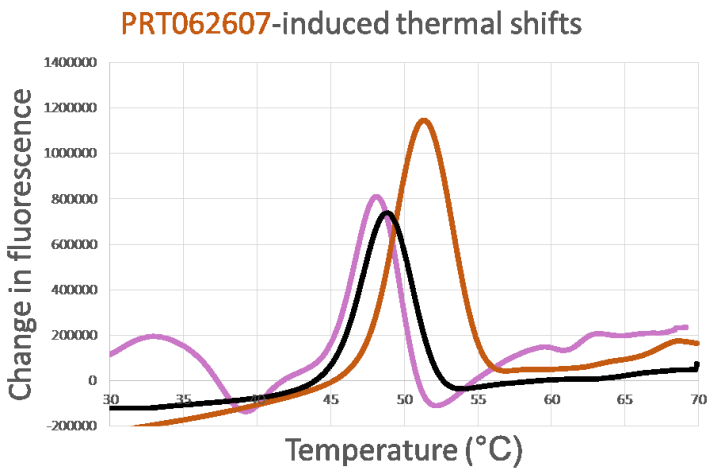

Figure 3: Thermal shift assay screening reveals PRT062607, but not Foretinib, as a TcPINK1 thermal stabilizer. Y-axis values represent values of the first temperature-wise derivative of measured fluorescence, and thus curve maxima are inflection points, or T_m.

Compound added	Compound structure	TcPINK1 KD T_m	ΔT_m
Foretinib MW: 632.66	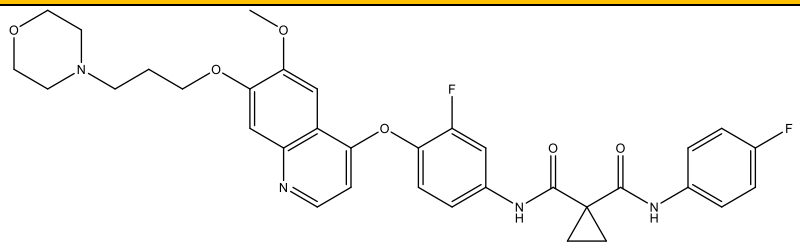	48.04°C	-0.84°C

Figure 4: Foretinib is a non-thermally stabilizing negative control. Molecular weight, structure, induced T_m, and ΔT_m are shown.

	PRT062607	CYC116
[Inhibitor] vs. response -- Variable slope (four parameters)		
Best-fit values		
Bottom	0.001845	0.005378
Top	0.2779	0.2119
HillSlope	2.432	3.923
IC50	18.02	28.09
logIC50	1.256	1.449
Span	0.2761	0.2065
Std. Error		
Bottom	0.01121	0.02066
Top	0.006392	0.009028
HillSlope	0.3713	1.971
IC50	1.305	3.565
Span	0.014	0.02379
95% CI (profile likelihood)		
Bottom	-0.0255 to 0.02352	-0.09621 to 0.04188
Top	0.2645 to 0.2925	0.1917 to 0.2397
HillSlope	1.766 to 3.317	1.2 to ???
IC50	15.43 to 21.21	20.43 to 45.35
logIC50	1.188 to 1.327	1.31 to 1.657
Goodness of Fit		
Degrees of Freedom	12	12
R square	0.9864	0.9285
Absolute Sum of Squares	0.002691	0.008407
Sy.x	0.01497	0.02647
Constraints		
IC50	IC50 > 0	IC50 > 0
Number of points		
# of X values	16	16
# Y values analyzed	16	16

Figure 5: Nonlinear regression of PRT062607 and CYC116 concentrations versus pUb production. Data analysis from pUb quantification from Phostag gels. All parameters computed by GraphPad Prism are shown.

[Inhibitor] vs. response – Variable slope (four parameters)	
Best-fit values	
Bottom	= 0
Top	0.5926
HillSlope	0.9903
IC50	192.3
logIC50	2.284
Span	= 0.5926
Std. Error	
Top	0.02344
HillSlope	0.4476
IC50	87.44
95% CI (profile likelihood)	
Top	0.547 to 0.7835
HillSlope	0.1899 to 2.363
IC50	102 to 3151
logIC50	2.009 to 3.498
Goodness of Fit	
Degrees of Freedom	6
R square	0.8087
Absolute Sum of Squares	0.008929
Sy.x	0.03858
Constraints	
Bottom	Bottom = 0
IC50	IC50 > 0
Number of points	
# of X values	9
# Y values analyzed	9

Figure 6: Nonlinear regression (with curve bottom set to 0) of PRT062607 concentrations vs. Mfn2 ubiquitination results. Data analysis from Mfn2 ubiquitination quantification from Western Blot. All parameters computed by GraphPad Prism are shown.

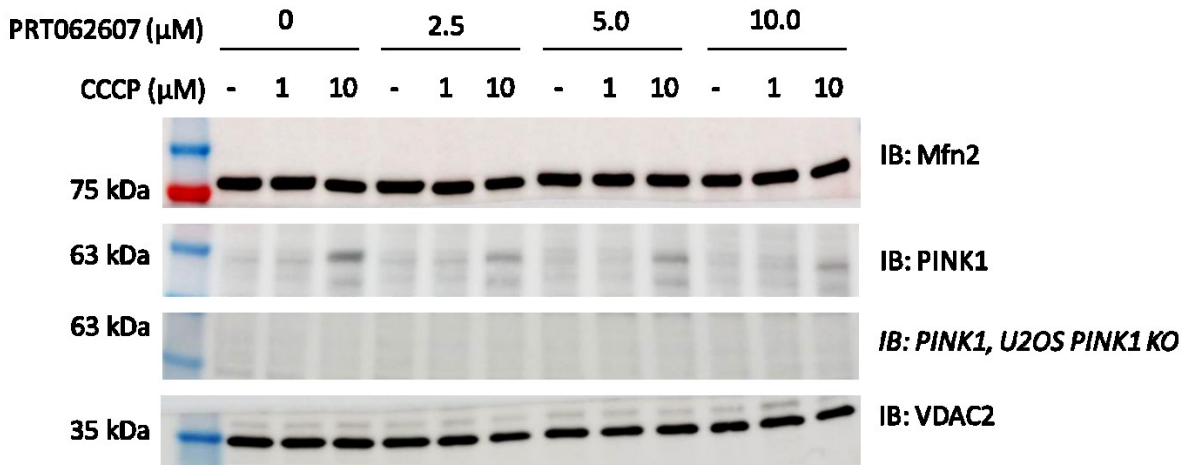

Figure 7: PRT062607 does not increase HsPINK1 stability in HeLa cells. The PINK1 immunoblot shows that PRT062607 does not increase HsPINK1 levels. The PINK1 signal is absent in PINK1 KO cells. The VDAC2 immunoblot serves as a mitochondrial loading control. Molecular weights are shown on the left.